

Functional characterization of transketolase-like
proteins and related model systems with
respect to thiamin diphosphate mediated
chemistry

Dissertation for the award of the degree
“Doctor rerum naturalium”
of the Georg-August-University Göttingen

submitted by
Stefan Schneider
born in Göttingen

Göttingen 2013

Members of the thesis committee

Prof. Dr. Kai Tittmann (Reviewer)

Department for Bioanalytics
Albrecht-von-Haller Institute for Plant Sciences
Georg-August-University Göttingen

Prof. Dr. Jörg Stülke (Reviewer)

Department for General Microbiology
Georg-August-University Göttingen

Prof. Dr. Matthias Dobbelstein

Institute of Molecular Oncology
Göttingen University Medical School

Affidativ

Herewith I declare, that I prepared this thesis "Functional characterization of transketolase-like proteins and related model systems with respect to thiamin diphosphate mediated chemistry" indipendently and with no other sources and aids than quoted.

Göttingen, 30.10.2013

Stefan Schneider

Table of content

1	Introduction	1
1.1	Metabolic adaptations as consequence of genetic alterations in cancer	1
1.2	Pentose phosphate pathway	5
1.3	Transketolase	7
1.3.1	Transketolase, general features and its contribution to human diseases	7
1.3.2	Structure of human transketolase.....	8
1.3.3	Cofactor activation and reaction mechanism of transketolases	9
1.4	The TKT isoforms Transketolase-like protein 1 and 2	12
1.4.1	Structural similarities of TKT, TKTL1 and 2.....	12
1.4.2	TKTL1 and tumorigenesis	15
1.4.3	TKTL1 putatively contributes to tumorigenesis by Hif1 α stabilization	16
1.4.4	The role of TKTL1 is contradictory.....	17
1.5	Phosphoketolase	18
1.5.1	Phosphoketolase of <i>Bifidobacteria</i>	18
1.5.2	Structure of XFPK from <i>Bifidobacterium breve</i>	20
1.5.3	Reaction mechanism of XFPK.....	22
1.6	Motivation	24
2	Material and methods	26
2.1	Materials	26
2.2	Devices	31
2.3	Programs	33
2.4	Media	33
2.5	Bacterial strains	34

Table of content

2.6	Vectors	35
2.7	Utilized primers.....	35
2.8	Methods.....	36
2.8.1	<i>Escherichia coli</i> cultivation	36
2.8.2	Transformation of <i>E. coli</i>	36
2.8.3	Isolation of plasmid DNA.....	36
2.8.4	Amplification of specific DNA fragments and site-directed mutagenesis by polymerase chain reaction	37
2.8.5	DNA-concentration determination.....	37
2.8.6	DNA-restriction	37
2.8.7	Separation of DNA-fragments by agarose-gel electrophoresis	37
2.8.8	DNA-ligation	37
2.8.9	CloneJet PCR cloning kit	38
2.8.10	Generation of a <i>hTKT</i> deletion construct by overlap extension PCR.....	38
2.8.11	DNA sequencing	38
2.8.12	Insect cell culture	38
2.8.13	Generation of pCOLD-TKTL1 and 2 fusion constructs.....	39
2.8.14	High density fermentation	39
2.8.15	Expression and purification of full length <i>hTKT</i> and the $\Delta 38$ deletion variant	40
2.8.16	Expression and purification of full length TKTL1 and 2.....	41
2.8.17	Expression and purification of xylulose 5-phosphate/fructose 6-phosphate phosphoketolase (XFPK) from <i>Bifidobacterium breve</i>	42
2.8.18	Sodium dodecyl sulfate-polyacrylamide-gel electrophoresis (SDS-PAGE)	42
2.8.19	Protein concentration determination according to Bradford	42
2.8.20	Detection of the proteins of interest by western blotting	42
2.8.21	Analytical gel filtration	43
2.8.22	Coupled optical enzymatic assay	43
2.8.23	Circular dichroism spectroscopy	44
2.8.23.1	Far-UV CD-based secondary structure element analysis	44

Table of content

2.8.23.2	Near-UV CD-based detection of a cofactor caused charge transfer absorption band	45
2.8.24	Cofactor binding studies by ¹ H NMR spectroscopy	46
2.8.25	Covalent reaction intermediate analysis by acidic quench ¹ H NMR spectroscopy.....	46
2.8.26	Analysis of XFPK catalysis derived acetate and <i>d4</i> -acetate by product ¹ H NMR spectroscopy	47
2.8.27	Determination of XFPK activity by the hydroxamate assay.....	47
2.8.28	Calorimetric based enzyme kinetics	47
2.8.29	Product analysis via mass spectrometry.....	48
2.8.30	Monitoring XFPK reaction intermediates by stopped flow absorbance spectroscopy.....	49
2.8.31	XFPK E437Q crystallization and data processing.....	50
3	Results	51
3.1	A Δ38 deletion variant of TKT as a minimal model for analysis of a putative TKTL1 function.....	51
3.1.1	Generation and purification of native TKT and TKT Δ 38	51
3.1.2	Analysis of secondary structure and thermal stability of native TKT and TKT Δ 38	51
3.1.3	Transketolase activity of TKT Δ 38	53
3.1.4	Analysis of cofactor binding competence of Δ 38 TKT by near-UV CD spectroscopy	54
3.1.5	Analysis of the oligomeric state of TKT and TKT Δ 38 by analytical gelfiltration	55
3.2	Phosphoketolase of <i>B. breve</i>	56
3.2.1	Expression and purification of wt XFPK and active site variants	56
3.2.2	Secondary structure and thermal stability of wt XFPK and variants.....	57
3.2.3	Analysis of enzymatic XFPK activity by discontinuous acetyl phosphate detection	58

Table of content

3.2.4	Analysis of protonic and tautomeric equilibria of enzyme-bound cofactor of XFPK by CD spectroscopy	63
3.2.5	pH dependence of the internal tautomeric equilibrium of XFPK-bound ThDP	64
3.2.6	Analysis of covalent reaction intermediates in XFPK formed during F6P conversion by ¹ H NMR spectroscopy	65
3.2.7	Analysis of intermediate formation in the course of XFPK mediated catalysis by stopped-flow UV/vis absorbance spectroscopy	66
3.2.7.1	Kinetic analysis of XFPK-driven F6P conversion.....	66
3.2.7.2	Reaction of XFPK-bound ThDP-intermediate with phosphate	68
3.2.8	¹ H NMR spectroscopic H/D exchange experiments to verify the presence of the enol form of AcThDP	69
3.2.9	Interactions of glutamate 437 with the pyrimidinium ring of ThDP	70
3.2.10	Structure of XFPK E437Q	73
3.3	Transketolase-like proteins 1 and 2	76
3.3.1	Recombinant expression of TKTL1 and 2 in <i>E. coli</i>	76
3.3.2	Recombinant expression of TKTL1 and 2 by usage of the Bac-to-bac™ expression system.....	77
3.3.3	Fed batch expression of TKTL1 and 2	78
3.3.4	A chaperone TKTL1 and 2 fusion construct for recombinant expression.....	79
3.3.5	Secondary structure and thermal stability of native TKTL1 and TKTL2	80
3.3.6	Enzymatic characterisation of TKTL1 and 2	82
3.3.7	Product analysis of a putative TKTL1 and 2 activity by mass spectrometry	83
3.3.8	Analysis of cofactor binding by near UV CD spectroscopy	85
4	Discussion	87
4.1	The Δ38 deletion variant of human transketolase as model for TKTL1	87
4.2	Elucidation of the catalytic mechanism of XFPK of <i>B. breve</i>	89
4.2.1	Purification and kinetic analysis of wt XFPK and active site variants	89
4.2.2	Protonic and tautomeric equilibria of XFPK and active site variants	90

Table of content

4.2.3	UV/vis stopped flow based analysis of enzyme-bound ThDP-intermediate formation	92
4.2.4	UV/vis stopped-flow based kinetic analysis of phosphate catalyzed enzyme bound ThDP-intermediate conversion	95
4.3	¹H NMR spectroscopic product analysis.....	97
4.3.1	Glutamate 437 seems to play a role in phosphorolysis.....	98
4.4	Transketolase-like protein 1 and 2.....	99
4.4.1	Expression and purification of a chaperone TKTL1 and 2 fusion construct	99
4.4.2	Biochemical analysis cofactor binding and of enzymatic TKTL1 and 2 activity	100
4.4.3	The role of TKTL1 in tumorigenesis needs to be further evaluated.....	102
5	Summary.....	104
6	Bibliography.....	107
7	Appendix.....	120

Figure list

Figure 1: The six hallmarks of cancer.	1
Figure 2: The conversion of glucose must be adjusted. It either serves for energy generation within glycolysis or NADPH/ nucleotide-synthesis within the PPP.	2
Figure 3: Metabolic adjustment by known oncogenes and tumor-suppressor genes.	3
Figure 4: The pentose phosphate pathway.	6
Figure 5: Structure of human transketolase.	8
Figure 6: Structure of thiamin diphosphate.	9
Figure 7: Tautomeric and ionization equilibria of ThDP prior to substrate addition.	10
Figure 8: Reaction cycle of TKTs.	11
Figure 9: Sequence alignment of hTKT (p29401) against TKTL1 (p51854).	14
Figure 10: The proposed mechanism of TKTL1-driven stabilization of Hif1 α	17
Figure 11: The bifid shunt of <i>Bifidobacteria</i>	19
Figure 12: Structure of <i>B. breve</i> XFPK.	20
Figure 13: The active centers of XFPK from <i>B. breve</i> and human TKT.	21
Figure 14: Reaction cycle of XFPK.	23
Figure 15: Coupled enzymatic assay for conversion of X5P and R5P by transketolase.	43
Figure 16: Expected m/z ratios for the used sugar phosphate and Coenzyme A substrates and products.	49
Figure 17: SDS-PAGE of purified native TKT and TKT Δ 38.	51
Figure 18 Far-UV spectra and thermal unfolding of native TKT and the TKT Δ 38 deletion variant.	52
Figure 19: Steady-state kinetic of enzymatic activity of native TKT as well as the TKT Δ 38 variant.	53
Figure 20: Cofactor binding analysis by near-UV CD and ¹ H NMR spectroscopy in full length TKT and the TKT Δ 38 deletion variant.	55
Figure 21: Analytical gel filtration experiments of full-length TKT and TKT Δ 38.	56
Figure 22: SDS-PAGE analysis of purified wt XFPK.	57
Figure 23: Far-UV spectra and thermal unfolding of wt XFPK.	58
Figure 24: Dependence of the reaction rate of wt XFPK on the F6P concentration.	59
Figure 25: ITC detected heat release during wt XFPK driven F6P cleavage.	60

Figure list

Figure 26: Determination of apparent enthalpy (ΔH_{app}) by complete substrate conversion.....	61
Figure 27: ITC based analysis of potential alternative substrate usage (S7P) and validation of activity of the different oligomeric states of wt XFPK.	62
Figure 28: Near-UV spectra analysis of wt XFPK at a concentration of 1 mg/mL enzyme in Hepes (pH 7.2).....	63
Figure 29: Near-UV spectra analysis of wt XFPK at different pH values.	64
Figure 30: Analysis of intermediate generation after wt XFPK driven conversion of F6P by ^1H NMR spectroscopy.	66
Figure 31: Stopped-flow absorbance spectra of F6P conversion by wt XFPK.	67
Figure 32: Time resolved PDA spectra of wt XFPK driven F6P conversion.	68
Figure 33: Rapid mixing experiment of wt XFPK bound enolAcThDP with the second substrate phosphate.....	69
Figure 34: ^1H NMR spectroscopic analysis of produced acetate after wt XFPK driven conversion of F6P in absence of phosphate.	70
Figure 35: Location of Glu 437 atop the pyrimidinring of the ThDP cofactor.....	71
Figure 36: Catalytic activity of XFPK E437Q.....	72
Figure 37: Time resolved PDA spectra of XFPK E437 driven F6P conversion.....	72
Figure 38: Near-UV spectra analysis of XFPK E437Q at a concentration of 1 mg/mL.	73
Figure 39: Electron density maps of resting ThDP in the XFPK E437Q variant.	74
Figure 40: Electron density maps of AcThDP in the XFPK E437Q variant.	76
Figure 41: SDS-PAGE analysis of TKTL1 and 2 expression in Hi 5 cells.....	78
Figure 42: SDS-PAGE analysis of purified fed-batch derived SUMO-TKTL 1.	79
Figure 43: SDS-PAGE analysis of purified TKTL1 and 2.	79
Figure 44: Far-UV spectra and thermal unfolding of TFKTL1 and 2 as well as the trigger-factor released TKTL1 and 2 constructs.	82
Figure 45: Steady-state kinetic analysis of enzymatic activity of TKTL1 and 2.	83
Figure 46: Total scan and ms/ms spectra of the putatively used substrates and generated products of a TKTL1 and 2 mediated enzymatic reaction.	84
Figure 47: Total scan and ms/ms spectra of the putatively used substrates and generated products of an TFKTL1 and 2 mediated enzymatic reaction.	84

Figure list

Figure 48: Total scan and ms/ms spectra of the putatively used substrates and generated products of an TFTKTL1 and 2 mediated enzymatic reaction.....	85
Figure 49: Cofactor binding analysis by near-UV CD.....	86
Figure 50: Structure of the active site of <i>human</i> TKT highlighting the 38 amino acids missing in the deletion variant.....	88
Figure 51: Tautomeric and ionization equilibria of ThDP in the resting state of ThDP-dependent enzymes.	90
Figure 52: Chemical structure of DhThDP including tautomeric states of the enolat-enamin in <i>E.coli</i> TKT.....	93
Figure 53: Catalytic steps mediated by the conserved active site His residues in XFPK...	94
Figure 54: Possible charge-transfer interaction of the aminopyrimidine- and the thiazolium ring of ThDP.	95
Figure 55: Phosphate catalyzed tautomerization of enolAcThDP to ketoAcThDP.	96
Figure 56: Microscopic steps of XFPK.....	99
Figure 57: Sequence alignment of <i>h</i> TKT (p29401) against TKTL2 (pQ9H0I9).....	120
Figure 58: XFPK variants (0.1 mg/mL) were analysed by far-UV CD to estimate their secondary structural content.	123
Figure 59: SDS PAGE analysis of purified XFPK variants.....	123
Figure 60: Temperature-induced unfolding of selected XFPK variants.	124
Figure 61: The active center histidine variants of XFPK were analyzed by near-UV CD spectroscopy for ThDP binding and generation of the AP, APH ⁺ and IP signal.....	127
Figure 63: Time resolved PDA spectra of XFPK driven F6P conversion.	128
Figure 62: Near-UV spectra analysis of XFPK at a concentration of 1 mg/mL enzyme in Hepes (pH 7.2).....	128
Figure 64: Analysis of intermediate generation after XFPK H97A variant driven conversion of F6P by ¹ H-NMR spectroscopy.....	129
Figure 65: Analysis of intermediate generation after XFPK H64A variant driven conversion of F6P by ¹ H-NMR spectroscopy.....	129
Figure 66: Simulated annealing 2 Fo - Fc omit map of dihydrothiachromin.	130
Figure 67: SDS-PAGE analysis of thrombin and HRV 3C digested TFTKTL1 and 2.	131
Figure 68: Steady-state kinetic analysis of enzymatic activity of TFTKTL1 and 2.	131

Figure list

Figure 69: Secondary structure signals as recorded by circular dichroism..... 132

Table list

Table 1: Used bacterial strains	34
Table 2: Used vectors	35
Table 3: Kinetic parameters of active site variants of XFPK.	56
Table 4: CDNN analysis of secondary structure contents of TFTKTL1, TFTKT2,	81
Table 5: X-ray statistics for <i>B.breve</i> XFPK in ground state with native cofactor ThDP, or refined with Dihydrothiachromin.....	121
Table 6: X-ray statistics for <i>B.breve</i> XFPK in complex with 1,2-dihydroxyethyl thiamindiphosphate (DhEThDP) or 2-acetyl thiamindiphosphate (AcThDP).	122

Abbreviations

Abbreviations

A260 or A280	absorption at 260 or 280 nm
app	apparent
BICINE	2-(Bis(2-hydroxyethyl)amino)acetic acid
<i>B. breve</i>	<i>Bifidobacterium breve</i>
CD	circular dichroism
Da	dalton
DHETHDP	dihydroxyethyl thiamin diphosphate
ϵ	molar extinction coefficient
E4P	D-erythrose 4-phosphate
<i>E. coli</i>	<i>Escherichia coli</i>
<i>EcTKT</i>	transketolase A from <i>Escherichia coli</i>
EDTA	ethylenediaminetetraacetate
Θ	ellipticity
F6P	D-fructose 6-phosphate
GAP	D-glyceraldehyde 3-phosphate
G3P-DH	glycerol 3-phosphate dehydrogenase
HEPES	(4-(2-hydroxyethyl)-1-piperazineethanesulfonic acid)
hTKT	human transketolase
IPTG	isopropyl- β -D-thiogalactoside
ITC	isothermal titration calorimetry
k	rate constant
λ	wavelength
LB media	Lysogeny-broth-Media
MES	2-(<i>N</i> -morpholino)ethanesulfonic acid
NADH/NAD ⁺	nicotinamide adenine dinucleotide (reduced form/oxidized form)
NADPH/NADP ⁺	nicotinamide adenine dinucleotide phosphate (reduced form/oxidized form)
NMR	nuclear magnetic resonance
nm	nano meter

Abbreviations

obs	observed
OD	optical density
pH	negative logarithm of H ⁺ concentration
PEG	polyethylene glycol
PIPES	1,4-Piperazinediethanesulfonic acid
PPP	pentose phosphate pathway
PMSF	phenylmethylsulfonylfluorid
R5P	D-ribose 5-phosphate
rpm	revolutions per minute
S7P	D-sedoheptulose 7-phosphate
SDS-PAGE	sodium dodecylsulfate polyacrylamide gelelectrophoresis
σ	estimated standard error, standard deviation or standard uncertainty
σ_A	Sigma-A, variance-term accounting for error and incompleteness in structure models
TCA	trichloro acetic acid
ThDP	thiamin diphosphate
TPI	triosephosphate isomerase
TRIS	tris (hydroxymethyl)-aminomethan
U	unit
UV/vis	ultraviolet and visible fraction of electromagnetic radiation
X5P	D-xylulose 5-phosphate

1 Introduction

1.1 Metabolic adaptations as consequence of genetic alterations in cancer

Cancer is the second most cause of death in the industrialized nations. Recent estimations turned out that for example up to almost 50 % of every individual citizen in Germany will develop cancer during its lifetime ¹. Moreover a meta-analysis estimated the costs for cancer treatment in the European Union to be 126 billion Euro per annum ². Therefore developing an effective treatment of cancer is a cross-national concern.

The cause for cancer can be found in a multistep process of accumulation of genetic alterations in non-cancerous cells. These genetic alterations are induced by a set of factors like chemical agents, ionizing radiation, virus infection or it originates from incorrect genome replication ³. Most of these genetic changes affect genes, encoding for proteins which are part of signal transduction cascades or are involved in cell-cycle control.

According to their way of action they are termed oncogenes or tumor-suppressor genes. Oncogenes are activated by mutations leading to a gain of function, whereas alterations of tumor-suppressor genes lead to a loss of function ⁴.

Although the amounts of genetic damages causing cancer seem numerous, the principles underpinning the characteristics of a malignant cell can be described by six general features ⁵. Hanahan and Weinberg state

that every cancer cell is self-sufficient in growth signaling, insensitive to antigrowth-signals, evasive of apoptosis-signals, limitless in replicative potential, sustaining in angiogenesis and prone to invade other tissues and form metastasis (Figure 1). Moreover, within the present decade, Hanahan and Weinberg extended their concept. They described four new abilities of malignant cells, two enabling characteristics and two emerging hallmarks ⁶. The enabling characteristics are the genome instability and



Figure 1: The six hallmarks of cancer. Picture adapted from Hanahan and Weinberg (2000).

1. Introduction

the tumor-promoting inflammation. The two emerging hallmarks are avoiding of immune destruction and deregulation of cellular energetics. Especially the latter has come into focus over the recent years since more and more functions of oncogenes and tumor-suppressor are described in terms of their involvement in the metabolism of cancerous cells ⁷.

Controlling cell proliferation (by tightly regulated signaling cascades and cell cycle control) are not the only bottlenecks tumors have to circumvent to maintain their antisocial behavior. They also have to surpass limitations in their energy- and nutrient supply by adjusting their metabolism. It was described that many enzymes of glucose metabolism are affected in tumors in terms of a deregulated expression rate or activity ^{8,9}. Moreover, glucose transport, lipogenesis, respiration and nucleotide synthesis are also subject to alterations to serve a tumor's metabolic demands ¹⁰. In this context an astonishing ability of cancerous cells was described 80 years ago by Otto Warburg. He discovered that tumors, although sufficient oxygen-concentrations are available, seem to rely mainly on glycolysis- rather than on respiration- to maintain their

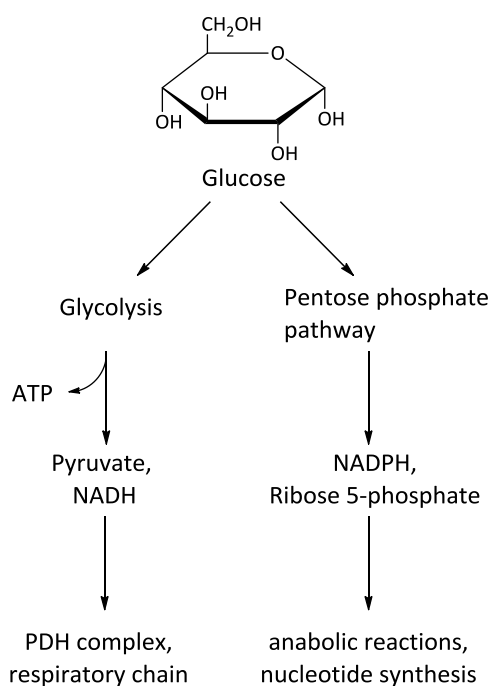


Figure 2: The conversion of glucose must be adjusted. It either serves for energy generation within glycolysis or NADPH/ nucleotide-synthesis within the PPP.

energy supply ^{11 12 13}. This kind of metabolic behavior was called "aerobic glycolysis". Why tumors do behave like this is still questionable. The more efficient production of ATP by respiration (~18 fold) ¹⁴ seems surprisingly not to be the favored way to generate energy by a lot of cancer entities. Within the last decades this aspect has been considered to be an alternative target for new antitumor-drugs ¹⁵. The favoured explanation for the use of "aerobic glycolysis" is that glycolysis is not primarily used for energy supply, but to produce molecules needed for cell division ¹⁶. Dividing cells have a high consumption of fatty acid-, amino acid- and nucleotide precursors. Moreover, the reducing equivalents in form of nicotinamide adenine dinucleotide

1. Introduction

phosphate (NADPH) are essential for certain anabolic reactions, forming these precursors. Therefore the cell has to adjust the fate of every glucose molecule in terms of either being used for energy supply in form of adenosine triphosphate (ATP) via glycolysis or as source for NADPH via the pentose phosphate pathway (PPP) (Figure 2). Malignant cells seem to adjust this described balance of glucose processing especially by inhibiting respiration and thereby increasing the availability of glucose for glycolysis and PPP especially¹⁶. Over the past years, more and more oncogenes as well as tumor-suppressor genes have been identified, affecting this balance by increasing the oxygen independent glucose metabolism. A set of proteins involved in this process are phosphoinositid-3 kinase/protein kinase B (PI3K/AKT), AMP-activated protein kinase/liver kinase B1 (AMPK/LKB1), p53 and MYC⁷ (Figure 3).

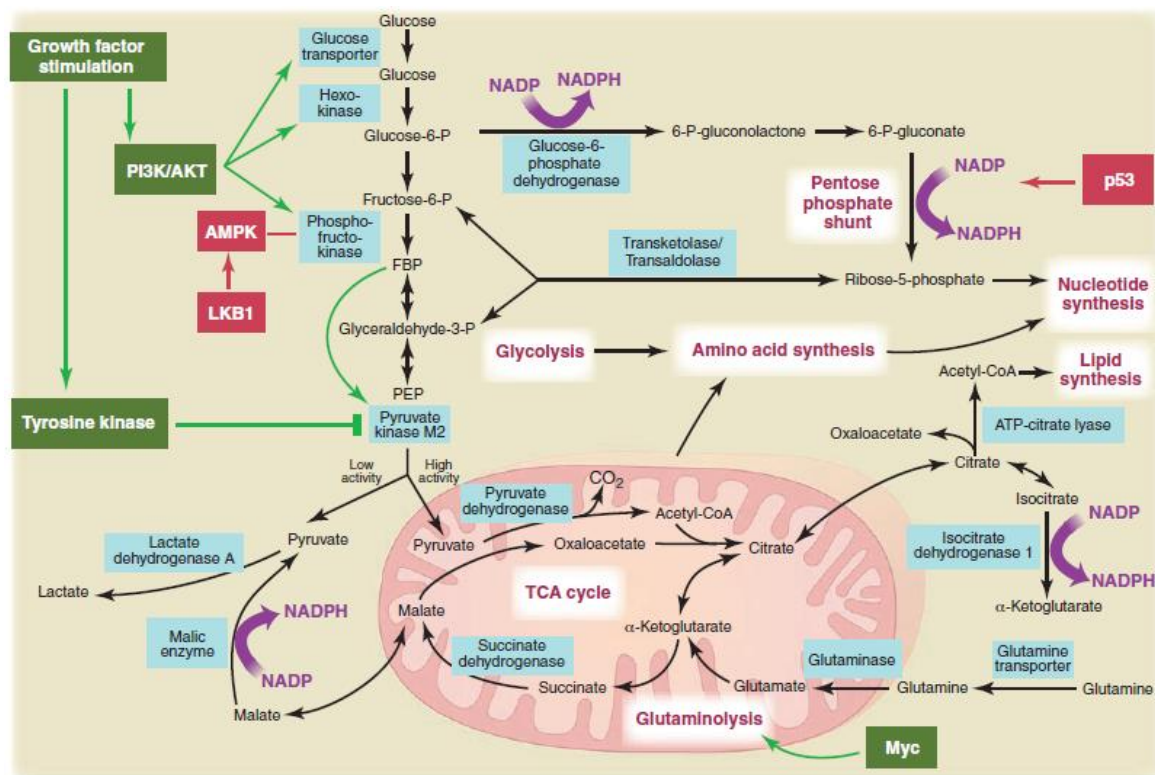


Figure 3: Metabolic adjustment by known oncogenes and tumor-suppressor genes. The scheme represents the known connection of oncogenes (green boxes) and tumor-suppressor genes (red boxes) to glycolysis, pentose phosphate pathway, oxidative phosphorylation and glutamine metabolism in proliferating cells. Adapted from Van der Heiden *et al.* 2009.

1. Introduction

PI3K is part of a signaling pathway being quite often affected in human cancers¹⁷. This pathway becomes permanently active by mutations in tumor-suppressor genes like the phosphatase tensin homolog protein (PTEN). One of the downstream targets of PI3K is AKT. Activation of AKT leads to several metabolic changes. It enhances glucose uptake by increasing the expression of glucose transporters (GLUT1) and by increasing the activity of hexokinase and phosphofructokinase the two enzymes catalyzing irreversible steps of glycolysis¹⁸.

AMPK is a crucial checkpoint for sensing low ATP concentrations. It inhibits glycolysis and cell proliferation and shifts towards a respiratory phenotype. Tumors must surpass this restriction to increase glucose-availability for glycolysis and PPP. This is caused by loss of the activity of the upstream tumor-suppressor gene LKB1, whose activity would otherwise lead to phosphorolytic activation of AMPK¹⁹.

Besides many other involvements in cancer development, p53 is also responsible for inhibiting glycolysis by an upregulation of the TP53-induced glycolysis and apoptosis regulator (TIGAR)²⁰. TIGAR decreases the levels of the glycolytic enzyme fructose-2, 6-bisphosphatase leading to downregulation of glycolysis. Moreover p53 induces expression of PTEN, a negative regulator of the PI3K pathway mentioned above. Thus, inactivation of p53-function leads to a switch towards a glycolytic phenotype in cancer²¹.

The oncogene MYC has, within its activity as transcription factor, a major role in the glutamine metabolism of proliferative cells. Glutamine is a critical supplemental factor of mammalian cells²². Besides this function MYC was also described to increase the expression of pyruvate kinase isoenzyme 2 (PKM2). Pyruvate kinase plays a pivotal role in glycolysis by transferring a phosphate group from phosphoenolpyruvate to adenosine diphosphate (ADP) leading to the production of ATP. PKM2 is a less active isoform and leads to a bottleneck within glycolysis, which increases the availability of glucose for the upstream localized PPP.

All these effects of known oncogenes and tumor-suppressor genes shift tumor cells towards an oxygen independent way of metabolism and are the events that lead to the deregulation of cellular energetics - one of the above mentioned hallmarks of cancer. It seems reasonable that this shift is not performed in terms of energy generation in form

1. Introduction

of ATP but more likely to increase the amount of glucose available for NADPH- and nucleotide-synthesis within the PPP.

1.2 Pentose phosphate pathway

The pentose phosphate pathway (PPP) (also termed hexose monophosphate shunt or phosphogluconate pathway) is responsible for the generation of NADPH, D-ribose 5-phosphate (R5P) and D-erythrose 4-phosphate (E4P). NADPH is required for anabolic reactions and to sustain a cell's redox state by donating reduction equivalents for glutathione production (glutathione is the most common used molecule for balancing a cell's redox-state)¹⁴. R5P serves as precursor for nucleotide synthesis whereas E4P is the starting point for aromatic amino acid synthesis in plants and some prokaryotes¹⁴. The PPP can be separated into an oxidative and a non-oxidative part (Figure 4). The oxidative part is initiated by the stepwise oxidation of D-glucose 6-phosphate (G6P). This irreversible step withdraws G6P from glycolysis and the fate of the glucose molecule is determined. In the next reaction 6-phosphogluconolactone is oxidatively decarboxylated which results in D-ribulose 5-phosphate formation. During this oxidation one mole D-glucose 6-phosphate leads to the production of 2 mole NADPH.

In the subsequent non-oxidative part of the PPP D-ribulose 5-phosphate is converted into either D-ribose 5-phosphate (R5P), by the activity of an isomerase, or D-xylulose 5-phosphate (X5P), by an epimerase. These two sugar phosphates now serve as substrates for the two enzymes transketolase (TKT) and transaldolase (TA), which are responsible for C₂- (TKT), or C₃- (TA) sugarphosphate fragment transfer. Starting from the two C₅ sugar phosphates the following products are formed: D-glyceraldehyde 3-phosphate (G3P), E4P, D-fructose 6-phosphate (F6P) and D-sedoheptulose 7-phosphate (S7P). As mentioned above the C₅ sugar phosphate R5P is used for nucleotide synthesis, whereas E4P serves as precursor for aromatic amino acid synthesis in plants and prokaryotes. G3P and F6P are incorporated into glycolysis vice versa, whereas S7P is an intermediate of the PPP only.

1. Introduction

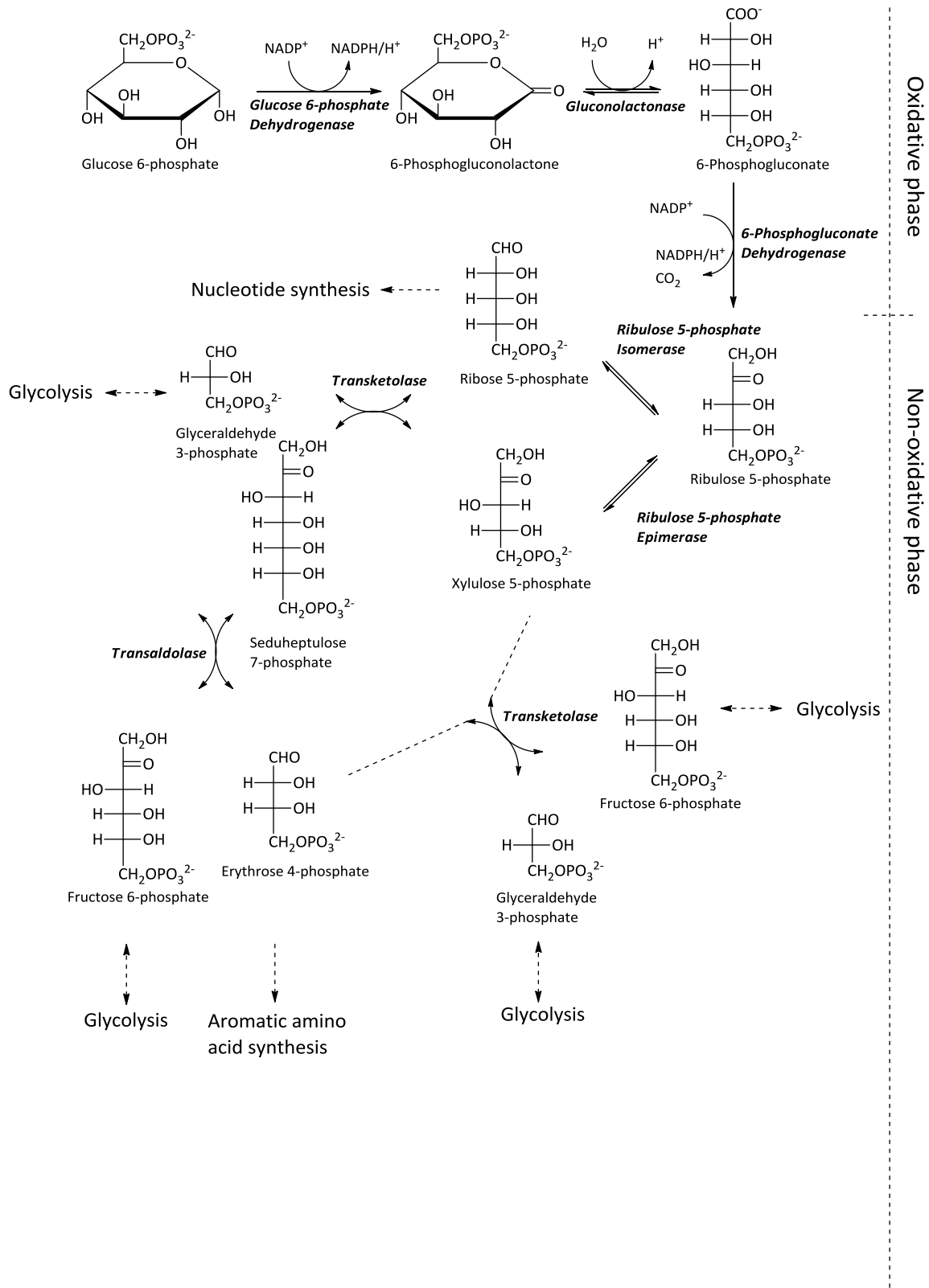


Figure 4: The pentose phosphate pathway. The oxidation of D-glucose 6-phosphate generates 2 mole of NADPH in the oxidative part of the PPP. The following non-oxidative reactions give rise to D-ribose 5-phosphate for nucleotide synthesis and D-erythrose 4-phosphate for aromatic amino acid synthesis. D-Fructose 6-phosphate and D-glyceraldehyde 3-phosphate represent connections to glycolysis.

1. Introduction

All cells can adjust the rate of glucose being metabolized either within glycolysis or the oxidative- or non-oxidative part of the PPP and recruit these metabolic pathways to serve their demands in terms of ATP-, NADPH-, aromatic amino acid- or nucleotide-synthesis¹⁶. In malignant cells this regulation seems to become decoupled in order to drive the generation of the above mentioned PPP products to a higher degree. The precursors are needed for the enhanced rate of cell division which reflects one of the above mentioned hallmarks of cancer. The two enzymes TA and TKT are indispensable for the non-oxidative part of the PPP and especially TKT and its isoforms were described to play a pivotal role in tumorigenesis.

1.3 Transketolase

1.3.1 Transketolase, general features and its contribution to human diseases

Transketolases (EC 2.2.1.1) are ubiquitously distributed enzymes and part of the PPP. They require thiamin diphosphate (ThDP), the biologically active form of vitamin B1, and bivalent cations for their catalytic activity^{23 24 25}. TKTs are involved in two metabolic pathways, namely the previously described PPP and the calvin-benson-bassham cycle of photosynthetic plants, where they are responsible for the regeneration of the CO₂ acceptor ribulose 1,5-bisphosphate¹⁴. Besides its well known metabolic function, TKT has been associated with a couple of diseases like diabetes, Alzheimer's disease, the neurological disorder Wernicke-Korsakoff syndrome and cancer^{26 27 28 29 30}. In case of cancer the impact of an altered TKT activity can be directly explained by its function within the PPP. It is assumed that up to 85 % of a cell's ribose, subsequently used for nucleotide synthesis, is produced by the PPP²⁸. Ribose is directly needed to fuel the cell division capacity of malignant cells, since it is the source of nucleotides and therefore for DNA replication. This circumstance makes TKT a promising target to inhibit uncontrolled cell division of tumor cells. In fact it was reported that inhibition of transketolase activity by ThDP analogs has a strong anti-proliferative effect on tumor cells^{31 32 33}.

1. Introduction

1.3.2 Structure of human transketolase

The structure of yeast TKT was first solved in 1992³⁴. In the following years structures of TKTs from all domains of life were determined. It has been shown that, although on the primary structure level the homogeneity of TKTs was not that striking, the quaternary structure of all investigated TKTs was strongly conserved³⁵. The structure of human TKT is shown below (Figure 5). Two kidney-formed monomers of transketolase form the active dimer of the enzyme. A monomer consists of an N-terminal pyrophosphate-domain, serving as an anchor for the pyrophosphate of the ThDP cofactor. In the center of the enzyme the pyrimidine-domain is located, responsible for binding the aminopyrimidine ring of the cofactor. The C-terminal domain was proposed to act as a nucleotide binding motif. However, biophysical characterizations do not underpin this assumption²⁵. The active centers of TKT are located at the subunit interface and amino acid residues of both monomer units contribute to its formation.

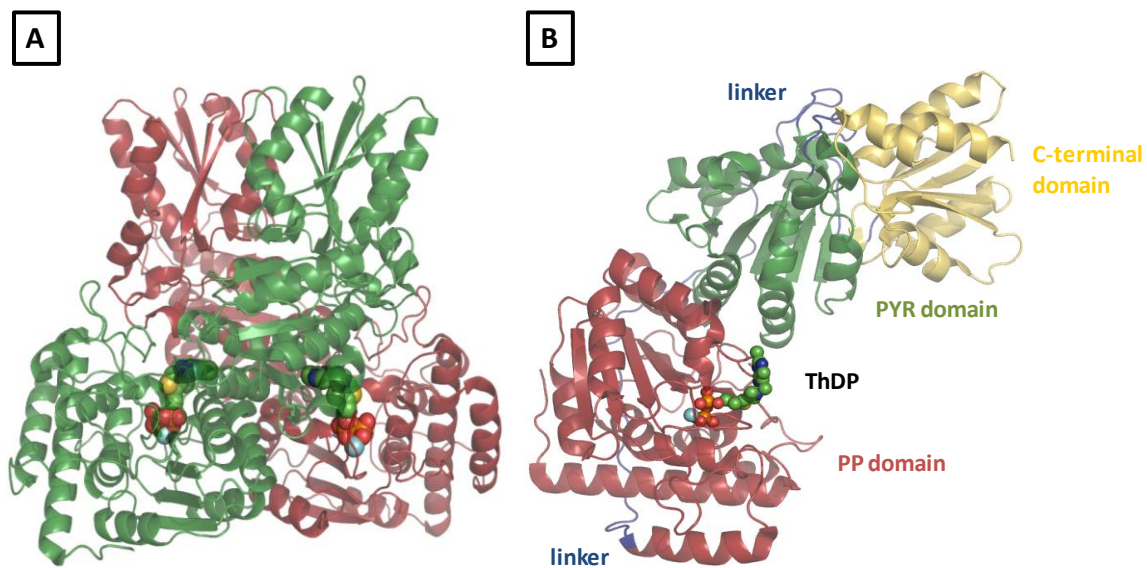


Figure 5: Structure of human transketolase. (A) Representation of the biologically active dimer of human transketolase. The monomers are colored in green and red, respectively. The cofactor ThDP and the bivalent calcium-cation (cyan) are depicted in ball representation. (B) Domain-structure of the human transketolase monomer. Shown are the PP-domain in red, the PYR-domain in green and the C-terminal domain in yellow. The two linker regions connecting the single domains are shown in blue (PDB file: **3MOS**). Adapted from Mitschke *et al.* 2010.

1. Introduction

1.3.3 Cofactor activation and reaction mechanism of transketoases

TKT catalysis requires ThDP and bivalent cations as cofactors. ThDP belongs to the yet best characterized cofactors^{36 37 38}. Its unique structure and chemical properties allow enzymes to perform a set of diverse reactions³⁹. Among those reactions the formation of carbon-carbon bonds, as it can be found in TKTs, belongs to the most sophisticated ones.

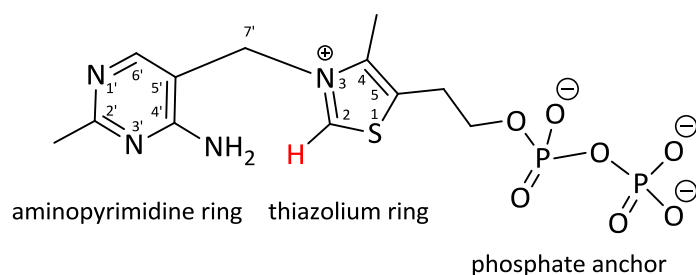


Figure 6: Structure of thiamin diphosphate.

Although the structure of ThDP is known since the 30's of the last century⁴⁰ it took until 1957 when Breslow identified the C2 carbon atom of the thiazolium ring as the critical factor for covalent catalysis^{41 42} (Figure 6). In the Breslow-mechanism the C2 of ThDP becomes activated by abstraction of its proton, leading to an active ylid which is necessary for ThDP-reactivity. In solution this Umpolung called reaction occurs in a negligible amount of ThDP molecules due to the low acidity of the C2 proton (pKa ~17-19)^{43 44}. In ThDP dependent enzymes the cofactor becomes orientated in such a way that the N4' of the aminopyrimidine ring and the C2 of the thiazolium ring are located in close vicinity (V-conformation)⁴⁵. This fact as well as the charge delocalization in the thiazolium part of the cofactor increases the proton abstraction at the C2 by the factor of 10^5 ^{46 47}.

Equilibria of tautomeric and ionized states of the aminopyrimidine ring of the cofactor have been describes as characteristic feature of enzyme-bound ThDP mediated catalysis^{37 48}. In almost all ThDP-enzymes the first step of ThDP-activation starts with protonation of the 4'-aminopyrimidene (AP) form of the cofactor by a conserved glutamate residue (Figure 7). This gives rise to the so called 4'-aminopyrimidinium form (APH⁺) of the cofactor. After deprotonation of the APH⁺ form at the N4' of the

1. Introduction

aminopyrimidinium ring the 1',4'-iminopyrimidine form (IP) is generated. These steps facilitate proton abstraction at the C2 of the thiazolium ring, which gives rise to the activated Ylid⁴⁹.

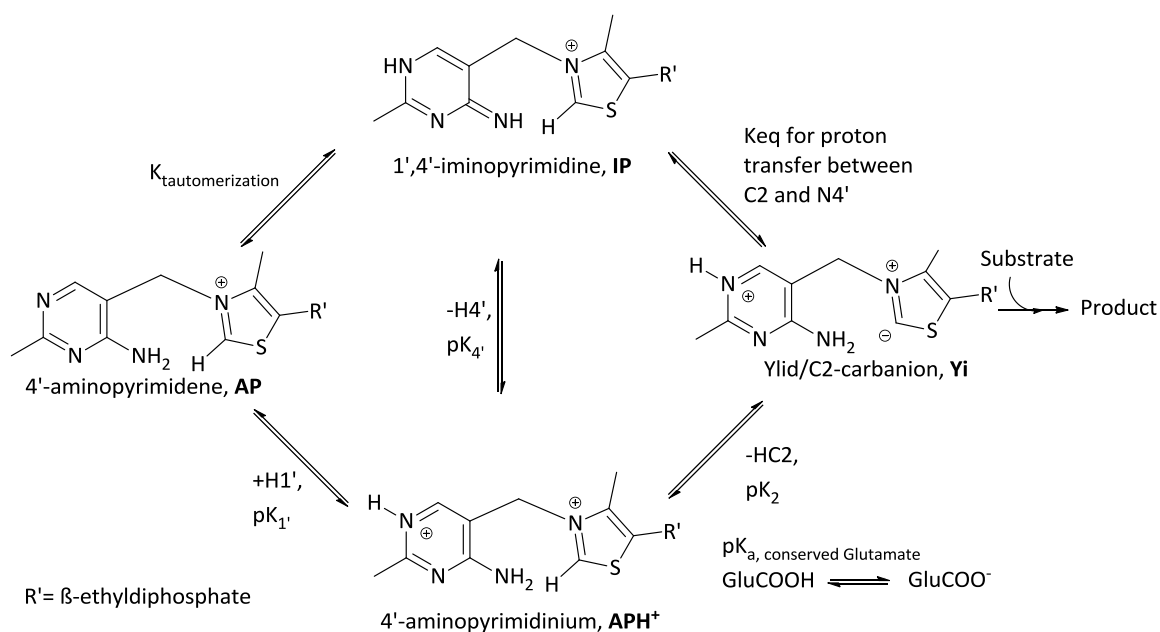


Figure 7: Tautomeric and ionization equilibria of ThDP prior to substrate addition. Adapted from Nemeria *et al.* (2007)

By using circular dichroism spectroscopy, different absorption spectra have been assigned to the tautomeric states of the cofactor. The AP form shows a negative absorption in the range of ~320-330 nm whereas the IP form gives rise to a positive signal between 300-310 nm. The APH⁺ signal has so far been described as spectroscopically silent⁴⁹.

In transketolases the activation of the ThDP occurs as described above leading to the activated ylid. After this activation a set of reversible reactions is initiated, beginning with the nucleophilic attack of the C2 of the thiazolium at the carbonyl function of the substrate (donor ketose), leading to the covalent ThDP adduct (Figure 8). Elimination of the first product (aldose phosphate) occurs after protonation of the 3'OH group of the intermediate, followed by a heterolytic bond cleavage of the C2 α -C3 α bond. This gives rise to the cofactor intermediate dihydroxy ethylthiamin diphosphate (DhETHDP). This

1. Introduction

intermediate is now able to react with the second substrate in a nucleophilic manner (acceptor aldose) leading to the second product of this reaction cycle⁵⁰.

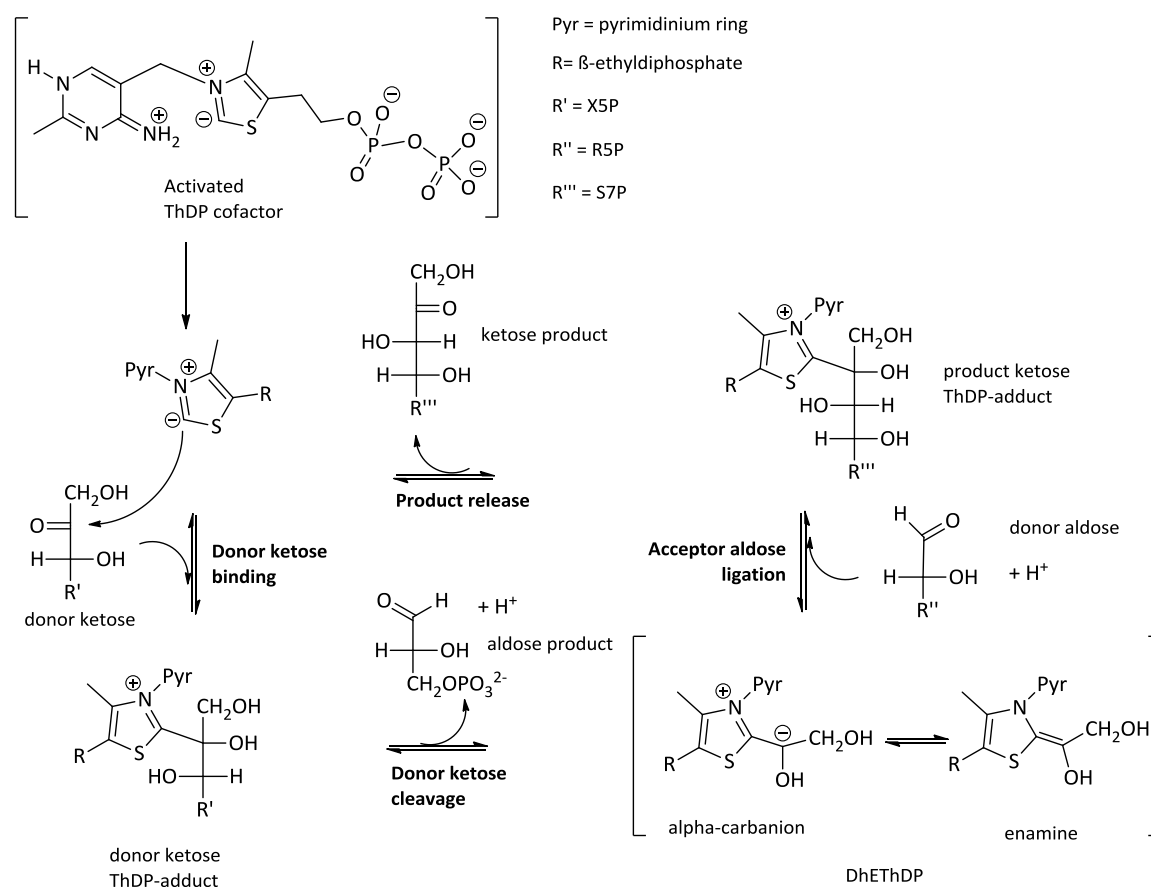


Figure 8: Reaction cycle of TKTs. The activated ThDP cofactor attacks the carbonyl function of a donor ketose in a nucleophilic manner which gives rise to the donor ketose ThDP-adduct. After release of the first product (aldose) the DhETHDP-intermediate is formed. This intermediate now attacks in a similar way an acceptor aldose which leads to the second product (ketose).

Besides this well understood reaction cycle of TKT it was recently shown that TKT can serve to elucidate the general assumption of enzymes to act as transition state stabilizers in more detail. High resolution crystal structures of human TKT revealed a distortion of the covalent bond between the substrate and the cofactor besides an elongated scissile C2 α -C3 α bond mentioned above within the substrate⁵¹. The unique overall structure of TKT seems to keep this transition state intermediate at a higher level of energy, preventing it from relaxing to its lowest energy state and facilitating catalysis.

1. Introduction

1.4 The TKT isoforms Transketolase-like protein 1 and 2

1.4.1 Structural similarities of TKT, TKTL1 and 2

TKTs have a central role in the primary glucose metabolism and seem also to be a critical determinant for driving a tumor's metabolism in terms of precursor generation for anabolic reactions. Moreover in the human genome two isoenzymes were discovered, namely transketolase-like protein 1 and 2 (TKTL1, TKTL2). Especially for TKTL1 a critical role in tumorigenesis has been proposed^{52 53}.

The sequence identity on the genome level between TKTL1 and TKT is 69 % whereas the identity of TKTL2 to TKT is 71 %⁵⁴. For several cancer entities such as breast cancer⁵⁵, glioblastoma⁵⁶ and cervix carcinoma⁵⁷ an increased expression of TKTL1 on the mRNA and protein level has been described. Besides it was demonstrated that an elevated expression rate of TKTL1 directly correlates with a lowered over time survival of patients suffering from cancer. Coy and coworkers hypothesized TKTL1 to be a crucial determinant in the aggressiveness of all in this regard investigated cancers. Contrary, no informations of the biological function of TKTL2 have been published so far.

The comparison of the amino acid sequence of TKT and TKTL1 results in an exon deletion observed in TKTL1, leading to the loss of 38 amino acids within the protein (Figure 9). Several residues that are inherently conserved amongst all so far investigated TKTs are located in the deleted part³⁵. One of the deleted residues corresponds to histidine 103 in yeast, whose exchange against alanine was reported to increase a one substrate reaction of TKT with X5P as substrate in the yeast homolog⁵⁸. Coy *et al.* reported a comparable one substrate reaction with TKTL1 and X5P as substrate, leading to the formation of G3P and a C2-fragment of unknown identity⁵³. This reaction is believed to follow a similar mechanism as it was described for phosphoketolases of heterofermentative lactic acid bacteria and *Bifidobacteria*⁵⁹. However the difference of TKT and TKTL1 is more dramatic than the exchange of this single amino acid. In total nine inherently conserved amino acids are exchanged or are totally missing in TKTL1 (Figure 9). Besides six invariant residues in the deleted 38 amino acid sequence (Gly 76, His 77, Tyr 83, Gly 90, His 110 and Pro 111), Ser 74, Gly 152 and Pro 426 are also exchanged. The exchange of glycine 152 against serine can be considered as most dramatic, since the affected GDG-motif is responsible for formation of the ThDP binding

1. Introduction

motif which is crucial for all ThDP-enzymes⁶⁰. These changes challenge the assumption, that TKTL1 can bind ThDP as cofactor and fulfill ThDP-dependent chemistry.

However, the authors assume that TKTL1 connects the PPP and the degradation of glucose in a way allowing tumors to drive lipid synthesis without the need of the citric acid cycle. The C2 fragment of unknown identity was assumed to be acetyl Coenzyme A, which can be further used to fuel lipid synthesis. Based on this activity the authors declare TKTL1 to be a crucial factor for the establishment of an aerobic glycolytic phenotype in cancer. Several studies have been published connecting an increased expression of TKTL1 on the mRNA- and protein-level to tumorigenesis⁵³.

1. Introduction

1.4.2 TKTL1 and tumorigenesis

Several physical and biochemical characteristics of different cancers and cancer derived cell lines have been associated with an increased TKTL1. In the following section a short synopsis is given, summarizing the most striking results on which metabolic changes have been correlated to an overexpression of TKTL1 in malignant cells.

- siRNA mediated suppression of TKTL1 in a colon carcinoma cell line (HCT-116) leads to a slower cell growth, a lowered glucose consumption and lactate production as well as an increased sensitivity to reactive oxygen species⁶¹
- comparable results were found for a cervical derived cell line (HeLa) and a gastric adenocarcinoma cell line (AGS cells), in which the total TKT activity was also affected^{57 62}
- TKTL1 expression was described to correlate with a higher rate of metastasis formation in histopathological thyroid and ovarian carcinoma samples^{63 64}
- in surgically removed breast cancer specimens an activation/upregulation of AKT and GLUT1 was correlated to an increased expression of TKTL1⁶⁵
- another group detected a correlation between TKTL1 and lactate dehydrogenase 5 expression in non-small lung cancer tissue samples, which contributes to the establishment of a fermentative phenotype of cancer⁶⁶
- a study of cervical carcinoma in terms of TKTL1 and phosphorylated AKT expression showed an increase of expression for both proteins, connected to a higher histopathological grade of the cervical tissue⁶⁷
- in a murine model TKTL1 was found to play a role in adjusting the downstream balance of the PPP, resulting in the production of anti inflammatory molecules by NADPH⁶⁸
- in 2012 Wanka *et al.* reported that TKTL1 seems to be a downstream target of the TP53 induced glycolysis and apoptosis regulator (TIGAR) in glioblastoma derived cell lines; inhibition of TKTL1 by siRNA reversed the protective effects of TIGAR in face of oxygen and glucose restriction⁶⁹

1. Introduction

Taken together these results indicate TKTL1 to be important for driving a tumors metabolism towards a more active glycolysis and PPP and thereby leading to independence from oxygen supply. Therefore it seems reasonable to assume that TKTL1 plays a crucial role for the production of R5P and NADPH by serving the tumors needs of these biomolecules for anabolic reactions and defense against reactive oxygen species. How TKTL1 overexpression contributes to the observed effects is still under investigation but recent results indicate an involvement of TKTL1 in the stabilization of the hypoxia inducible factor 1 α (Hif1 α).

1.4.3 TKTL1 putatively contributes to tumorigenesis by Hif1 α stabilization

Sun and coworkers showed that expression of TKTL1 on the mRNA and protein level is driven by promoter hypomethylation in head and neck squamous cell carcinoma (HNSCC) cell lines O11, O28 and 22A⁷⁰. In a previous study the same group reported TKTL1 overexpression in HNSCC cell lines FaDu and UM22B to have proliferative effects, whereas a knockdown of TKTL1 reversed this outcome⁷¹. In the recent study Sun *et al.* could show that TKTL1 overexpression leads to an increase of F6P and G3P production (both products of the PPP and glycolysis). Production of pyruvate, lactate and ATP was also raised, as well as glucose consumption. Some of these metabolic effects have been described earlier for a colon carcinoma cell line, as mentioned above (HCT-116)⁶¹. The authors furthermore investigated, whether the hypoxia inducible transcription factor 1 α (Hif1 α) is affected by the elevated levels of the mentioned metabolites, as it was already described in an earlier study⁷².

Hif1 is an oxygen-sensitive transcription factor, adjusting a cells adaptation to changing oxygen availability⁷³. It is a heterodimer consisting of a Hif1 α and a Hif1 β monomer. Hif1 α is localized in the cytosol, whereas Hif1 β is located in the nucleus. Under normoxic conditions the constitutively expressed Hif1 α becomes hydroxylated at distinct proline residues by the activity of prolyl-hydroxylases. The marked Hif1 α is now prone to degradation by the proteasom. If the cell faces oxygen restriction Hif1 α is accumulated in the cytosol by inhibition of the prolyl-hydroxylase activity (PHD) and is being translocated into the nucleus. Here it forms, together with Hif1 β , the active transcription factor Hif, leading to downstream activation of several target genes. On the one hand

1. Introduction

these genes are responsible for recruiting new blood vessels, to stimulate oxygen supply of the tumor (angiogenesis). On the other hand they also stimulate cell proliferation to escape the hypoxic environment. The last adaption of Hif1 leads to an increase of expression of glycolytic enzymes and glucose transporters which switches the metabolism towards oxygen independent glycolysis and PPP ⁷⁴. Indeed, Sun *et al.* could show that Hif1 α is stabilized even in the presence of ample oxygen concentrations. This leads to an activation of several Hif-downstream targets like hexokinase 2, aldolase and phosphoglycerate kinase, crucial enzymes of glycolysis. This stabilization of Hif1 α by TKTL1 even in the presence of oxygen seems to be a reasonable explanation how TKTL1 promotes aerobic glycolysis in cancer and increases the rate of glycolysis and PPP (Figure 10).

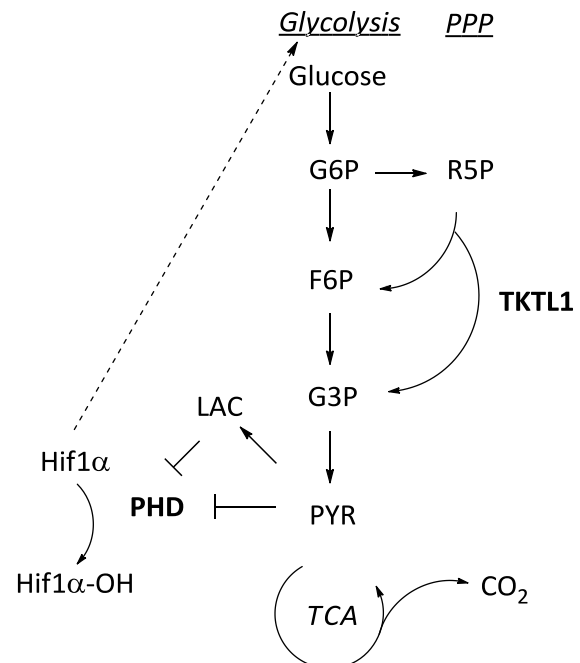


Figure 10: The proposed mechanism of TKTL1-driven stabilization of Hif1 α . Adapted from Sun *et al.* (2010).

1.4.4 The role of TKTL1 is contradictory

The concept of TKTL1 promoted tumorigenesis leading to higher rates of metastasis formation and lowered over time survival of patients by the described mechanisms is not accepted by all scientists. There are well-founded doubts about the concept of a glycolytic phenotype established by TKTL1 ⁷⁵. The main argument of these scientists is the unspecificity of the antibody used for detection of TKTL1 in surgically removed specimens and western blots. This antibody was generated by Coy and coworkers in 2005 (JFC12T10) and is used for most studies dealing with TKTL1 expression analysis since then ⁵³. Mayer *et al.* performed a set of experiments aiming to detect TKTL1 on the mRNA (by qRT-PCR) as well as on the protein level (by western blotting and histopathological immunostaining). For western blot analysis different cell lysate fractions were generated from HeLa and MCF-7 cells. By blotting the lysate and

1. Introduction

subsequent exposure to the JFC12T10 the blots gave rise to a set of bands between 44 to 95 kDa that could not be explained. Besides the western blot analysis Mayer *et al.* performed qRT-PCR of six different cell lines (HeLa, MCF-7, A549, HT1080, M21 and TF-1). In none of the end-point RT-PCR analysis a significant overexpression of TKTL1 could be detected in comparison to TKT.

The nonspecific behavior of the antibody was also reported by another group ⁷⁶. Hartmannsberger *et al.* detected several protein bands of varying size from 40-78 kDa in western blot applications of different cell lines (PCI-1/13, FaDu, HeLa, THP-1, SkBr3, HCT-8) by use of the JFC12T10 antibody. Significant TKTL1 expression could only be detected in a HEK293 cell which was transfected with a TKTL1 construct and in THP-1 cells ⁷⁶. siRNA mediated knock down led to a decrease in one of the detected bands (65 kDa), but the other bands were unaffected. These bands might represent alternative splice variants of TKTL1, missing the target sequence of the siRNA. However it is more likely that the bands between 40 and 78 kDa correspond to unspecific stained proteins. Derived from these inconsistencies immunohistochemical stainings and deduced expression strengths of TKTL1 in the corresponding tumor tissue samples have to be interpreted with caution if the mentioned antibody is used.

Despite the questionable specificity of the TKTL1 antibody (JFC12T10) and rather reproducible qRT-PCR analysis TKTL1 is believed to have an effect on tumorigenesis as outlined previously by stabilizing Hif1 α . But whether TKTL1 leads to the observed effects caused by an enzymatic activity of TKTL1 itself or by increasing the activity of other metabolic enzymes is still not clear. As mentioned above TKTL1 is proposed to perform a reaction similar to the X5P cleavage reaction of phosphoketolases ⁵³.

1.5 Phosphoketolase

1.5.1 Phosphoketolase of *Bifidobacteria*

Phosphoketolases are the central metabolic enzyme of heterofermentative lactic acid bacteria and *Bifidobacteria* ⁵⁹. Phosphoketolases of heterofermentative lactic acid bacteria use X5P solely as substrate. Therefore they are termed xylulose 5-phosphate phosphoketolase (XPK) (E4.1.2.9). XPK are responsible for cleaving X5P into G3P (a

1. Introduction

glycolysis intermediate) and acetyl phosphate, a compound further used for ATP production.

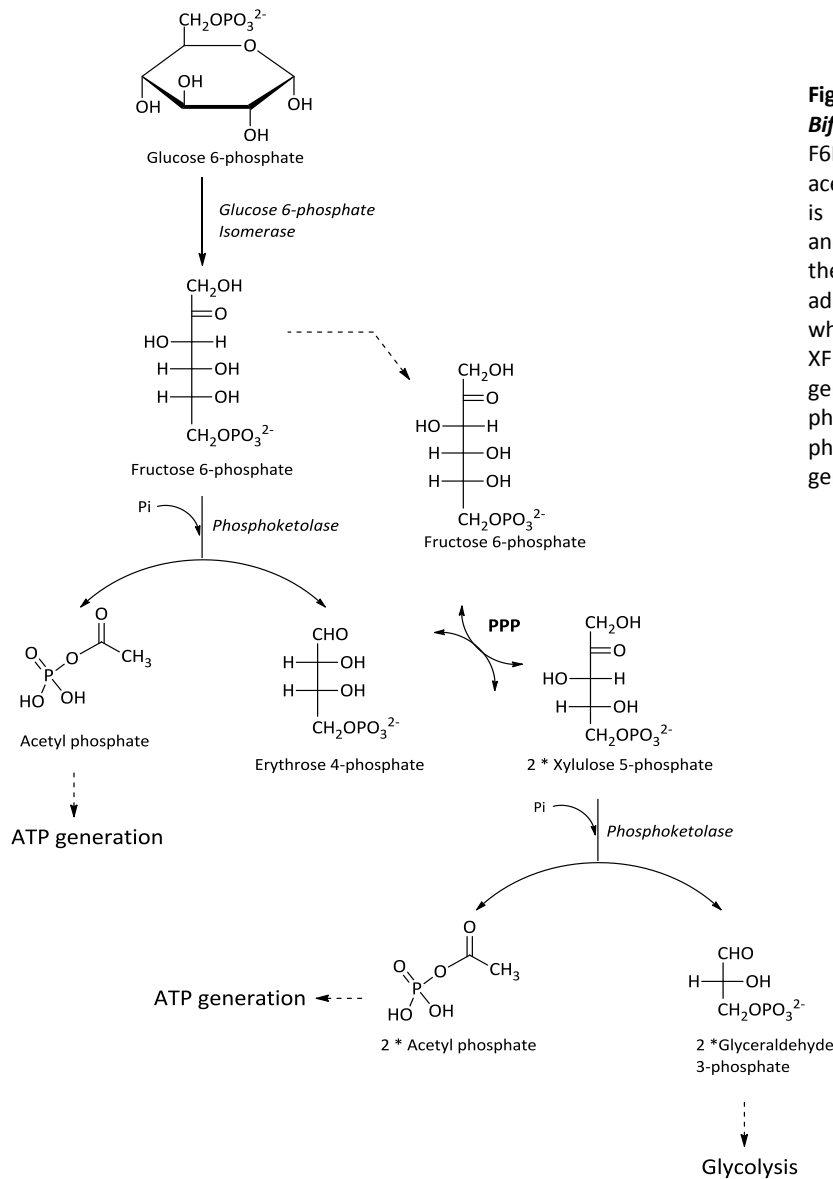


Figure 11: The bifid shunt of *Bifidobacteria*. G6P derived F6P is cleaved by XFPK into acetyl phosphate and E4P. E4P is cycled, together with another F6P molecule, through the PPP, giving rise to two additional X5P molecules which are also cleaved by XFPK. This final cleavage generates another acetyl phosphate and G3P. Acetyl phosphate is utilized for ATP generation.

In *Bifidobacteria* phosphoketolases are able to use X5P as well as F6P as substrates and are therefore termed xylulose 5-phosphate/fructose 6-phosphate phosphoketolases (XFPK) (EC 4.1.2.22). In the so called bifid shunt of *Bifidobacteria* XFPK is the main metabolic enzyme (Figure 11). Here XFPK cleaves F6P into E4P and acetyl phosphate. Acetyl phosphate is used for ATP generation. E4P instead is, together with another F6P molecule, cycled through the PPP leading to formation of two molecules X5P, which are

1. Introduction

finally also processed by XFPK. This leads to the generation of two additional acetyl phosphate molecule and G3P which fuels glycolysis in an above described manner.

1.5.2 Structure of XFPK from *Bifidobacterium breve*

Although already described since the 1950's⁷⁷ as active in several procaryotic and eukaryotic specimens, little was known about the enzymatic and structural properties of phosphoketolases until recently. In 2010 the structures of XFPK from *Bifidobacterium longum* and *B. breve* were published, revealing some structural properties of this enzyme^{78 79 80}. Since XFPK and TKT are both ThDP-dependent enzymes acting on the same set of substrates (X5P, F6P), XFPK was thought to share some structural similarities with TKT. And indeed the solved structure of XFPK revealed a high degree of similarity to TKT. As it was observed for TKT, two kidney-shaped monomers contribute to the formation of the biologically active dimer of XFPK (Figure 12)^{78 80}. XFPK consists of three domains which can be assigned comparable to TKT. The N-terminal PP-domain is responsible for binding of the pyrophosphate-portion of the ThDP-cofactor, whereas the PYR-domain interacts with the aminopyrimidine ring of ThDP. The C-terminal has so far no described function.

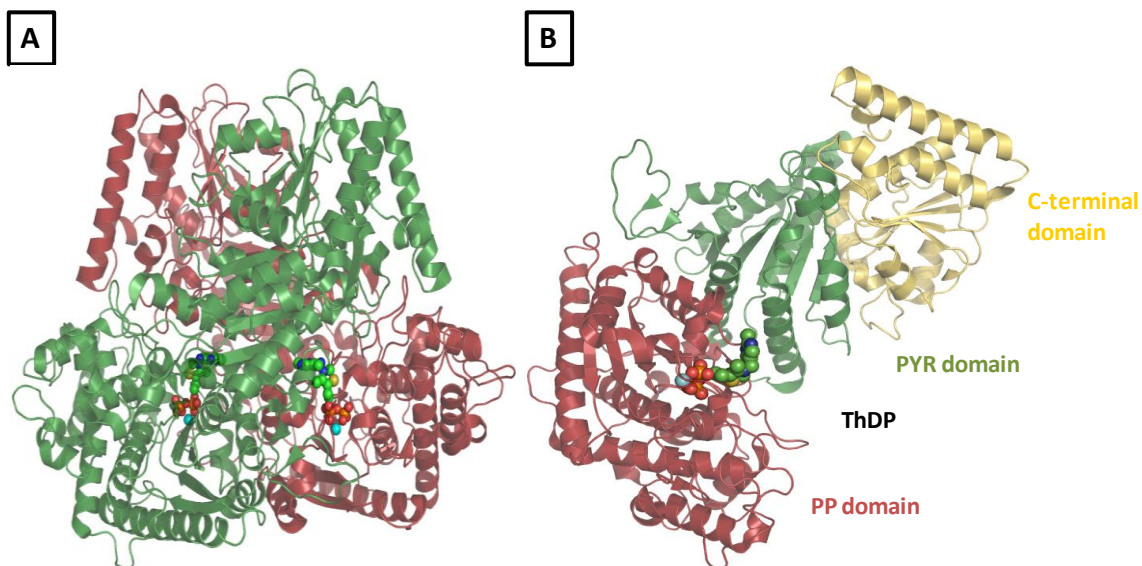


Figure 12: Structure of *B. breve* XFPK. A) Representation of the biologically active dimer of *BbXFPK*. The monomers are colored in green and red, respectively. The cofactor ThDP as well as the bivalent magnesium-cation (cyan) is depicted in ball representation. B) Domain-structure of the *BbXFPK* monomer. Shown are the PP-domain in red, the PYR-domain in green and the C-terminal domain in yellow (PDB file: **3AHC**). Adapted from Suzuki *et al.* 2010.

1. Introduction

The active centers of the two monomers are located at the interface and several amino acid residues of both monomer subunits contribute to the construction of the active centers.

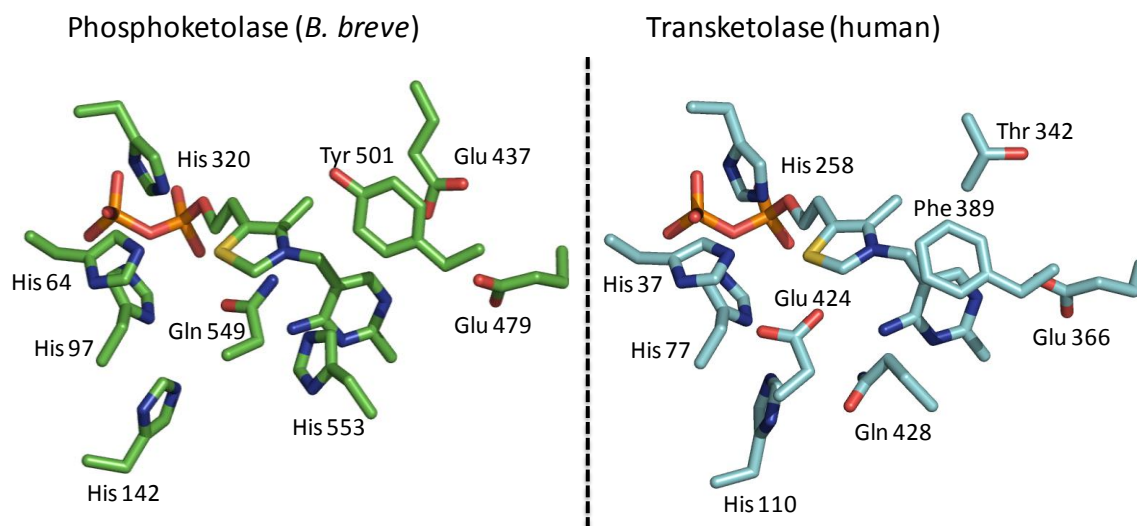


Figure 13: The active centers of XFPK from *B. breve* and human TKT. Most of the residues are conserved except those that are responsible for binding of the second substrate (phosphate) in XFPK (Gln 549, Glu 437 and Tyr 501). Gln 428 is a human transketolase specific exchange. The corresponding His 553 in XFPK is conserved among all other TKTs.

As shown above (Figure 13) the active centers of human TKT and XFPK from *B. breve* share a high degree of similarity. The four histidines (His 64/37, His 97/77, His 142/110 and His 320/258) are conserved. Besides, the replacement of histidine 553 against glutamine 428 is a human transketolase specific change. In all TKTs from other organisms this histidine is conserved³⁵. In XFPK these histidine residues are important for the single catalytic steps by acting as acid/base catalysts as it will be discussed later. Asparagine 549 and tyrosine 501 are part of the phosphate binding site and are therefore specific for XFPKs as TKTs do not act on inorganic phosphate as substrate. A very interesting exchange can be found in close vicinity to the aminopyrimidine portion of the ThDP cofactor. Threonine 342 is exchanged against glutamate 437 in XFPKs. This charged residue might affect the tautomerization/charge equilibria of the cofactor as described above and might be an explanation for the different catalytic activity of XFPKs in comparison to TKTs (carbolyase versus carbolygase).

1.5.3 Reaction mechanism of XFPK

The consistence of TKT and XFPK on the structural level is also reflected in the reaction both enzymes catalyze. In case of XFPK a donor ketose (X5P or F6P) is attacked at its carbonyl function in a nucleophilic manner, resulting in the ketose-ThDP adduct. After aldose cleavage DhEThDP is formed. Histidine 64 and histidine 320 are believed to be involved in the first catalytic step by protonating the donor-sugar at the 3'-OH leading to the first product (G3P) and intermediate (DhEThDP)⁸⁰. At this point the reaction steps catalyzed by TKT and XFPK diverge. TKT ligates the C2-fragment to an acceptor aldose, leading to the formation of the second sugar-phosphate product. In XFPK, on the contrary, water elimination occurs. In this model histidines 97, 142 and 553 are supposed to be responsible for protonation of DhEThDP which leads to water elimination and formation of the second intermediate (enolAcThDP). After tautomerization of the enolAcThDP the ketoAcThDP intermediate is formed which is believed to be attacked by inorganic phosphate in a nucleophilic manner, yielding acetyl phosphate as a final product (Figure 14). According to Yevenes and Frey, water-elimination and tautomerization are irreversible steps in XFPK-driven catalysis⁸¹.

1. Introduction

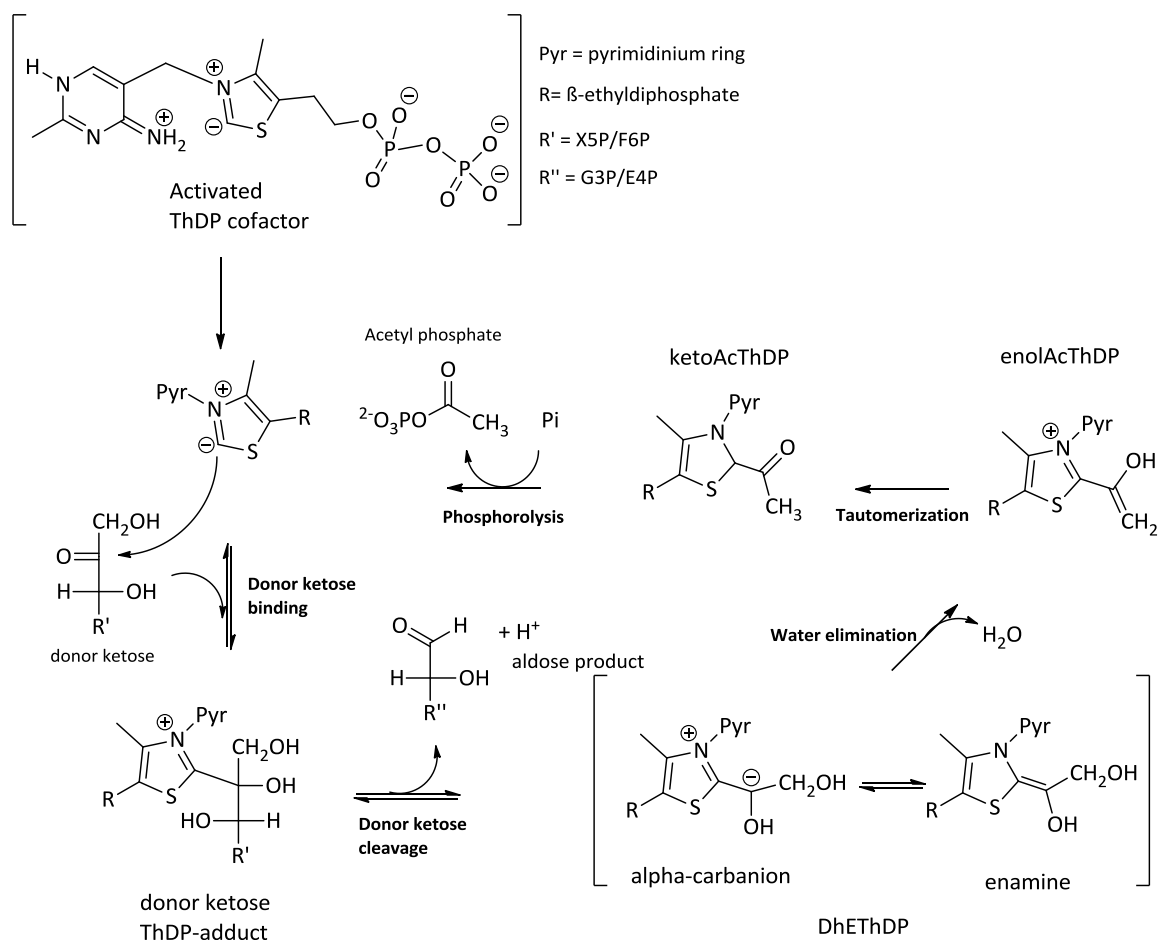


Figure 14: Reaction cycle of XFPK. The activated ThDP cofactor attacks the carbonyl function of a donor ketose in a nucleophilic manner, which gives rise to the donor ketose ThDP-adduct. After release of the first product (aldose) the DhETHDP-intermediate is formed. Subsequently a water-elimination takes place leading to the enolAcThDP intermediate. After tautomerization the ketoAcThDP is assumed to be attacked in a nucleophilic manner by inorganic phosphate leading to the product acetyl phosphate. Adapted from Yevenes and Frey (2008).

It is still unclear if acetyl thiamin diphosphate (AcThDP) is indeed an intermediate occurring during XFPK mediated catalysis, or if water-elimination and nucleophilic attack of phosphate occur in a concerted mechanism. The latter seems more likely since phosphate was shown to be a nucleophile too weak to attack AcThDP diphosphate in aqueous solution⁸². The reaction with water is much more preferred (0.2 s^{-1}) which results in formation of acetate⁸³. In XFPK this reaction must be suppressed as it was shown for pyruvate oxidase (POX) of *Lactobacillus plantarum*, another phosphate using enzyme, where hydrolysis of the formed AcThDP occurs with 0.03 s^{-1} ⁸⁴. Moreover pyruvate processing in POX leads to the stepwise transfer of two electrons from the formed hydroxymethyl thiamine diphosphate intermediate (HeThDP) to a flavin cofactor. Within this stepwise oxidation of HeThDP a radical transition state is formed,

1. Introduction

which is nucleophilic attacked by phosphate, coupled to the transfer of the second electron⁸⁵. By this concerted mechanism the low nucleophilicity of the phosphate can be overcome, leading to the formation of acetyl phosphate. However in XFPK no such mechanism has been described.

It is also possible that the second substrate, phosphate, plays a more sophisticated role in the catalytic model of XFPK. Besides for several enzymes a mechanism is proposed in which a phosphate-containing substrate acts as acid/base catalyst, or anchor of a water molecule. This was shown for serine proteases, GTPases and type II restriction endonucleases⁸⁶. Although such results were deduced from structural data and model system based approaches, it is imaginable that in case of XFPK phosphate acts as catalyst and facilitates tautomerization of the enolAcThDP to the ketoAcThDP.

1.6 Motivation

Cancer is a disease caused by stepwise genetic alterations in non-cancerogenous cells. Most of these alterations affect genes of signaltransduction cascades, transcriptionfactors or cell cycle control proteins. Additionally, over the recent years more and more evidences have been found that alterations in metabolic enzymes seem to play an important role in cancer development too. Such alterations include mutations in metabolic enzymes itself, an adjustment of their transcription-rate or an altered catalytic activity. Of great interest is the pentosephosphate pathway (PPP) since it is the main source of nucleotides and reductive equivalents, making it indispensable for cell division and anabolic reactions. In the PPP the two enzymes transketolase (TKT) and transaldolase (TA) are in the focus of research. Inhibition of TKT was shown to have inhibitory growth-effects on malignant cells. Besides a TKT isoenzyme has been discovered which seems to cover the question of an altered PPP-activity in malignant cells. This transketolase-like protein 1 (TKTL1) was shown to be overexpressed on the mRNA- as well as on the protein-level in several cancer entities. Moreover, its increased expression rate seems to correlate with the overall survival of patients suffering from cancer. How TKTL1 is influencing this process is still under investigation but the most accepted model suggests TKTL1 to have a catalytic activity which connects the PPP with

1. Introduction

other metabolic pathways like the synthesis of lipids and increases the overall flux through the PPP itself.

Since the proposed catalytic function of TKTL1 has not been elucidated in detail it was the aim of this thesis to address this question. For that purpose TKTL1 was recombinantly expressed and analyzed by spectroscopic methods. Furthermore two model systems were established to elucidate the putative functions of TKTL1 in a comparative manner. The first alternative system is a deletion variant of native human TKT, lacking 38 amino acids that are missing in TKTL1. By spectroscopic methods and an enzymatic assay the question was addressed if the missing 38 amino acid residues are important for cofactor binding and catalysis. The second model system was the phosphoketolase of *Bifidobacterium breve* whose structure was recently published. By comparing structural information as well as spectroscopic analysis of the proposed reaction mechanism it served to be compared to a putative TKTL1 mediated reaction.

2 Material and methods

All molecular and microbiological methods were performed, if not mentioned otherwise, as described in *Current Protocols in Molecular Biology*⁸⁷. For all described molecular biological methods heat-sterilized glass envelopes (3 h at 180 °C) as well as sterile plastic articles were used. For media, buffers and solutions double-distilled water (ddH₂O) was used and autoclaved if required (121 °C, 20 min). Heat-labile solutions were sterilized by filtering (0.22 µm pore size).

2.1 Materials

All chemicals were purchased from Sigma-Aldrich (Munich, Germany), Carl Roth GmbH & Co. KG (Karlsruhe, Germany) or AppliChem GmbH (Darmstadt, Germany), if not stated otherwise.

Acetic acid	Carl Roth GmbH & Co. KG (Karlsruhe, Germany)
Acetyl coenzyme A, sodium salt	Sigma-Aldrich (Munich, Germany)
Acetyl phosphate	Carl Roth GmbH & Co. KG (Karlsruhe, Germany)
Acrylamide	Carl Roth GmbH & Co. KG (Karlsruhe, Germany)
Agar	AppliChem GmbH (Darmstadt, Germany)
Agarose	AppliChem GmbH (Darmstadt, Germany)
Ammonium chloride	Carl Roth GmbH & Co. KG (Karlsruhe, Germany)
Antifoam 204	Sigma-Aldrich (Munich, Germany)
Phenylmethylsulfonyl fluoride (PMSF)	AppliChem GmbH (Darmstadt, Germany)
2-(Bis(2-hydroxyethyl)amino)acetic acid (BICINE)	AppliChem GmbH (Darmstadt, Germany)
Calcium chloride hexahydrate	Carl Roth GmbH & Co. KG (Karlsruhe, Germany)

2. Material and methods

Carbenicillin	AppliChem GmbH (Darmstadt, Germany)
Coenzyme A hydrate	Sigma-Aldrich (Munich, Germany)
Coomassie Brilliant Blue G250	AppliChem GmbH (Darmstadt, Germany)
Cover plates, 18 mm (siliconized)	Jena Bioscience GmbH, (Jena, Germany)
Cryoloops (0.05 – 0.1 mm)	Hampton Research Corp, (CA, USA)
Crystallization plates, greased	Hampton Research Corp, (CA, USA)
Deuterium oxide 99.9%	Sigma-Aldrich (Munich, Germany)
Dimethylsulfoxide (DMSO)	Sigma-Aldrich (Munich, Germany)
Ethylenediaminetetraaceticacid (EDTA)	AppliChem GmbH (Darmstadt, Germany)
Ethanol (denatured)	Carl Roth GmbH & Co. KG (Karlsruhe, Germany)
Ethanol (purest)	Nordhäuser Spirituosen GmbH (Nordhausen, Germany)
Formamide	Sigma-Aldrich (Munich, Germany)
D-fructose 6-phosphate, disodium salt hydrate	Sigma-Aldrich (Munich, Germany)
D-glucose	Carl Roth GmbH & Co. KG (Karlsruhe, Germany)
D-ribose 5-phosphate, disodium salt hydrate	Carl Roth GmbH & Co. KG (Karlsruhe, Germany)
D-seduheptulose 7-phosphate	Provided by Dr. Stefan Lüdtkke
D-xylulose 5-phosphate, sodium salt	Carl Roth GmbH & Co. KG (Karlsruhe, Germany)
Ethylene glycol	Carl Roth GmbH & Co. KG (Karlsruhe, Germany)
Glycerol	Carl Roth GmbH & Co. KG (Karlsruhe, Germany)
Glycine	Carl Roth GmbH & Co. KG (Karlsruhe, Germany)
Glycylglycine	AppliChem GmbH (Darmstadt, Germany)

2. Material and methods

2-[4-(2-hydroxyethyl)piperazin-1-yl]ethanesulfonic acid (HEPES)	AppliChem GmbH (Darmstadt, Germany)
Hydrochloric acid (37 %)	Th.Geyer GmbH & CoKG (Renningen, Germany)
β -hydroxypyruvate, sodium salt (97 %)	Sigma-Aldrich (Munich, Germany)
Hydroxylamine hydrochloride	Sigma-Aldrich (Munich, Germany)
Imidazol	AppliChem GmbH (Darmstadt, Germany)
Iron(III) chloride, hexahydrate	Carl Roth GmbH & Co. KG (Karlsruhe, Germany)
1,4-Piperazinediethanesulfonic acid (PIPES)	AppliChem GmbH (Darmstadt, Germany)
Kanamycine sulfate	Carl Roth GmbH & Co. KG (Karlsruhe, Germany)
Magnesium chloride, hexahydrate	Carl Roth GmbH & Co. KG (Karlsruhe, Germany)
Magnesium sulfate, hydrate	Carl Roth GmbH & Co. KG (Karlsruhe, Germany)
Medi test glucose test stripes	Macherey-Nagel (Düren, Germany)
Manganese chloride	Carl Roth GmbH & Co. KG (Karlsruhe, Germany)
2-(<i>N</i> -morpholino)ethanesulfonic acid(MES)	AppliChem GmbH (Darmstadt, Germany)
β -Mercaptoethanol	Carl Roth GmbH & Co. KG (Karlsruhe, Germany)
Methanol	Carl Roth GmbH & Co. KG (Karlsruhe, Germany)
Nicotinamid adenine dinucleotid (NADH)	Sigma-Aldrich (Munich, Germany)
Phosphoric acid (85 %)	Carl Roth GmbH & Co. KG (Karlsruhe, Germany)
Polyethylene glycol (PEG 6000)	Carl Roth GmbH & Co. KG (Karlsruhe, Germany)
Potassium chloride	Carl Roth GmbH & Co. KG (Karlsruhe, Germany)

2. Material and methods

Roti NC nitrocellulose membrane	Carl Roth GmbH & Co. KG (Karlsruhe, Germany)
Sodium acetate trihydrate	AppliChem GmbH (Darmstadt, Germany)
Sodium chloride	AppliChem GmbH (Darmstadt, Germany)
Sodium dodecylsulfate (SDS)	AppliChem GmbH (Darmstadt, Germany)
Sulfuric acid	Carl Roth GmbH & Co. KG (Karlsruhe, Germany)
N,N,N',N' - Tetramethylethylenediamin (Temed)	Carl Roth GmbH & Co. KG (Karlsruhe, Germany)
Thiamin chlorid	AppliChem GmbH (Darmstadt, Germany)
Thiamin diphosphate	Sigma-Aldrich (Munich, Germany)
Trichloroacetic acid	Sigma-Aldrich (Munich, Germany)
3-(Trimethylsilyl) propionic-2,2,3,3-d ₄ acid sodium salt (TSP)	AppliChem GmbH (Darmstadt, Germany)
Tris-(hydroxymethyl)-amino methane (TRIS)	AppliChem GmbH (Darmstadt, Germany)
Tryptone	AppliChem GmbH (Darmstadt, Germany)
Whatman chromatography paper	GE Healthcare Europe (Munich, Germany)
Yeast extract	AppliChem GmbH (Darmstadt, Germany)
Yeast extract for high-density fermentation	Ohly GmbH (Hamburg, Germany)

Kit systems

Nucleospin TM Plasmid Kit	Macherey Nagel (Düren, Germany)
Quick-Change TM Mutagenesis Kit	Stratagene (Amsterdam, Netherlands)
ABI Prism [®] BigDye Terminator Cycle Sequencing Ready Reaction Kit	Life Technologies GmbH (Darmstadt, Germany)
CloneJet PCR cloning kit	MBI Fermentas (St. Leon-Roth, Germany)
Bac-to-Bac [®] expression system	Invitrogen, (Karlsruhe, Germany)
BM Chemiluminescence Western Blotting Substrate (POD)	F.Hoffmann-La Roche AG, (Basel, Switzerland)

2. Material and methods

DNA Marker

Gene Ruler™ 1kb DNA-Ladder MBI Fermentas (St. Leon-Roth, Germany)

Protein Marker

Unstained Protein Molecular Weight Marker MBI Fermentas (St. Leon-Rot, Germany)

Prestained Protein Molecular Weight Marker MBI Fermentas (St. Leon-Rot, Germany)

Enzymes

T4-DNA-Ligase MBI Fermentas (St. Leon Rot, Germany)

Restrictionendonukleases MBI Fermentas (St. Leon Rot, Germany)

DNAse AppliChem GmbH (Darmstadt, Germany)

Phusion™ High Fidelity- DNA polymerase MBI Fermentas (St. Leon Rot, Germany)

Triosephosphat isomerase (TIM) + Glycerol Sigma-Aldrich (Munich, Germany)

3-phosphate dehydrogenase (G3P-DH) mix

Lysozyme AppliChem GmbH (Darmstadt, Germany)

PreScission Protease GE Healthcare Europe (Munich, Germany)

Thrombin from bovine plasma Sigma-Aldrich (Munich, Germany)

SUMO-Protease Life Technologies GmbH (Darmstadt, Germany)

Solutions

dNTP mix (10 mM) MBI Fermentas (St. Leon Rot, Germany)

Antibodies

Mouse IgG Penta His Antibody Qiagen (Hilden, Germany)

Goat IgG anti mouse conjugated with horse raddish peroxidase (HRP) Jackson ImmunoResearch Europe Ltd., (Suffolk, United Kingdom)

2. Material and methods

2.2 Devices

Micro pulser electroporator	BioRad Laboratories GmbH (Munich, Germany)
Incubation shaker, Unitron	Infors AG (Bottmingen, Switzerland)
Biofermenter, Biostat C	Sartorius AG (Göttingen, Germany)
Laminar flow Prettl®-Telsta Bioll-A	Telstar (Terrassa, Spain)
Optima LE-80K Ultracentrifuge	Beckman Coulter GmbH (Krefeld, Germany)
Universal 320R	Hettich GmbH & Co. KG (Tuttlingen, Germany)
Avanti™J-25 Centrifuge	Beckmann Coulter GmbH (Krefeld, Germany)
Avanti™J-30I Centrifuge	Beckmann Coulter GmbH (Krefeld, Germany)
Avanti™J-20XPI Centrifuge	Beckmann Coulter GmbH (Krefeld, Germany)
Centrifuge tubes	Beckmann Coulter GmbH (Krefeld, Germany)
pH-electrode FiveEasy™ FE20	Mettler Toledo (Gießen, Germany)
Microfluidizer, M-110S	Microfluidics (Newton, MA, USA)
Sonoplus GM 70	Bandelin GmbH & Co. KG (Berlin, Germany)
ÄKTAprime plus	GE Healthcare Europe (Munich, Germany)
ÄKTapurifier	GE Healthcare Europe (Munich, Germany)
HisPrep FF 16/10	GE Healthcare Europe (Munich, Germany)
Sephadex 200	GE Healthcare Europe (Munich, Germany)

2. Material and methods

HiPrep 26/10 desalting	GE Healthcare Europe (Munich, Germany)
Uno Q&S ion exchange column	BioRad (Munich, Germany)
Superdex 200 10/30 Analytical gel filtration column	GE Healthcare Europe (Munich, Germany)
Superloop (10 mL, 50 mL, 150 mL)	GE Healthcare Europe (Munich, Germany)
Gel filtration standard	BioRad Laboratories GmbH (Munich, Germany)
Vivaspin concentrator 6, 20 mL (30000, 50000 MWCO)	Sartorius AG (Göttingen, Germany)
Electrophoresis device, EV 231	Consort bvba (Turnhout, Belgium)
Mini-PROTEAN® Tetra cell system	BioRad Laboratories GmbH (Munich, Germany)
SE250 small format vertical Electrophoresis system	Hoefer Inc., (MA, USA)
Thermocycler, TProfessional standard 96 well gradient	Whatman Biometra (Göttingen, Germany)
Gel documentation chamber raytest Ida	Herolab (Wiesloch, Germany)
Sterile filters, 0.22 µM	VWR International GmbH (Darmstadt, Germany)
Precision cuvettes, suprasil	Hellma GmbH & Co.KG (Mühlheim, Germany)
UV-Vis spectrometer, V-650	Jasco GmbH, (Groß-Umstade, Germany)
ITC-system, ITC ₂₀₀	GE Healthcare Europe (Munich, Germany)
Filters for NMR samples, 0.45 µM	GE Healthcare Europe (Munich, Germany)
ARX 400 MHz	Bruker Biospin GmbH (Karlsruhe, Germany)
Stopped-flow system SX.20	Applied Photophysics Ltd., UK

2. Material and methods

X-ray MM-007 rotating-anode generator, Rigaku Corp., (MI, USA)

Micromax 007- HF X-stream 2000, R-AXIS

IV++ imaging-plate system

2.3 Programs

SigmaPlot 11.0	Systat Software Inc. (Erkrath, Germany)
Origin 7	OriginLab Corp., MA, USA
Multalin	http://multalin.toulouse.inra.fr/multalin/ ⁸⁸
ESPRIT	http://espript.ibcp.fr/ESPrIPT/ESPrIPT/ ⁸⁹
PYMOL	DeLano Scientific LLC
MestreNova	Mestrelab research (Santiago de Compostela, Spain)
Kaleidagraph	Synergy Software, NJ, USA

2.4 Media

Lysogeny-broth-medium (LB) ⁹⁰

Tryptone/Peptone from casein (pancreatic digested)	0.1 % (w/v)
Yeast extract	0.05 % (w/v)
NaCl	0.1 % (w/v)

Super-broth-medium (SB) (3xLB)

Tryptone/Peptone from casein (pancreatic digested)	0.3 % (w/v)
Yeast extract	0.15 % (w/v)
NaCl	0.3 % (w/v)

LB-plates

1.5 % (w/v) Agar was added to LB-medium, as well as the required antibiotic (concentrations see below).

2. Material and methods

Antibiotic concentrations

Kanamycine:	35 µg/mL
Carbenicillin:	100 µg/mL

2.5 Bacterial strains

Table 1: Used bacterial strains

Organism	Strain	Genotype	Reference	Supplier
<i>E. coli</i>	XL-Blue	recA1endA1gyrA96 thi-1hsdR17 supE44 relA1lac[F`proAB lac9zM15 Tn19(Tetr)]	-	Stratagene, (Heidelberg, Germany)
<i>E. coli</i>	BL21 Star	F`ompT hsdS _B (r _B ⁻ m _B ⁻) gal dcm araB::T7RNAP-tetA	-	Invitrogen, (Karlsruhe, Germany)
<i>E. coli</i>	DH5α	fhuA2 Δ(argF- ⁹¹ lacZ)U169 phoA glnV44 Φ80 Δ(lacZ)M15 gyrA96 recA1 relA1 endA1 thi-1 hsdR17		Invitrogen, (Karlsruhe, Germany)

2. Material and methods

2.6 Vectors

Table 2: Used vectors

Vector	Selection marker	Supplier
pET28a	Kanamycine	Novagen (Schwalbach/Ts, Germany)
pMK-RQ	Kanamycine	Geneart (Regensburg, Germany)
pET-SUMO	Kanamycine	Invitrogen (Karlsruhe, Germany)
pCOLD	Carbenicillin	TaKaRa Bioscience Inc. (Otsu, Japan))

2.7 Utilized primers

Sequencing primers

T7 promotor	TAATACGACTCACTATAGGG
T7 terminator	AGCTAGTTATTGCTCAGCGG
hTKT_1	CTCAGAACAAAACGATCGTTA
hTKT_2	CTGACCGTGGAAGATCATT
TKTL1_1	TCCGGATCGCTCTGTTTA
TKTL2_1	AATAAAGCGATCATTATCCG
TKTL1/2_2	GTATTATTACCGTGGAAGATCAT
BbXFPK_1	CCATGATGAACACGGTGTCTGC
BbXFPK_2	GCAGTCCAACAAGCTCGTCAACC
BbXFPK_3	CCGCTTCCAACCGCCTGAACGC
BbXFPK_4	GCTGGCGATGTGCCGACCCAGG
pCOLD_1	TGGCAGGGATCTTAGATTCTG

2. Material and methods

Mutagenesis primers

pBAC sense	GGCCATGCGGATCCATGGCGGATGCCGAAGCG
pBAC antisense	GGCCATGCGGATCCATGATGGCAAATGATGCC
BbXFPK E437Q sense	GCATCTTCGGACCGGACGAAACCGCTTCCAACCGCC
BbXFPK E437Q antisense	GGCGGTTGGAAGCGGTTTCGTCCGGTCCGAAGATGC
hTKT deletion sense	CGTTTTGTTCTGAGCAAAAAACAGGCGTTTACCGATGTG
hTKT deletion antisense	CATCGGTAAACGCCTGTTTTTTGCTCAGAACAAAACGATCG

2.8 Methods

2.8.1 *Escherichia coli* cultivation

Escherichia coli (*E. coli*) strains used for this thesis were either cultivated on solid or liquid LB-media. Precultures were incubated shaking in LB-medium at 37 °C and 200 rpm. Expressioncultures grew in SB-medium over night at 12 °C and 180 rpm in baffled flasks. Plasmid-containing clones were selected by choosing the required antibiotics. Carbenicillin was used for all pCOLD-TKTL1 and 2 constructs, kanamycine for all pET28a derived ones, namely the full-length TKT, TKTΔ38, pETSUMO-TKTL1, pETSUMO-TKTL2 and XFPK of *Bifidobacterium breve*.

2.8.2 Transformation of *E. coli*

Preparation of the desired *E. coli* strains and transformation was performed as described by Inoue *et al.*⁹².

2.8.3 Isolation of plasmid DNA

For plasmid isolation 5 mL LB-medium were incubated with the desired plasmid-containing *E.coli* strain and incubated shaking over night at 37 °C and 200 rpm. Plasmid preparation was performed according to the Nucleospin™ Plasmid Kit (Macherey-Nagel). Obtained plasmids were stored at -80 °C.

2.8.4 Amplification of specific DNA fragments and site-directed mutagenesis by polymerase chain reaction

Polymerase chain reaction (PCR) was used to amplify desired DNA-fragments as well as to construct selected variants. For all applications Phusion™ High Fidelity DNA-polymerase was used according to the manufacturers' manual (MBI Fermentas [St. Leon Rot, Germany]).

2.8.5 DNA-concentration determination

Concentration of double stranded DNA was determined spectroscopically by using the absorption at 260 nm. Correlation of absorption and DNA-concentration is as follows:

$$A_{260} = 1 = 50 \mu\text{g/mL pure ds DNA}$$

2.8.6 DNA-restriction

DNA-restriction was performed according to the manufacturer's manual of the used endonucleases (MBI Fermentas [St. Leon-Roth, Germany]).

2.8.7 Separation of DNA-fragments by agarose-gelelectrophoresis

Agarose-gelelectrophoresis was used for separation and size determination of DNA-fragments. For that purpose 1 % agarose gels (w/v) were used. Before electrophoresis sample buffer (EDTA 250 mM, SDS 0.1 % [w/v], glycerol 40 % [w/v], bromophenol blue 0.025 % [w/v], xylene cyanol 0.025 % [w/v]) was added to the samples. GeneRuler™ DNA-Ladder served as size standard. Electrophoresis was carried out at 120 V for 50 minutes in 1xTAE buffer (TRIS HCl [40 mM], acetic acid [20 mM], EDTA [1 mM], pH 7). Gels were stained in an ethidiumbromide solution (2 µg/mL) for 10 minutes. Visualization of DNA bands was performed in a gel documentation chamber under UV-light.

2.8.8 DNA-ligation

DNA ligation was performed by use of T4 DNA-ligase according to the manufacturers' manual (MBI Fermentas [St. Leon-Roth, Germany]).

2. Material and methods

2.8.9 CloneJet PCR cloning kit

The CloneJet PCR cloning kit was used to ligate blunt end PCR products into the pJET amplification vector. This was carried out as described in the manufacturers' manual (MBI Fermentas [St. Leon-Roth, Germany]).

2.8.10 Generation of a *hTKT* deletion construct by overlap extension PCR

An overlap extension method was used to create the 38 amino acid deletion variant⁹³. This was carried out by using the Phusion™ High Fidelity DNA polymerase system. The *hTKT* sense and antisense deletion primers listed in the primer list were used as well as T7 sense and antisense primers. In a first step the two domains intended to be fused (aminoacids 1–75 and 114–623) were amplified individually by using the following primer combinations: T7 forward/deletion reverse and T7 reverse/deletion forward. In a subsequent PCR reaction the amplicons were fused by usage of T7 forward and T7 reverse primers. The shortened *hTKT* construct was cloned into the amplification plasmid pJET (Fermentas) and transferred as NcoI/XhoI fragment into pET28a expression vector.

2.8.11 DNA sequencing

DNA-sequencing was used to confirm the correctness of the used DNA-constructs. Sequencing was either performed with the ABI Prism BigDye Terminator Cycle Sequencing Ready Reaction Kit, or by a company (Seqlab, Göttingen, Germany). Amplicons generated with the BigDye Sequencing Kit were analyzed for their sequence by courtesy of Andreas Nolte (Department of Developmental Biochemistry, Georg-August-University Göttingen).

2.8.12 Insect cell culture

Expression of TKTL1 and 2 was performed by use of the Bac-to-Bac® expression system (Invitrogen, [Karlsruhe, Germany]). The *Spodoptera frugiperda* derived cell lines Sf-9 and Sf 21 as well as the *Trichoplusia ni* derived cell line Hi5™ were used according to the manufacturers' manual. Baculovirus constructs carrying the genes of TKTL1 and 2 were previously generated as described in the manual. All cell cultural experiments were

2. Material and methods

performed by courtesy of Michael Franke (Department for Molecular Structural Biology, Georg-August-University Göttingen).

2.8.13 Generation of pCOLD-TKTL1 and 2 fusion constructs

The genes encoding for codon optimized TKTL1 and 2 were amplified by use of Phusion DNA-polymerase as described above. The amplicons were fused as KpnI/XhoI fragments into the pCOLD expression plasmid in-frame harboring an N-terminal trigger-factor/hexahistidine tag.

2.8.14 High density fermentation

To generate high amounts of TKTL1/2 high density fermentation was carried out in a biofermenter. Two 200 mL overnight precultures containing 35 µg/mL kanamycine were generated from a single colony of *E coli* BL21 Star harboring either the pETSUMO-TKTL1 or 2 construct. These cultures were used to inoculate a 6 L fermentation batch for cell cultivation.

Fermentation medium:

300 g yeast fermentation extract

3 g NH₄Cl

30 g glucose

4 g MgSO₄

66 g K₂HPO₄

1 mL Antifoam 204

1 mg/mL thiamin dichlorid

35 µg/mL kanamycine

The fermentation batch was stirred at 400-1500 rpm and aerated with a flow of 3–24 L/min of air, to maintain an O₂-level of 30 % at a temperature of 37 °C. A neutral pH was established by computer controlled addition of 10 % NaOH or 10 % H₃PO₄. After glucose was consumed (verified by medi test glucose test stripes) feeding was started by adding a proper amount of feeding solution into the fermentation batch until the desired OD₆₀₀ was reached (~60-80).

2. Material and methods

Feeding solution:

600 g yeast fermentation extract

600 g glucose

add to 2 L with ddH₂O

TKTL1 and 2 expression was induced after cooling the fermenter down to 18 °C by addition of 100 µM IPTG. After 12 hours the cells were harvested by centrifugation (2921 g, 30 min, 4 °C), the yield was in the range of 1.5-2 kg of wet cell material.

2.8.15 Expression and purification of full length hTKT and the Δ38 deletion variant

The pET28a vector encoding for C-terminal His-tagged full length human transketolase was provided by Dr. Kathrin Schröder-Tittmann (Department for Bioanalytics, Georg-August-University Göttingen). The full length construct and the Δ38 deletion variant of human transketolase were transformed into *E. coli* BL21 Star cells by the method of Inoue ⁹². Transformed cells were grown on LB/Agar plates containing 35 µg/mL kanamycine over night at 37 °C. A single colony was used to inoculate 200 mL of an overnight culture and expression was carried out as described in section 2.8.1.

For protein purification, 20 g of cells were thawed and resuspended on ice in 60 mL of buffer containing 20 mM TRIS-HCl pH 7.6, 500 mM NaCl, 20 mM imidazole, 1 mM CaCl₂ and 100 µM ThDP. Moreover, DNase (5 µg/mL), MgCl₂ (1 mM), Lysozyme (0.2 mg/mL) and PMSF (1 mM) were added. The suspension was stirred on ice for 30 min. Cells were disrupted by repeated passages through a microfluidizer. Cell debris was removed by centrifugation at 54000 x g for 30 min at 4 °C. The supernatant was loaded onto a HisPrep FF 16/10 column previously equilibrated with 20 mM TRIS-HCl, pH 7.6, 500 mM NaCl, 20 mM imidazole, 1 mM CaCl₂ and 100 µM ThDP. TKTΔ38 was eluted with a linear gradient (0-100%) of elution buffer (20 mM TRIS-HCl, pH 7.6, 500 mM NaCl, 1 mM CaCl₂, 100 µM ThDP and 300 mM imidazole) over a total volume of 20 column volumes. Fractions containing TKTΔ38 were pooled and loaded onto a HiPrep™ 26/10 desalting column equilibrated with 50 mM glycylglycine, pH 7.6 containing 1 mM CaCl₂, 100 µM

2. Material and methods

ThDP and 500 mM NaCl. Finally, the protein concentration was adjusted to 15-25 mg/mL by ultra filtration using a microconcentrator (VIVASPIN, Sartorius) with a molecular weight cut-off of 50000 at 4 °C. Protein homogeneity was judged by SDS-PAGE analysis.

2.8.16 Expression and purification of full length TKTL1 and 2

The pCOLD vector encoding for N-terminal trigger factor/His-tagged full length human transketolase-like protein 1 and 2 were transformed into *E. coli* BL21 Star cells by the method of Inoue ⁹². Transformed cells were grown on LB/Agar plates containing 100 µg/mL carbenicillin over night at 37 °C. A single colony was used to inoculate 200 mL of an overnight culture and expression was carried out as described in section 2.8.1 .

For protein purification of the pCOLD- and the pETSUMO-constructs, 20 g of cells were thawed and resuspended on ice in 60 mL of buffer containing 20 mM TRIS-HCl pH 8, 500 mM NaCl, 20 mM imidazole, 1 mM CaCl₂ and 200 µM ThDP. Moreover, DNase (5 µg/mL), MgCl₂ (1 mM), Lysozyme (0.2 mg/mL) and PMSF (1 mM) were added. The suspension was stirred on ice for 30 min. Cells were disrupted by repeated passages through a microfluidizer. Cell debris was removed by centrifugation at 54000 g for 30 min at 4 °C. The supernatant was loaded onto a HisPrep FF 16/10 previously equilibrated with 20 mM TRIS-HCl, pH 8, 500 mM NaCl, 1 mM CaCl₂ and 200 µM ThDP. Bound proteins were eluted with a one step gradient (0-100 %) of elution buffer (20 mM TRIS-HCl, pH 8 containing 1 mM CaCl₂, 200 µM ThDP, 500 mM NaCl and 300 mM imidazole). Fractions containing the desired protein were pooled and loaded onto a HiLoad™ 16/60 superdex 200 pg gel filtration column equilibrated with 50 mM glycylglycine, pH 7.6 containing 500 mM NaCl, 1 mM CaCl₂ and 200 µM ThDP. Finally, the protein concentration was adjusted to 15-25 mg/mL by ultra filtration using a microconcentrator (VIVASPIN, Sartorius) with a molecular weight cut-off of 50000 at 4 °C. Protein homogeneity was judged by SDS-PAGE analysis.

2.8.17 Expression and purification of xylulose 5-phosphate/fructose 6-phosphate phosphoketolase (XFPK) from *Bifidobacterium breve*

The pET 28a vector harboring N-terminally His-tagged XFPK of *B. breve* was kindly provided by Prof. Dr. Shinya Fushinobu (University of Tokyo, Japan). Expression and purification was performed according to Suzuki *et al.* 2010⁷⁹.

2.8.18 Sodiumdodecylsulfate-polyacrylamide-gelelectrophoresis (SDS-PAGE)

Homogeneity of purified proteins was judged by one dimensional SDS-PAGE according to Laemmli⁹⁴. 20 µL of a sample, with a concentration of 0.4 mg/mL, was mixed with 20 µL of 2xLaemmli buffer, heated at 98 °C for 5 minutes and used for electrophoresis. Gels containing 12 % acrylamid were run at 30 mA for 50 minutes.

2.8.19 Protein concentration determination according to Bradford

A colometric method according to Bradford was used for protein concentration determination⁹⁵. By use of a bovine serum albumin standard solution a reference linear slope was generated. Absorption of the colored protein-bradford reagent (methanol 5 % [v/v], acetic acid 10 % [v/v] and coomassie brilliant blue G250 [0.25 % [w/v]]) complex was determined at a wavelength of 595 nm.

2.8.20 Detection of the proteins of interest by western blotting

Western blot analysis was performed to verify TKTL1 and 2 expression in baculovirus infected insect cell lines. After SDS-PAGE of the desired samples as described above, proteins were blotted onto a nitrocellulose membrane in a Mini-PROTEAN® Tetra cell system. Blotting was performed for 1 h at 350 mA and 4 °C in blotting buffer (TRIS base 25 mM, glycine 192 mM and methanol 20 % [v/v]). Unspecific binding sites were blocked with 3 % (w/v) dry milk powder in TBS-T buffer for 1 h (TRIS base 50 mM, NaCl 150 mM Tween20 0.05 % [v/v], pH 7.6). The following incubation with primary antibody (mouse IgG anti pentaHistidine 1:10000 in TBS-T) was performed over night at 4 °C. Primary antibody was removed by three washing steps with TBS-T buffer, followed by secondary

2. Material and methods

antibody (Goat IgG anti mouse conjugated with horse raddish peroxidase (HRP), 1:10000 in TBS-T) incubation for 2 h at 4 °C. After three more washing steps chemiluminescence reaction was performed by use of the BM Chemiluminescence Western Blotting Substrate (POD) according to the manufacturers' manual (F.Hoffmann-La Roche AG, [Basel, Switzerland]). The blot was exposed to a roentgen film in a photo cassette for different time points (1-120 sec).

2.8.21 Analytical gel filtration

Analytical gel filtration experiments were carried out on an ÄKTA Purifier HPLC-system by loading 200 µL of protein solution (4 mg/mL) on a Superdex 200 10/30 column. Oligomerization degree was estimated by use of a gel filtration-standard (BioRad Laboratories GmbH [Munich, Germany]).

2.8.22 Coupled optical enzymatic assay

The enzymatic activity of TKTΔ38, full-length TKT, TKTL1 and TKTL2 for conversion of physiological substrates X5P and R5P into products G3P and S7P was measured in a coupled spectrophotometric assay using the auxiliary enzymes triosephosphate isomerase (TPI) and *sn*-glycerol-3-phosphate:NAD⁺2-oxido-reductase (G3PDH) (Figure 15)⁹⁶. This assay detects formation of the product G3P that derives from TKT-catalyzed cleavage of substrate X5P. The concomitant oxidation of NADH was followed spectrophotometrically at 340 nm in 50 mM glycyglycine, pH 7.6 containing 500 mM NaCl at 30 °C. The assay contained as final concentration 220 µM NADH, 3.6 units of TIM/G3PDH enzyme mix, 1 mM thiamine diphosphate, 1 mM CaCl₂, 5 mM of X5P and R5P, and varied concentrations of TKTΔ38 and full-length TKT (0.05 – 2 mg/mL).

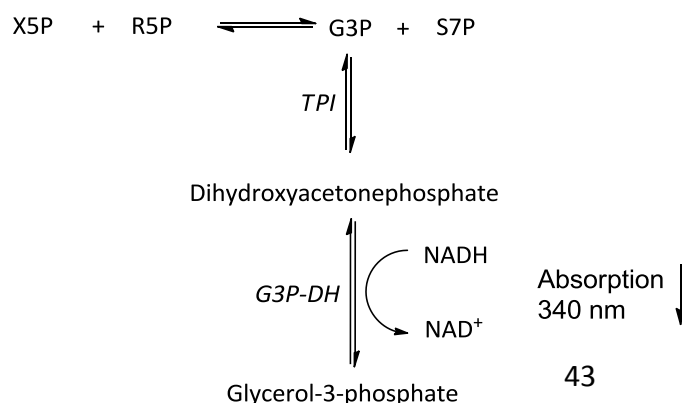


Figure 15: Coupled enzymatic assay for conversion of X5P and R5P by transketolase.

2. Material and methods

2.8.23 Circular dichroism spectroscopy

2.8.23.1 Far-UV CD-based secondary structure element analysis

For analyzing secondary structure contents of proteins, far UV circular dichroism (CD) was used⁹⁷. Spectra of full length TKT as well as TKTΔ38, TKTL1, TKTL2 and XFPK (wt and variants) were recorded at 20 °C in a 1 mm quartz cuvette by usage of a CD spectrometer equipped with a peltier temperature control element. The protein concentration was adjusted to 0.1 mg/mL in 50 mM sodium phosphate buffer, pH 7.6 containing 2.5 mM MgCl₂ and 100 μM ThDP. To prevent protein aggregation of TKTΔ38, the buffer additionally contained 500 mM NaCl. The buffer corrected spectra were converted to mean residue ellipticity

$$[\theta]_{MRW,\lambda} = \frac{MRW * \theta\lambda}{10 * d * c} \quad [1]$$

with Θ as the measured ellipticity at the given wavelength λ , the pathlength d , the concentration c (in g/L) and MRW which is the molecular weight of the corresponding protein divided by its amino acid chain length – 1. The unit of the mean residue ellipticity is deg * cm² * d mol⁻¹.

The program CDNN⁹⁸ was used to analyze secondary structure contents. The stability of the proteins was investigated by thermal denaturation at a wavelength of 222 nm within a temperature range of 293-367 K. The heating rate was adjusted to 1 K/min, the data interval was set at 0.5 K at an accumulation time of 12 sec. Spectra were recorded before (at 293 K) and after (367 K and 293 K) thermal denaturation. Transition point of thermal denaturation was fitted according to Pace *et al*⁹⁹.

2. Material and methods

$$y = \frac{\{(y_f + m_f \cdot T) + (y_u + m_u \cdot T) \cdot \exp\left[\left(\frac{\Delta H_m}{RT}\right) \cdot \left(\frac{T - T_m}{T_m}\right)\right]\}}{1 + \exp\left[\left(\frac{\Delta H_m}{RT}\right) \cdot \left(\frac{T - T_m}{T_m}\right)\right]} \quad [2]$$

y	=	Circular dichroism signal at 222 nm
y _f , y _u	=	Intercepts of pre- and posttransition baselines
m _f , m _u	=	Slopes of pre- and posttransition baselines
T	=	Temperature in Kelvin
T _m	=	Midpoint of the thermal unfolding curve
ΔH _m	=	Enthalpy change for unfolding at T _m
R	=	Gas constant

This equation was described as characteristic for reversible folding proteins. Since none of the investigated proteins showed such behaviour, absolute transition points can not be determined. A comparison of the stability of the respective variants is nevertheless possible.

2.8.23.2 Near-UV CD-based detection of a cofactor caused charge transfer absorption band

All so far known TKTs give rise to a negative CD signal centered around 320 nm which reflects a charge transfer interaction between the aminopyrimidine- and the thiazolium portion of the cofactor (AP signal)^{100 101}. We investigated full length TKT as well as TKTΔ38, TKTL1, TKTL2 and XFPK (wt and variants) for cofactor binding. For that purpose near-UV spectra were recorded in a 10 mm quartz cuvette at 20 °C. The buffer corrected spectra were recorded either in 50 mM glycylglycine buffer, pH 7.6 (for TKT, TKTΔ38, TKTL1 and 2) or in 20 mM HEPES buffer, pH 7.2 (for wt XFPK and variants) at a protein concentration of 1-2 mg/mL, the scanning range was from 400–290 nm. To elucidate dynamical changes of the respective charge/tautomeric states of the bound ThDP cofactor, signal spectra were recorded with different pH-values. The pH was adjusted by dissolving XFPK (1mg/mL) in MES/PIPES/TRIS buffer (20 mM each) with the desired pH-values ranging from 6-9.

2. Material and methods

2.8.24 Cofactor binding studies by ^1H NMR spectroscopy

To verify whether the TKT Δ 38 variant, TKTL1 and TKTL2 contained tightly bound ThDP cofactor, acid quench/NMR experiments were performed. For that purpose 400 μL of the corresponding freshly prepared protein was dialyzed against cofactor-free buffer. Afterward 400 μL of protein (7.5 mg/mL in 50 mM glycylglycine buffer, pH 7.6 containing 500 mM NaCl) were quenched by addition of 200 μL quench solution (650 μL D_2O , 250 μL TCA 50 % [w/v] in H_2O and 100 μL HCl 37%). The denatured protein was pelletized by centrifugation (10 min, 4 $^\circ\text{C}$ and 15000 rpm) and the supernatant filtered through a 0.22 μm nylon-membrane filter. NMR-samples were measured by Cindy Wechsler (Department for Bioanalytics, University of Göttingen) or Prof. Dr. Kai Tittmann (Department for Bioanalytics, University of Göttingen) on a 400 MHz Bruker NMR-spectrometer with 3-(trimethylsilyl) propionic-2,2,3,3- d_4 acid as internal standard at desired conditions¹⁰².

2.8.25 Covalent reaction intermediate analysis by acidic quench ^1H NMR spectroscopy

^1H NMR acidic quench spectroscopy was established to analyze microscopic steps of ThDP-dependent catalysis¹⁰³. The desired enzymes were incubated with the substrate of choice at pre steady-state or steady-state conditions and quenched by a strong acidic solution after desired time points. The acid-stable ThDP-intermediates were analyzed by ^1H NMR spectroscopy. By this method a qualitative analysis of the occurring intermediates, starting from the Michaelis complex up to the different cleavage-raised intermediates can be performed.

For detection of the different intermediates present in XFPK, the wild-type enzyme and several variants were incubated with F6P solely, or in presence of the second substrate phosphate. To prevent falsification from free ThDP in the buffer, the enzyme was dialyzed against cofactor-free buffer. A typical experiment was performed by incubating 200 μL XFPK-solution (15 mg/mL) with 200 μL of 50 mM F6P, or F6P/Pi (all in 20 mM HEPES-NaOH, pH 7.2) at room temperature. After a few seconds the reaction was quenched by addition of 200 μL quench solution (650 μL D_2O , 250 μL TCA 50 % [w/v] in H_2O and 100 μL HCl 37%). The denatured protein was pelletized by centrifugation

2. Material and methods

(10 min, 4 °C, and 15000 rpm) and the supernatant filtered through a 0.22 µm nylon-membrane filter. NMR-samples were measured by Cindy Wechsler (Department for Bioanalytics, University of Göttingen) or Prof. Dr. Kai Tittmann (Department for Bioanalytics, University of Göttingen) on a 400 MHz Bruker NMR-spectrometer with 3-(trimethylsilyl) propionic-2,2,3,3-d₄ acid as internal standard at desired conditions¹⁰².

2.8.26 Analysis of XFPK catalysis derived acetate and d4-acetate by product ¹H NMR spectroscopy

¹H NMR spectroscopy was used to analyze H/D exchange at the terminal methyl group of acetate derived from XFPK driven F6P conversion. A typical experiment contained 2 mg/mL of the desired enzyme in 50 mM HEPES buffer (pH 7.2) containing 1 mM MgCl₂ and 200 µM thiamine diphosphate. F6P were dissolved in the same buffer and added to a final concentration of 5 mM. Reaction was incubated at 37 °C for 10 min. The reaction was either performed in aqueous buffers or in deuterium oxide based buffers. Protein was separated by ultra filtration using a microconcentrator (VIVASPIN, Sartorius) with a molecular weight cut-off of 5000 at 4 °C. Flow through was analyzed for products by ¹H NMR spectroscopy by Prof. Dr. Kai Tittmann (Department for bioanalytics, University of Göttingen, Germany) on a 400 MHz Bruker NMR-spectrometer with 3-(trimethylsilyl) propionic-2,2,3,3-d₄ acid as internal standard at desired conditions.

2.8.27 Determination of XFPK activity by the hydroxamate assay

Activity of wt XFPK and selected variants was analyzed by monitoring the amount of formed acetyl phosphate in form of a colored compound as described earlier^{80 104 105}.

2.8.28 Calorimetric based enzyme kinetics

A calorimetric based method was used for determination of kinetic parameters of XFPK as described earlier¹⁰⁶. For the kinetic measurements of XFPK different variants and substrates were used. In a general experiment XFPK at varying concentrations in HEPES buffer (20 mM, pH 7.2) containing 1 mM MgCl₂, 50 mM Na₂HPO₄ and 200 µM ThDP was incubated with different substrate concentrations. The exact specified parameters of the

2. Material and methods

reactants and the Microcal ITC₂₀₀ instrument settings are depicted in the corresponding graphs in the results part of this work.

2.8.29 Product analysis via mass spectrometry

Sugarphosphate derived products of a putative enzymatic TKTL1 and TKTL2 activity were measured by mass spectrometry. A typical experiment contained 2 mg/mL of the desired enzyme in 50 mM glycyl-glycine buffer (pH 7.6) containing 1 mM CaCl₂ and 100 μM ThDP. X5P, R5P and Coenzyme A were dissolved in the same buffer and added to a final concentration of 1 mM. Reaction was incubated at 37 °C for 10 min. Protein was separated by ultra filtration using a microconcentrator (VIVASPIN, Sartorius) with a molecular weight cut-off of 5000 at 4 °C. Flow through was analyzed for products by courtesy of Dr. Cornelia Herfurth (Department for Plant Biochemistry, University of Göttingen) via nano electrospray ionisation mass spectrometry. For a measurement the product containing flow through was dissolved in 85 % (v/v) methanol, 15 % (v/v) acetonitril and 0.1 % (v/v) acetic acid. After acidification of the sample the molecules undergo ionization when transferred into the electron spray ionization device of the mass spectrometer. The generated ions were trapped and analyzed according to their mass over charge (m/z) ratio. Moreover it was possible to analyze ions with an m/z ratio of interest by collision induced dissociation (CID) in helium gas followed by daughter ion generation. Characteristic daughter ions for possible products are phosphate (97 m/z), G3P (170.1 m/z), X5P (229.1 m/z), R5P (229.1 m/z) as well as Coenzyme A (768 m/z) and acetyl Coenzyme A (810 m/z) with their respective fragmentation product with a m/z of 408¹⁰⁷ (Figure 16).

2. Material and methods

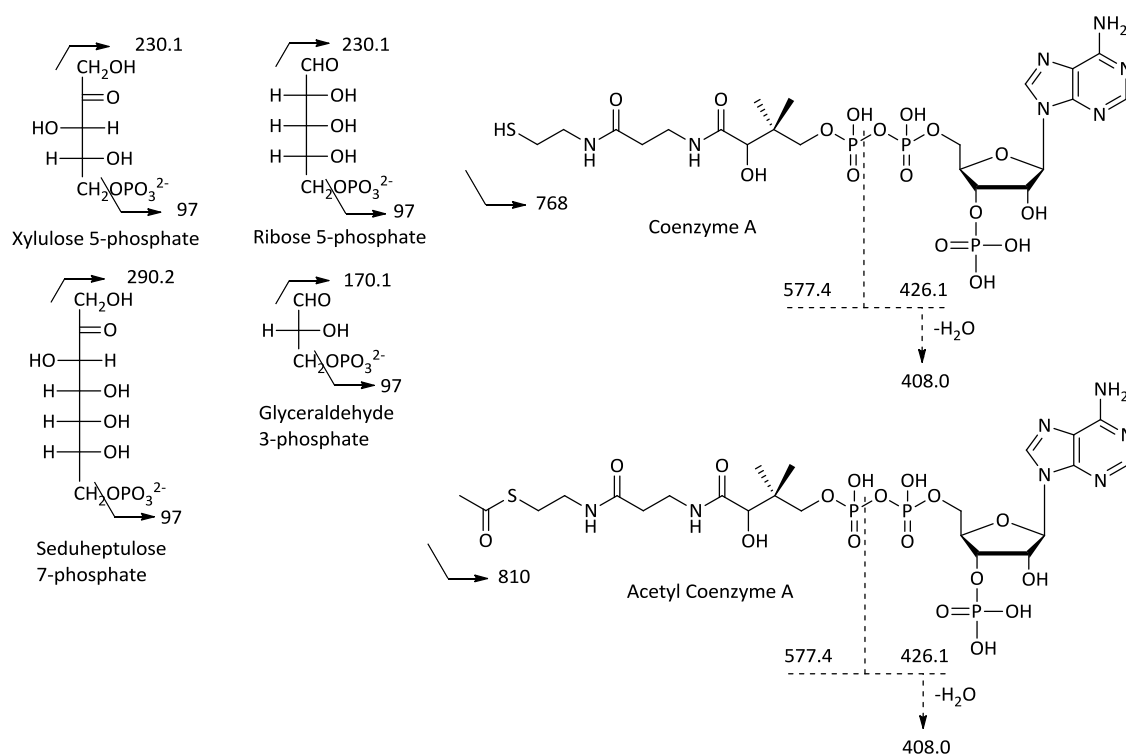


Figure 16: Expected m/z ratios for the used sugar phosphate and Coenzyme A substrates and products.

2.8.30 Monitoring XFPK reaction intermediates by stopped flow absorbance spectroscopy

Stopped-flow and sequential stopped-flow/UVvis measurements of XFPK were performed to characterize fast kinetic events. Experiments were performed by use of a photo diode array. Experiments were performed at 18 °C with an optical path length of 1 cm. Single mixing experiments were carried out by use of the photo diode array with mixing ratios of 1:1.

To analyze if certain reaction intermediates are already formed after addition of only the first substrate F6P without anorganic phosphate sequential stopped flow experiments were performed. Premixture containing high amounts of enzyme and F6P were mixed manually. In single mixing experiments the premix and a phosphate solution were used as described above. The respective buffer-, cofactor- and enzyme concentrations of the experiments are depicted in the in the figures of the results part.

2. Material and methods

2.8.31 XFPK E437Q crystallization and data processing

Crystallization of the XFPK E437Q variant was performed by the hanging drop vapor diffusion method according to Suzuki *et al.*⁸⁰. XFPK variant E437Q was purified as holo enzyme and adjusted to a protein concentration of 20–30 mg/mL in 5 mM HEPES-NaOH pH 7.2, 0.25 mM MgCl₂ and 25 μM ThDP. 1.5 μL of protein solution was mixed in a 1:1 ratio with reservoir solution containing 20–30 % PEG 6000 (w/v) in BICINE buffer (0.1 M, pH 9) at 18 °C. Crystals grew within a few days at 18 °C.

For data collection crystals were soaked in 24 % PEG 6000 (w/v) in BICINE (0.1 M, pH 9) containing 20 % (v/v) ethylene glycol. Soaked crystals were flash frozen and stored in liquid nitrogen. Soaking experiments were performed with F6P at different concentrations (27 mM and 54 mM) as reported elsewhere for varying periods of time⁷⁹. Crystals were tested for preliminary diffraction quality in-house on a nitrogen cryostream (130-140 K, XSTREAM2000, Rigaku/MSK, Japan) with an R-Axis IV++ imaging-plate system (Rigaku/MSK, Japan) using CuKα radiation generated by a Rigaku MM-007 rotating-anode generator. High resolution data sets were collected by Dr. Piotr Neumann (Department for Molecular Structural Biology, University of Göttingen, Germany) at the Positron-Elektron-Tandem-Ring-Anlage (Petra) of the German electron synchrotron facility (DESY) in Hamburg.

Processing of the collected data was performed with *XDS*¹⁰⁸ by courtesy of Dr. Piotr Neumann. The obtained models were iteratively refined and improved by use of *PHENIX*¹⁰⁹ and final validation was performed with *MOLPROBITY*. Restraints for additional ligands (ThDP-intermediates, buffer molecules and substrates) were generated with the *PRODRG* server¹¹⁰. For collection- and structure refinement statistics see Appendix. The final model was validated with *COOT*¹¹¹ and electron density maps ($|F_o| - |F_c|$, $2|F_o| - |F_c|$) were generated with *PHENIX*. Preparation of the final figures was performed with *PYMOL* (DeLano Scientific).

3 Results

3.1 A $\Delta 38$ deletion variant of TKT as a minimal model for analysis of a putative TKTL1 function

3.1.1 Generation and purification of native TKT and TKT $\Delta 38$

The 38 amino acid sequence missing in TKTL1 compared to TKT was removed by an overlap extension PCR based method⁹³. The genes, which are optimized for codon usage in *E.coli*, were expressed by a protocol previously established for TKT⁵⁰. Full length TKT and TKT $\Delta 38$ were purified to homogeneity in the milligram scale (~40 g

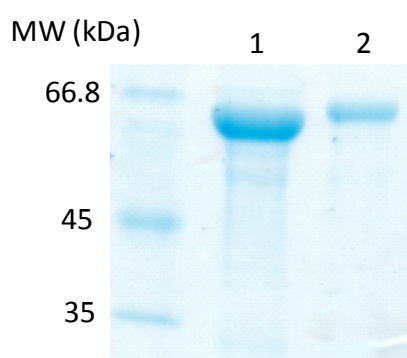


Figure 17: SDS-PAGE of purified native TKT and TKT $\Delta 38$. As expected, the deletion variant migrates with a smaller apparent molecular weight than the wt enzyme. (1) TKT $\Delta 38$, (2) TKT.

protein from a 20 g cell pellet) (Figure 17). First purifications based on the established protocol showed that the deletion variant undergoes precipitation under low salt conditions (50 mM glycyl glycine, pH 7.6 containing 1 mM CaCl₂ and 100 μ M ThDP). Sodium chloride at concentrations above 500 mM turned out to be a suitable additive to prevent denaturation of the variant. Therefore, all further purifications were performed with 500 mM sodium chloride in all buffers.

3.1.2 Analysis of secondary structure and thermal stability of native TKT and TKT $\Delta 38$

The increased tendency of the deletion variant to precipitate under low salt buffer conditions indicates a lower stability in comparison to full length TKT. Therefore a CD based secondary structure analysis was performed to enlight structural changes and the decreased stability in the variant in comparison to the wild type.

The CD spectrum recorded for full length TKT corresponds to a typical (α/β)-protein with two negative bands at 208 nm and 220 nm, and a positive signal at 195 nm. By using the CDNN software the α -helical fraction was estimated to be 35 % whereas the β -sheet content was 16 %. These values resemble the secondary structural content of TKT

3. Results

derived from crystallographic data (36 % α -helices and 16 % β -sheets estimated by use of the program PROMOTIF, pdb code: 3MOS).

Due to the strong CD absorbance of chlorid ions the CD spectrum of TKT Δ 38 is limited to wavelengths above 200 nm (Figure 18). Despite this restriction the overall quality of the spectrum is good. Unstructured elements - which would contribute to a strong negative absorption around 190 nm - could not be detected. Noteworthy is a smaller absorption at 222 nm compared to TKT corresponding to a loss of α -helical content. This is an expected finding since the deleted 38 amino acids form two short helices⁵⁰. The CDNN based analysis of TKT Δ 38 is in good agreement with this result because the calculated α -helical part is lowered to 31 % whereas the β -sheet content is only slightly affected (17 %). A sample CD spectrum of secondary structure contribution to ellipticity signals can be found in the appendix.

Next, the stability of both proteins was analyzed by thermal unfolding which turned out to be an irreversible process in both cases (Figure 18). Unfolding of TKT usually followed a one phase transition with a transition point at 345 K (data not shown). On the contrary, TKT Δ 38 was not stable under the same conditions and precipitated immediately. To overcome this restriction 500 mM NaCl were added and TKT Δ 38 turned out to be stable at 293 K. The apparent melting temperature for this variant was \sim 317 K. In comparison, full length TKT showed a two phase transition under high salt conditions - a minor one at 326 K and a major one at 337 K.

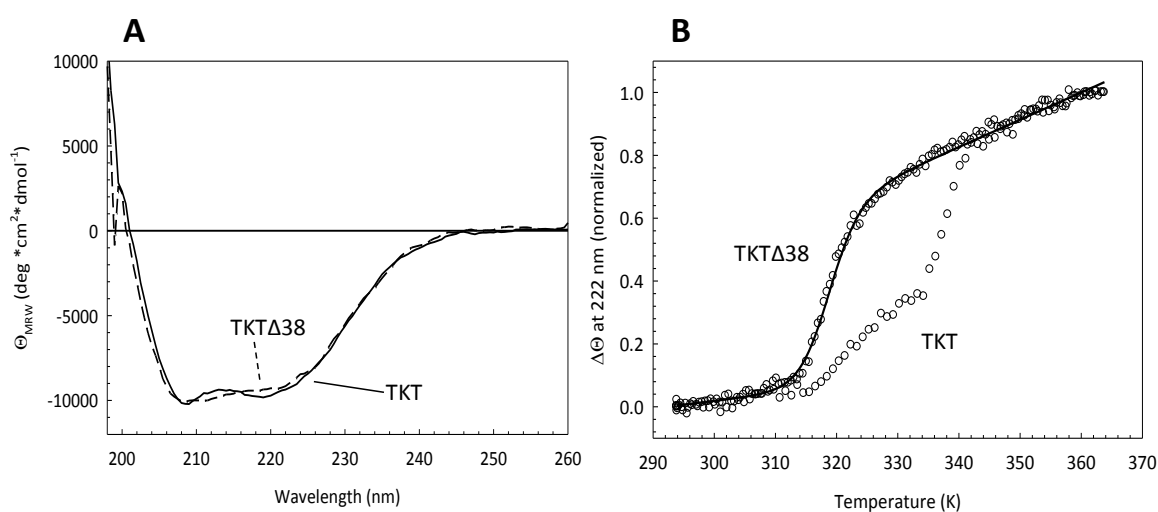


Figure 18 Far-UV spectra and thermal unfolding of native TKT and the TKT Δ 38 deletion variant. (A) Far-UV CD spectra of native TKT and the TKT Δ 38 deletion variant were recorded at a protein concentration of 0.1 mg/mL in 50 mM sodium phosphate buffer, pH 7.6 containing 500 mM NaCl, 2.5 mM MgCl₂ and 100 μ M ThDP at 20 $^{\circ}$ C. (B) Thermal unfolding of TKT and TKT Δ 38 was recorded at 222 nm in the same buffer as mentioned above.

3. Results

3.1.3 Transketolase activity of TKT Δ 38

Enzymatic activity measurements of TKT Δ 38 were performed as outlined in section 2.8.22. The substrates X5P and R5P are converted by all known TKTs to S7P and G3P. For the activity assay G3P is further processed by auxiliary enzymes (TPI and G3PDH) linked to the oxidation of NADH. As control native TKT was used. Since the deletion variant is unstable under low salt conditions the reaction batch contained 500 mM sodium chloride to prevent enzyme precipitation. In high salt buffer native TKT exhibited a slightly lowered enzymatic activity in comparison to low salt conditions as reported earlier (~ 1 U/mg versus 2.7 U/mg (Figure 19)⁵⁰. Contrary, no enzymatic activity could be detected for the TKT Δ 38 variant, even at an enzyme concentration of 2 mg/mL. Whether the lack of enzymatic activity is caused by the absence of catalytically essential amino acids or improper binding of the cofactor can not be distinguished by this experiment.

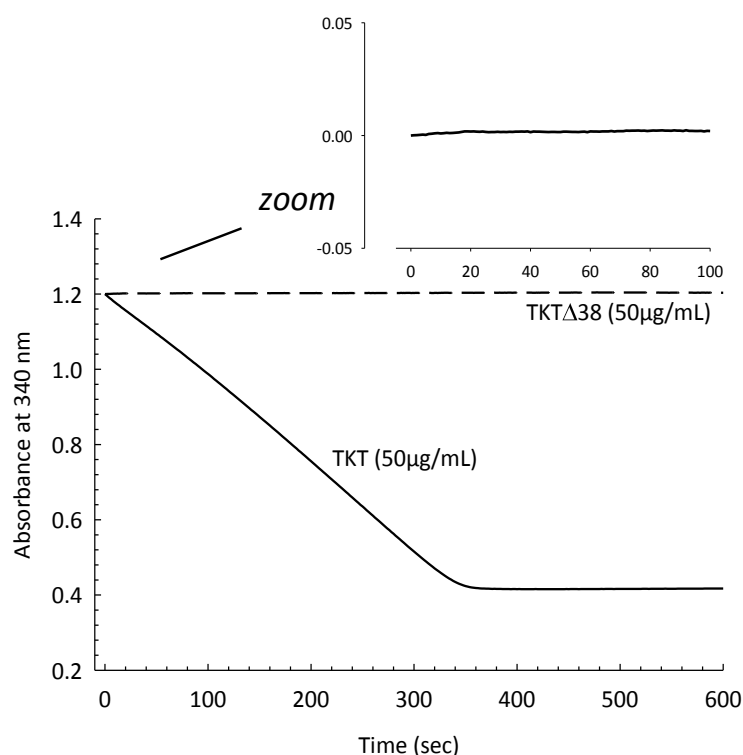


Figure 19: Steady-state kinetic of enzymatic activity of native TKT as well as the TKT Δ 38 variant. Conversion of native substrates X5P and R5P (2 mM each) to S7P and G3P which is linked to the consumption of NADH was monitored at 340 nm. No enzymatic activity could be detected for the TKT Δ 38 variant.

3.1.4 Analysis of cofactor binding competence of $\Delta 38$ TKT by near-UV CD spectroscopy

Binding of the ThDP cofactor to TKT $\Delta 38$ as well as TKT was analyzed to address the question, whether the lack of enzymatic activity in the deletion variant is caused by imprecise or absent cofactor binding. All so far characterized TKTs show a characteristic absorbance pattern in near-UV CD which were assigned to different tautomerization and ionization states of the aminopyrimidine ring system of ThDP (see introduction).

TKTs reveal a broad, negative signal between 320 to 350 nm when complexed with ThDP^{100 101}. Indeed, such a negative signal at 325 nm can be detected in TKT wild type, confirming previous results^{112 113} (Figure 20). No such signal was observed in the deletion variant under the same conditions, as well as after adding a huge excess of both of the cofactors to the buffer (up to 10 mM ThDP and Ca²⁺). This outcome either corresponds to the absence of enzyme bound ThDP in the deletion variant or an affected chemical state of the bound ThDP resulting in spectroscopically silent cofactor.

To rule out that ThDP is bound in a spectroscopically silent state a ¹H NMR spectroscopic approach was used. For that purpose the enzyme is initially saturated with cofactor and transferred into cofactor-free solution. Afterwards the enzyme is precipitated by addition of an acidic solution and the enzyme-bound cofactor is liberated^{103 50}. The acid-stable ThDP can be analyzed quantitatively by ¹H NMR spectroscopy after removal of the precipitated protein. While ThDP was found after acidic treatment of full length TKT no cofactor was detected in the deletion variant (Figure 20). Summarizing both, the near-UV CD and ¹H NMR spectroscopy experiments strongly indicate that TKT $\Delta 38$ is unable to bind the ThDP cofactor.

3. Results

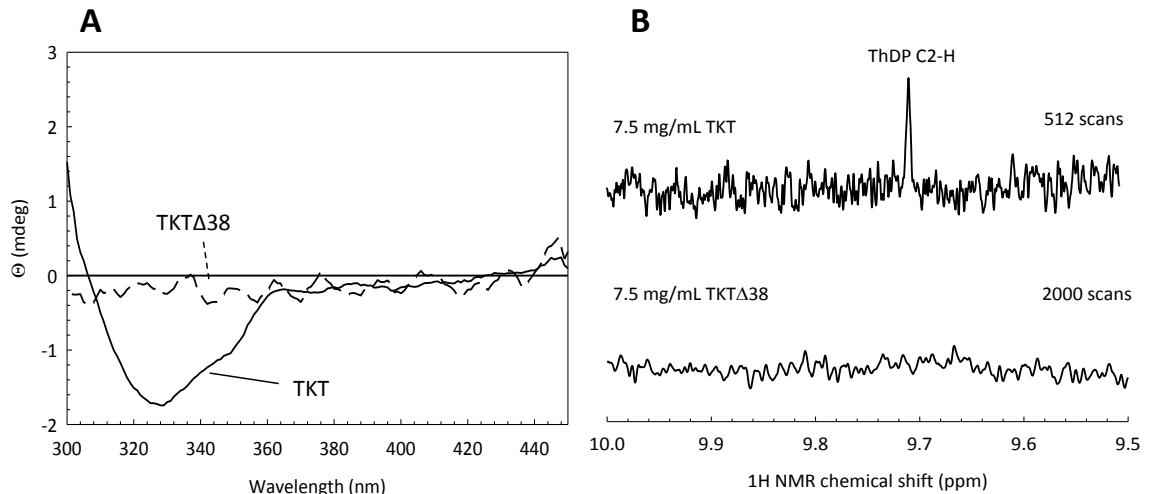


Figure 20: Cofactor binding analysis by near-UV CD and ^1H NMR spectroscopy in full length TKT and the TKT Δ 38 deletion variant. (A) Near-UV spectra analysis of TKT and TKT Δ 38 at a concentration of 2 mg/mL enzyme in glycyl Glycine buffer, pH 7.6 containing 500 mM NaCl. Noteworthy is the missing absorption at 320 nm for TKT Δ 38. (B) ^1H NMR spectroscopic analysis of supernatant obtained after acid quench treatment of TKT and TKT Δ 38. Shown is the downfield section of the NMR-spectrum (10-9.5 ppm). Within this range a signal is located at \sim 9.705 for TKT which can be assigned to the C2-H of the thiazolium portion of the ThDP cofactor. No corresponding signal was detected in TKT Δ 38 deletion variant.

3.1.5 Analysis of the oligomeric state of TKT and TKT Δ 38 by analytical gelfiltration

Another possible explanation for the absence of enzymatic activity in the deletion variant could be its inability to form the catalytically active homodimer. To address this question analytical gel filtration experiments were performed with native TKT and TKT Δ 38.

Both proteins elute in a single peak, reflecting one dominant oligomeric state in each case (Figure 21). The difference in the retention time of the deletion variant is considerably affected, which results in a retention time not corresponding to a putative mass difference of 4 kDa as it was expected for the TKT Δ 38. Native TKT shows a mass of 135 kDa (theoretical M_r for the expected homodimer \sim 125 kDa). The observed mass of the deletion variant was with 70 kDa significantly lower indicating that TKT Δ 38 exists mainly as monomer (theoretical M_r \sim 64 kDa).

It can be concluded that the deleted 38 amino acids do not only impair cofactor binding but also the formation of the catalytic active dimer of TKTs.

3. Results

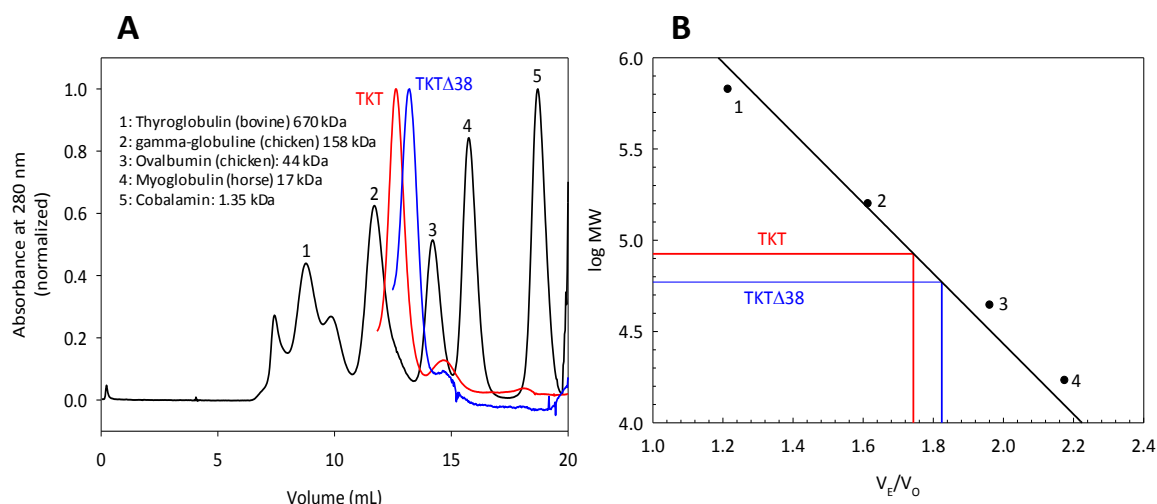


Figure 21: Analytical gel filtration experiments of full-length TKT and TKTΔ38. (A) Elution profiles of a protein standard mixture, native TKT and TKTΔ38 (detected at 280 nm). **(B)** Plot of log molecular weight (MW) versus V_E/V_0 (V_E elution volume, V_0 void volume).

3.2 Phosphoketolase of *B. breve*

3.2.1 Expression and purification of wt XFPK and active site variants

Wild-type XFPK and several active site variants (H64A, H97A, H142A, H320A and H553A) were expressed as C-terminal hexahistidine fusion proteins and purified stepwise by immobilized metal ion affinity chromatography (IMAC), ion exchange chromatography (IEX) and size exclusion chromatography (SEC) as previously described. For all of these variants a decrease or even loss of activity has been reported, highlighting the importance of the respective histidines for XFPK catalysis⁸⁰.

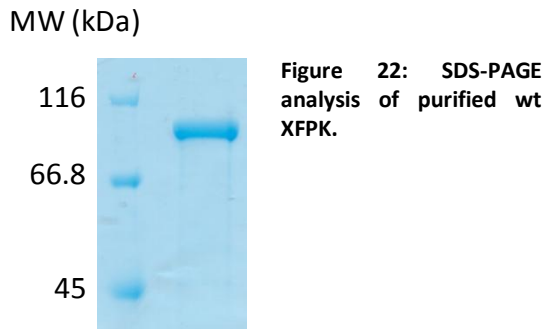
Table 3: Kinetic parameters of active site variants of XFPK.

Adapted from to Suzuki *et al.* (2010), (NA no activity).

variant	k_{cat} (min^{-1})	$K_{M\ app}$ (F6P)	$K_{M\ app}$ (Pi)	T_m (K)
wt	1540 ± 60	9.7 ± 0.3	1.2 ± 0.2	319.5
H64A	NA	NA	NA	327.5
H97A	NA	NA	NA	313.5
H142A	12.2 ± 0.9	7.4 ± 0.6	1.7 ± 0.2	314.5
H320A	NA	NA	NA	319.9
H553A	NA	NA	NA	315.9

3. Results

All proteins could be purified to homogeneity in miligram scale (up to 200 mg from a 20 g cell pellet). The His-tagged enzymes consist of 845 amino acids with a predicted molecular weight of 94.9 kDa. As it can be seen in Figure 22 the wild-type shows an estimated size as predicted (for SDS-PAGE analysis of the variants see appendix).



3.2.2 Secondary structure and thermal stability of wt XFPK and variants

To analyse the influence of amino acid exchanges in the active site on the thermodynamic stability, far-UV CD spectra were collected for all purified proteins. XFPK wt and the variants show a typical far-UV spectra as it can be expected for an (α/β)-protein (see appendix). The only exception was the H142A variant, which precipitated during CD experiments (at 20 °C). This is an unexpected finding since kinetic characterization and crystallization of this variant was previously successful⁸⁰.

Next, thermal unfolding was used to elucidate the stability of wt and variants. This process turned out to be irreversible for all characterized XFPK variants. As it can be seen in Figure 23 thermal unfolding followed a one phase transition, with the transition point located at ~319.5 K for the wild-type. All variants except H64A have a significantly decreased thermal stability (see appendix). Their transition points are in the range ~313-328 K (see Table 3). Moreover, the wild-type seems to be stable under initial conditions (20 °C) whereas the variants already start to lose secondary structure elements under initial temperature conditions 293-303 K. The low stability of H142A observed in far-UV spectra experiments is underpinned by thermal unfolding results since it shows the lowest thermal stability.

3. Results

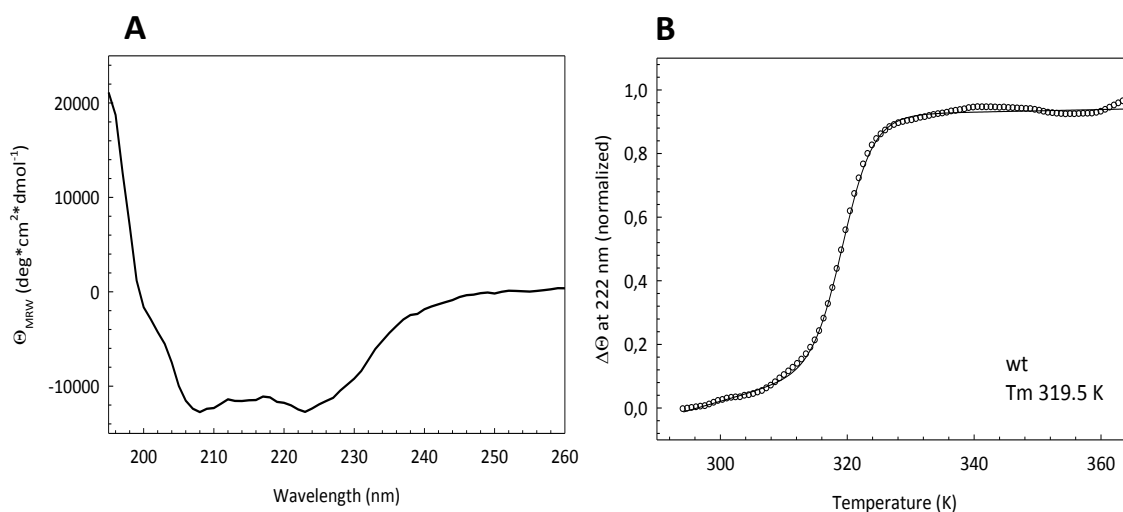


Figure 23: Far-UV spectra and thermal unfolding of wt XFPK. (A) Far-UV CD spectra of wild-type XFPK was recorded at a protein concentration of 0.1 mg/mL in 50 mM sodium phosphate buffer, pH 7.6 containing 2.5 mM MgCl₂ and 200 μ M ThDP at 20 $^{\circ}$ C. (B) Thermal unfolding of XFPK was recorded at 222 nm in the same buffer as mentioned above.

3.2.3 Analysis of enzymatic XFPK activity by discontinuous acetyl phosphate detection

Enzymatic activity of XFPK was analyzed by detecting the formation of the acetyl phosphate derived chromophoric complex hydroxamate as described earlier^{104 80}. The observed kinetic parameters for donor substrate F6P resembled those, that have previously been published (K_M 24.6 \pm 4.3 mM and k_{cat} 18.6 \pm 1.3 s $^{-1}$) (see Table 3) (Figure 24) Determination of kinetic constants for the alternative donor substrate X5P could not be performed, since this sugar phosphate was not available.

3. Results

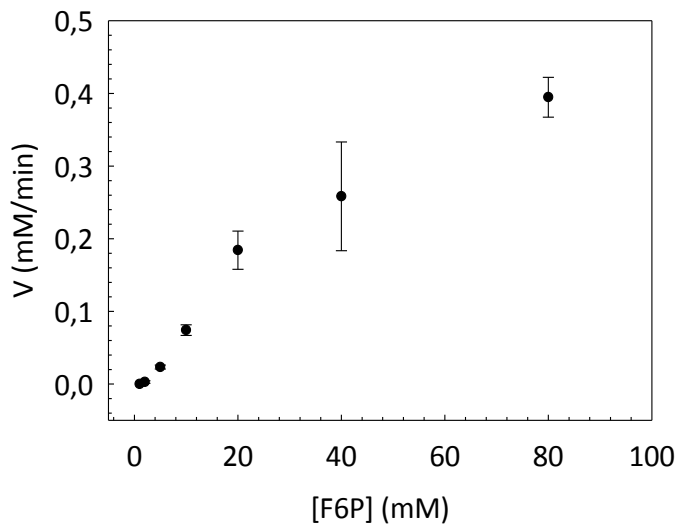


Figure 24: Dependence of the reaction rate of wt XFPK on the F6P concentration. Rate constants of substrate dependent acetyl phosphate formation were plotted according to the Michaelis-Menten equation. K_M 24.6 ± 4.3 mM and k_{cat} 18.6 s^{-1} were decreased in comparison to previously published results.

Given that the detection of acetyl phosphate by the hydroxamate assay mentioned above is a time consuming and error-prone method to determine kinetic parameters of XFPK, an isothermal titration calorimetry (ITC) based method was established. ITC is commonly used to quantitatively characterize interactions between biomacromolecules or other compounds^{114 115}. Moreover, ITC was adopted as a suitable tool for characterizing enzyme kinetics which is in particular interesting in cases where no suitable assay is available^{116 106 117}. In two different experimental setups the kinetic parameters K_M and V_{max} can be obtained. The first experiment is the successive titration of substrate into the ITC cell containing the enzyme. After each injection the steady-state corresponding to the respective substrate concentration is established, resulting in a shift of the baseline that corresponds to the current reaction rate. This allows the detection of reaction rates at different substrate concentrations in one single titration experiment and thus the direct determination of K_M ¹⁰⁶. To determine V_{max} the amount of substrate that is consumed over time (ΔP in $\mu\text{M}/\text{sec}$) must be calculated from the total heat over time (ΔH in $\mu\text{cal}/\text{sec}$) (see appendix). Therefore, the molar enthalpy of the reaction ΔH_{app} is calculated from the heat, which is generated after injection and complete conversion of a distinct amount of substrate to the enzyme.

3. Results

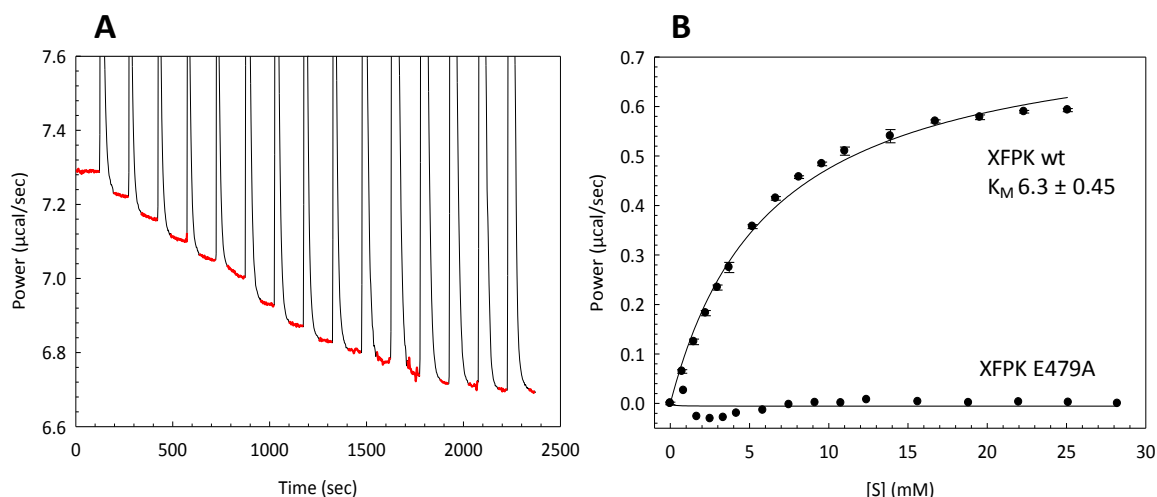


Figure 25: ITC detected heat release during wt XFPK driven F6P cleavage. (A) 525 nM XFPK in 20 mM HEPES (pH 7.2) containing 1 mM $MgCl_2$, 50 mM Na_2HPO_4 and 200 μM ThDP were incubated for 2 min at 25 °C in the ITC cell until thermal equilibrium was established. Afterwards, successive injections of 5 times 0.5, 5 times 1 and 5 times 2 μL of 350 mM F6P were performed every 150 seconds. (B) Integrated signals of the pseudo-first order reactions (red baselines in Figure A) plotted against the used substrate concentration. By this the K_M can be obtained directly (6.3 mM). The catalytically inactive variant E479A served as negative control.

As depicted in Figure 25 after initial thermal equilibration, injections of F6P to XFPK lead to a significant release of heat (decrease of instrumental power) demonstrating that the cleavage of F6P into acetyl phosphate and E4P is an exothermic reaction. To estimate the reaction rate, the difference between the initial baseline and the respective baselines after each single injection step were determined. A fit of the released power over time in dependence on the substrate concentration gives rise to K_M which was determined by fitting the data according to Michaelis-Menten equation (K_M 6.3 ± 0.45 mM). This is in fair agreement with previously published data (9.7 mM) and proves the applicability of the ITC-based assay.

To characterize all kinetic parameters of XFPK according to equations 4-7 (see appendix), the apparent enthalpy ΔH_{app} was determined. This was performed by titrating substrate with a final concentration of 3 mM to the enzyme (5.3 μM) and recording of complete turnover. After the baseline has returned to its origin another titration was performed to elucidate if the product inhibits the reaction. As depicted in Figure 26 after a first injection the substrate becomes totally consumed resulting in an over all heat release of ~ 4360 cal/mol (for calculations see appendix). A second and third titration did not lead to a comparable amount of heat release which is presumably caused by product inhibition as it was previously reported for XPKs⁸¹. To validate this assumption, single

3. Results

injection experiments were performed with increasing amounts of F6P (0.3-30 mM). In theory the released heat per mole substrate should be independent of the used substrate concentration. While this assumption holds true for F6P concentrations up to 3 mM (~4200-4400 kcal/mol) we observe significant deviations at higher concentrations (~1800-3200 kcal/mol) (Figure 26).

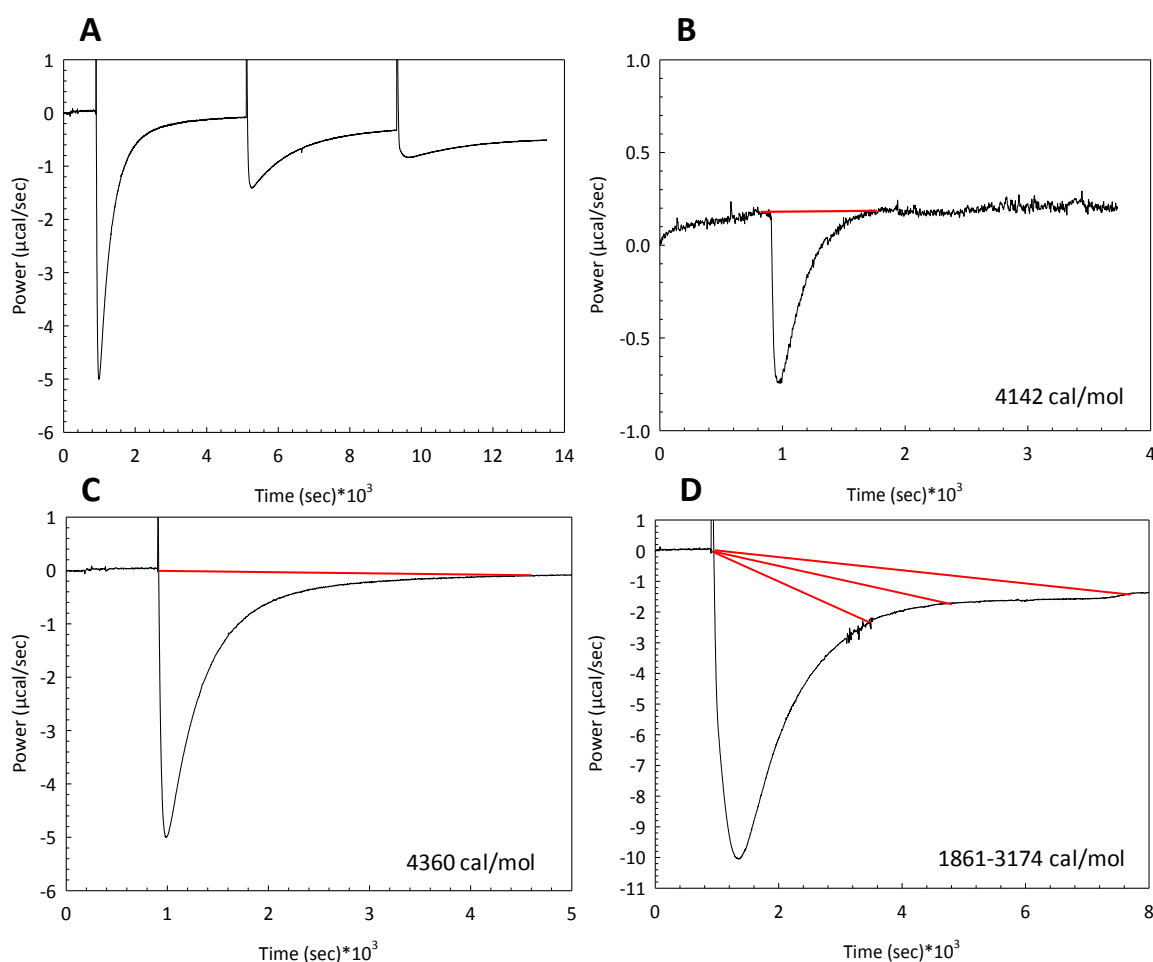


Figure 26: Determination of apparent enthalpy (ΔH_{app}) by complete substrate conversion. (A) Injection of 1.3 μL of a 350 mM F6P solution into the ITC cell (final concentration 3.11 mM) containing 5.3 μM XFPK in 20 mM HEPES (pH 7.2), 1 mM MgCl_2 , 50 mM Na_2HPO_4 and 200 μM ThDP. F6P cleavage was monitored until the original baseline value was reached. A second and third titration of substrate gave not the same amount of heat release. (B) Injection of 1.3 μL of a 35 mM F6P solution into the ITC cell (final concentration 0.31 mM) containing 5.3 μM XFPK in 20 mM HEPES (pH 7.2), 1 mM MgCl_2 , 50 mM Na_2HPO_4 and 200 μM ThDP. F6P cleavage was monitored until the original baseline value was reached. The integral of the thermogram corresponds to a heat release of 4124 cal/mol. (C) Injection of 1.3 μL of a 350 mM F6P solution into the ITC cell (final concentration 3.11 mM) containing 5.3 μM XFPK in 20 mM HEPES (pH 7.2), 1 mM MgCl_2 , 50 mM Na_2HPO_4 and 200 μM ThDP. F6P cleavage was monitored until the original baseline value was reached. The integral of the thermogram corresponds to a heat release of 4360 cal/mol. (D) Injection of 13 μL of a 35 mM F6P solution into the ITC cell (final concentration 31 mM) containing 5.3 μM XFPK in 20 mM HEPES (pH 7.2), 1 mM MgCl_2 , 50 mM Na_2HPO_4 and 200 μM ThDP. F6P cleavage was monitored for over 2 hours. The baseline did not return to its origin and integration of the thermogram values between 1861 and 3174 cal/mol depending on the end point selection. (Baselines of integration are shown in red).

3. Results

This restriction makes the ITC method not useful for a complete kinetic characterization of XFPK but a rough estimation of K_M is still accessible (due to product inhibition K_M is also decreased; therefore derived data have to be discussed with caution).

ITC was applied to elucidate whether XFPK is able to convert the seven-carbon sugar phosphate S7P, an intermediate of the PPP (see section 1.2). The analysis of this titration experiment revealed that S7P is not converted by XFPK. Last the different oligomeric fractions of XFPK were analyzed for catalytic activity (Figure 27). It was reported that only the homohexameric fraction of XFPK shows significant activity⁸⁰. While tetramers and hexamers possess similar turnover rates and K_M , we observe a ten-fold lower affinity for donor F6P in the dimer fractions as well as a reduced but still detectable turnover (Figure 27).

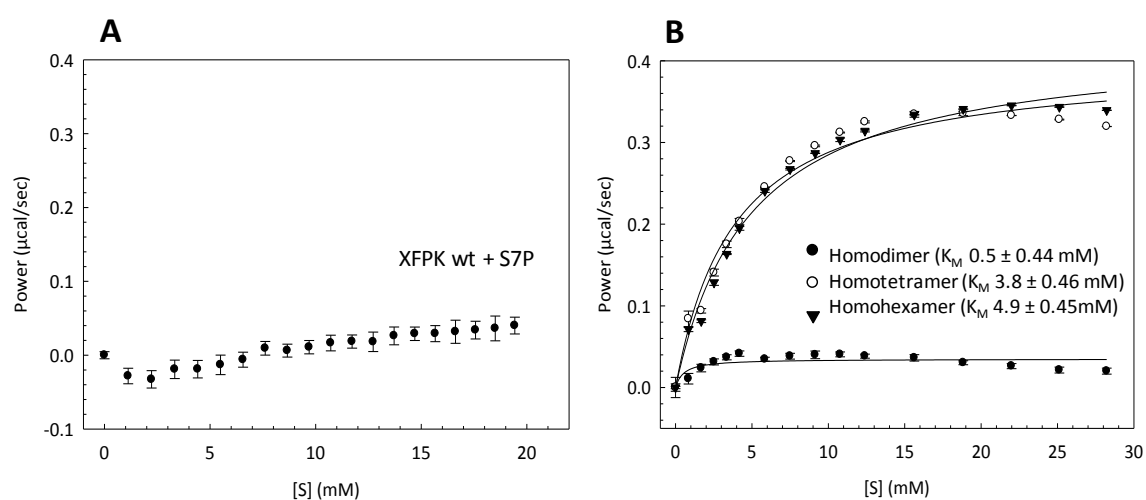


Figure 27: ITC based analysis of potential alternative substrate usage (S7P) and validation of activity of the different oligomeric states of wt XFPK. (A) 525 nM XFPK in 20 mM HEPES (pH 7.2) containing 1 mM MgCl_2 , 50 mM Na_2HPO_4 and 200 μM ThDP were incubated for 2 min at 25 $^\circ\text{C}$ in the ITC cell until thermal equilibrium was established. Afterwards 20 successive injections 2 μL of 311 mM F6P were performed every 120 seconds. (B) 525 nM XFPK monomer, dimer and trimer in 20 mM HEPES (pH 7.2) containing 1 mM MgCl_2 , 50 mM Na_2HPO_4 and 200 μM ThDP were incubated for 120 seconds at 25 $^\circ\text{C}$ in the ITC cell until thermal equilibrium was established. Afterwards 5 successive injections of 0.5, 1 and 2 μL of 311 mM F6P were performed every 120 minutes.

As XFPK is inhibited by the product erythrose 4-phosphate the kinetic analysis was restricted to the estimation of K_M . Moreover, this aspect has not been further investigated by use of the hydroxamate assay, due to its inconvenience.

3.2.4 Analysis of protonic and tautomeric equilibria of enzyme-bound cofactor of XFPK by CD spectroscopy

Since the active centers of TKT and XFPK share a high homology we expected to observe a similar spectroscopic signature for the UV-CD experiment with XFPK as previously described (section 3.1.4). However, no negative signal around 320 nm could be detected in XFPK even after addition of up to 10 fold excess of ThDP and Mg^{2+} (Figure 28). On the other hand, two signals can be seen below 300 nm, one positive signal at 290-300 nm and a negative signal at 280-290 nm. These signals have previously been assigned to different tautomerization and ionization states of the ThDP-cofactor⁴⁸. The positive signal is supposed to reflect the so called 1',4'-iminopyrimidine (IP) form of the cofactor whereas the negative signal putatively represents the 4'-aminopyrimidinium (APH⁺) state although it was described to be located at 260-270 nm (Figure 7). XFPK shows such signals even in the absence of ThDP in the buffer indicating that ThDP is tightly bound to the active center.

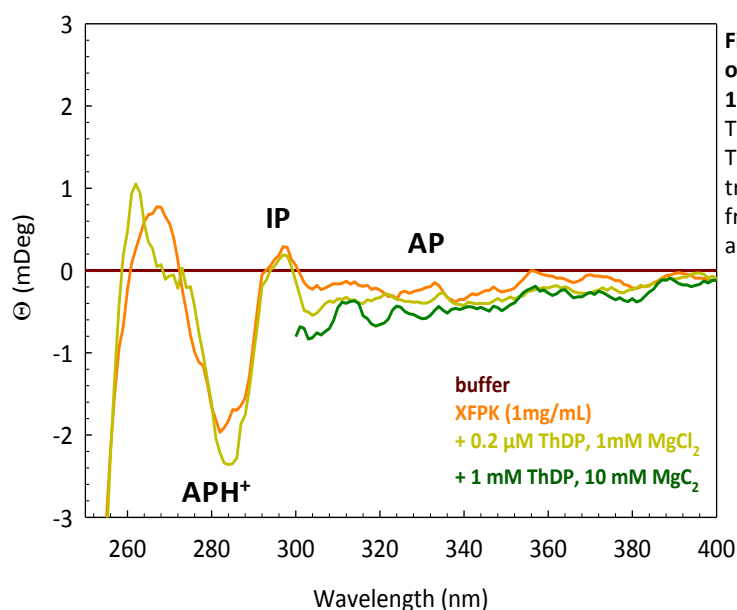


Figure 28: Near-UV spectra analysis of wt XFPK at a concentration of 1 mg/mL enzyme in Hepes (pH 7.2). The spectrum after adding 1 mM ThDP and 10 mM $MgCl_2$ was truncated below 300 nm since the free ThDP cofactor shows a high absorbance below this wavelength.

3.2.5 pH dependence of the internal tautomeric equilibrium of XFPK-bound ThDP

On the basis of CD spectra for enzyme-bound ThDP at different pH values the pK_as of AP, APH⁺ and the IP form have previously been determined for different ThDP enzymes⁴⁹. Based on these experiments it was suggested that all postulated tautomeric states exist at the active site in ThDP-dependent enzymes under physiological conditions. However, their relative abundances significantly differed among the studied proteins. To get an insight of such equilibria in XFPK-bound ThDP, pH-titration experiments in the range of pH 6-9 where performed within the present work. At higher or lower pH values the wt as well as the variants denatured.

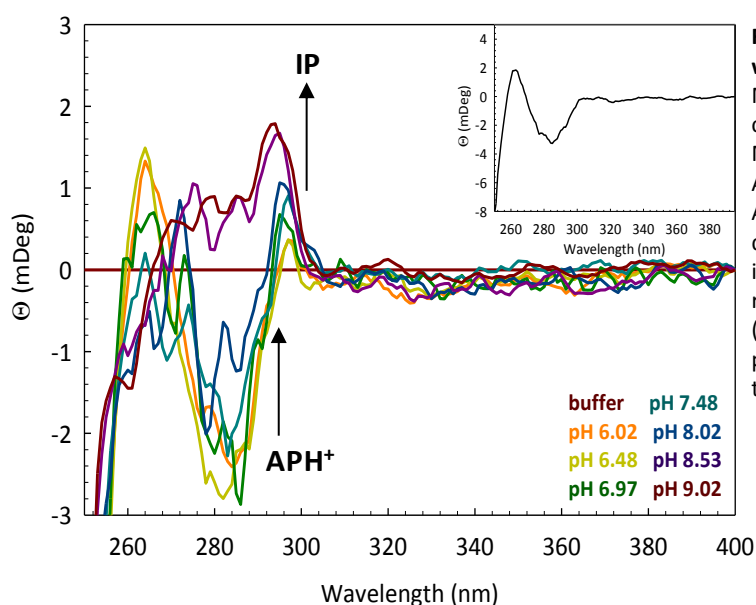


Figure 29: Near-UV spectra analysis of wt XFPK at different pH values. Measurements were performed at a concentration of 1 mg/mL enzyme in MES/PIPES/TRIS buffer (20 mM, pH 6-9). All spectra are core for volume changes. An increase of the pH-value leads to a decrease of the APH⁺ signal and an increase in the IP signal. The insert (top right) shows the difference spectra (spectrum at pH 6.02 minus spectrum at pH 9.02) reflecting the overall change in the wavelength range below 300 nm.

Increasing the pH value of the buffer leads to depletion of the APH⁺ signal and an accumulation of the IP signal (Figure 29). This is an expected finding since the addition of hydroxyl ions should lead to deprotonation of the APH⁺ form. An AP derived signal is undetectable although the presence of this tautomer was expected under low pH conditions⁴⁹.

Titration experiments performed with the active center histidine variants were not that conclusive (see appendix). Although a slight comparable tendency as described for the wild type could be detected, it seems that transferring the variants into cofactor-free

3. Results

buffer leads to the formation of apo-enzyme and a loss of CD signal. This finding indicates the importance of each active site histidine for cofactor binding.

3.2.6 Analysis of covalent reaction intermediates in XFPK formed during F6P conversion by ^1H NMR spectroscopy

It is still questionable, whether the AcThDP intermediate is formed directly during XFPK mediated donor conversion, or if dehydration of the DhETHDP intermediate and nucleophilic attack of phosphate takes place in a concerted manner (see section 1.5.3). To address this question ^1H NMR spectroscopy was performed. For that purpose the reaction was either carried out in presence of F6P alone, or with F6P and phosphate, the two native substrates of XFPK.

In absence of phosphate two distinct NMR signals at 7.36 and 7.37 ppm can be detected, which are specific for the AcThDP intermediate as reported earlier (Figure 30)⁸². Moreover, a multiplet signal centered at 6.39 ppm can be detected which was assigned unambiguously to the methylene bridge of the carbinolform of AcThDP. This species has a characteristic coupling constant of 16 Hz⁸². Contrary, when XFPK was incubated with F6P and phosphate the only detectable signal at 7.31 ppm which is specific for DhThDP¹⁰³. Whether AcThDP is indeed an intermediate of this reaction or just an artificial “dead-end” product which is formed in absence of substrate phosphate could not be answered yet. NMR measurements of the variants could not be performed to a greater extent. Preliminary results for the histidines 64, 97 and 320 can be found in the appendix. The histidines 97 and 320 show no ThDP-signal, indicating the formation of apoenzyme while transferring the enzymes into cofactor-free buffer. The histidine 64 variant shows characteristic signals for ThDP-intermediates, but they could not be allocated to a distinct species, since the ThDP seems to have lost its phosphate anchor (which leads to formation of several signals in the intermediate-region of the NMR-spectra).

3. Results

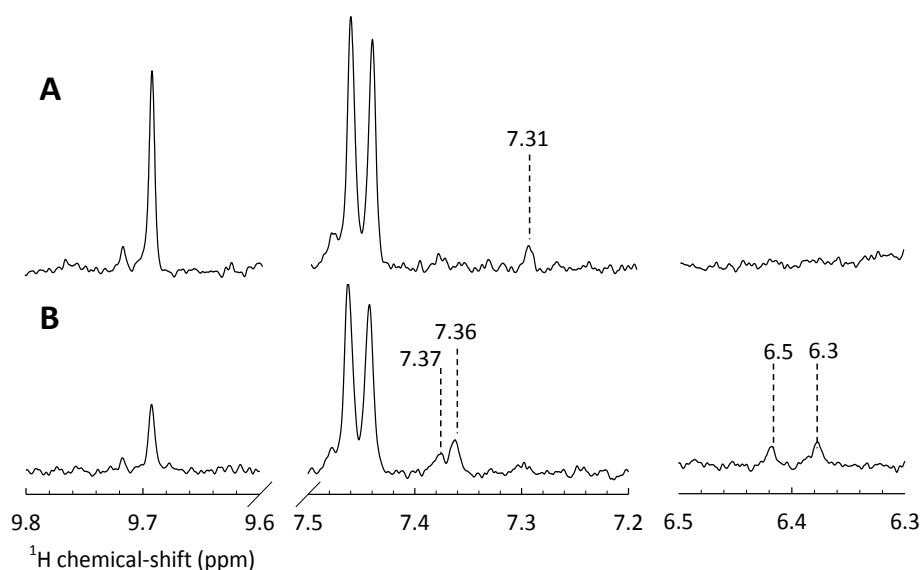


Figure 30: Analysis of intermediate generation after wt XFPK driven conversion of F6P by ¹H NMR spectroscopy. (A) Addition of F6P and phosphate leads to generation of DhThDP as detectable intermediate at 7.31 ppm. (B) Incubation of XFPK with F6P only leads to generation of AcThDP, whose signals can be detected at 7.36 and 7.37 ppm, respectively. Moreover, an AcThDP-specific multiplet centered at 6.4 ppm with a coupling constant of 16 Hz is observable.

3.2.7 Analysis of intermediate formation in the course of XFPK mediated catalysis by stopped-flow UV/vis absorbance spectroscopy

3.2.7.1 Kinetic analysis of XFPK-driven F6P conversion

To resolve F6P conversion by XFPK in more detail we performed rapid mixing, single-jump stopped-flow experiments with UV/vis detection. It was shown for *E.coli* TKT that F6P addition leads to a significant absorption spectrum with a maximum between 295-305 nm and between 320-335 nm¹¹³. It is supposed that these signals correspond to the IP (295-305 nm) and the AP (320-335 nm) state of the aminopyrimidine moiety of ThDP. First, stopped-flow experiments were performed with different F6P concentrations in the absence of phosphate to visualize the spectral signature of intermediates in XFPK. We could not detect any absorbance signal below 400 nm in a Jasco spectrophotometer (data not shown) or in the stopped-flow device. Unexpectedly, a positive absorption signal centered at 420 nm could be detected (Figure 31). While such red-shifted absorbance signals have yet been detected in several ThDP-dependent enzymes¹¹³ this is the first observation of such an intermediate derived signal in any XFPK. Diederichs

3. Results

and Lüdtke clearly assigned the molecular origin of this signal in *Ec*TKT using fast kinetics and NMR-spectroscopy. In *Ec*TKT this red-shifted, broad signal is generated by the DhEThDP intermediate (personal communication Dr. Stefan Lüdtke). In our experiments the signal strength at 420 nm increases with increasing substrate concentrations. These results indicate that spectral signatures of the formed intermediate are not unique to TKT and can also be found in other ThDP-dependent enzymes. It is still questionable whether the detected signal corresponds indeed to DhThDP, or AcThDP but our NMR results suggest this species to be the latter.

For the conversion of F6P and phosphate with transiently formed AcThDP no signal at 420 nm could be detected suggesting that this intermediates' longevity is too short to be resolved by our experimental setup.

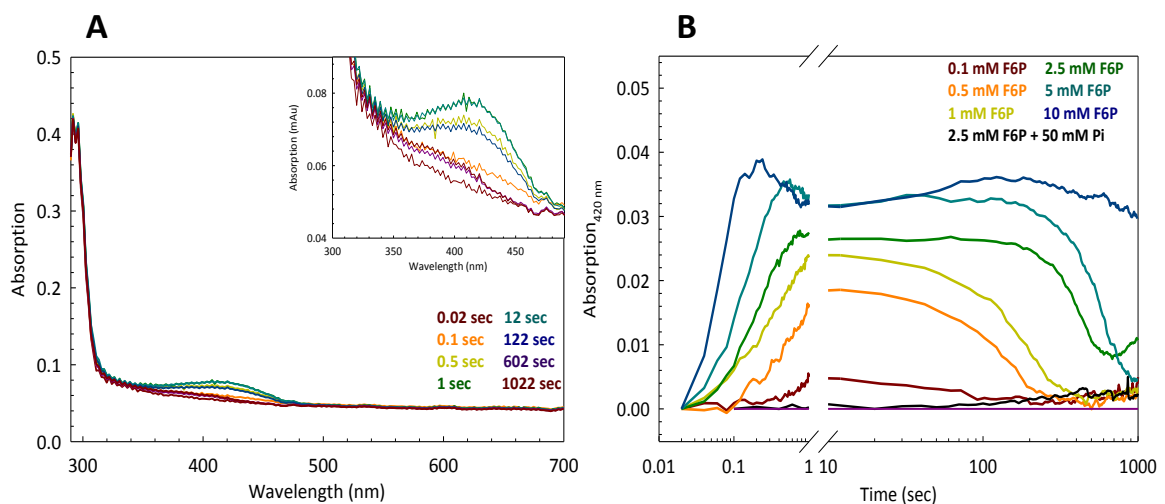


Figure 31: Stopped-flow absorbance spectra of F6P conversion by wt XFPK. (A) Photo diode array (PDA) spectra of XFPK in 20 mM HEPES (pH 7.2) containing 1 mM MgCl₂ and 200 μM ThDP after addition of 2.5 mM F6P at 25 °C in a stopped-flow spectrometer with a pathlength of 10 mm. Inset: zoom into the region 300 to 500 nm. **(B)** Time resolved PDA spectra of XFPK in 20 mM Hepes (pH 7.2) containing 1 mM MgCl₂ and 200 μM ThDP after addition of increasing F6P concentrations and phosphate.

Both kinetic phases (formation and depletion) of the 420 nm signal were fitted according to a first order exponential equation (Figure 32). By fitting the obtained rate constants with a hyperbolic equation, k_{\max} could be determined with $77 \pm 11 \text{ s}^{-1}$ and K_{sapp} with $44.6 \pm 10 \text{ mM}$.

3. Results

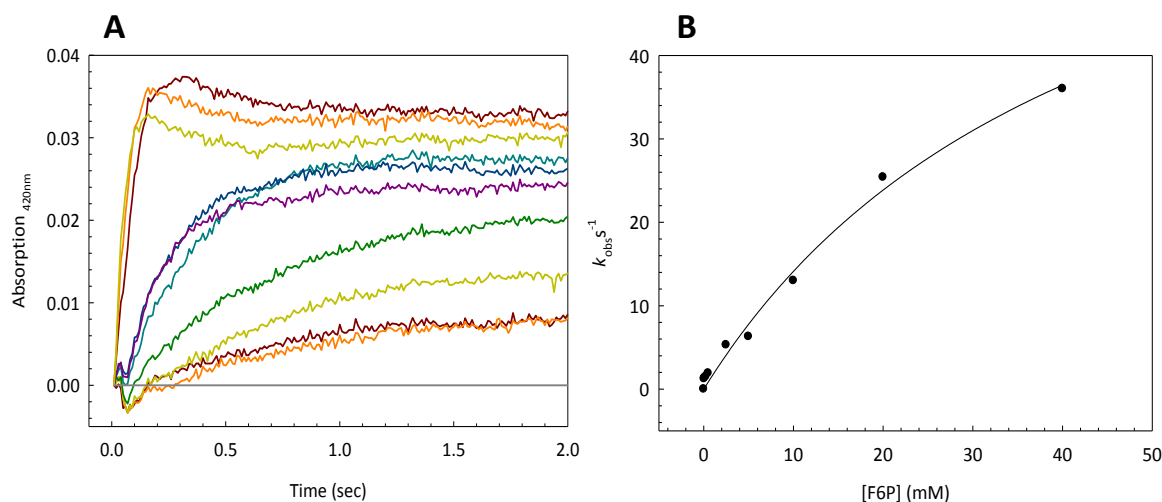


Figure 32: Time resolved PDA spectra of wt XFPK driven F6P conversion. (A) First phase of F6P conversion by XFPK in 20 mM HEPES (pH 7.2) containing 1 mM $MgCl_2$ and 200 μM ThDP at 25 °C in a stopped-flow spectrometer with a pathlength of 10 mm. (B) Obtained rate constants for formation of the intermediate plotted against the different F6P concentrations giving rise to k_{max} with $77 \pm 11 s^{-1}$ and K_{sapp} with $44.6 \pm 10 mM$.

While applying this experimental setup on the different histidine variants it seems that they are unable to generate this absorption pattern in presence or absence of phosphate (see appendix). Only the H142A variant, which was reported to show slight catalytic activity, gives rise to a weak signal. Since the residues have been described as important for generation of the DhThDP or the AcThDP-intermediate it is most likely that the observed signal can be assigned to the enol-form of the latter. In this regard the depletion of the spectroscopic signal can be deduced to the slow tautomerization of the enolAcThDP followed by hydrolysis with water as previously described for AcThDP if no phosphate is present⁸³.

3.2.7.2 Reaction of XFPK-bound ThDP-intermediate with phosphate

In order to analyze the reactivity of the XFPK bound intermediate towards phosphate a double-jump stopped-flow experiment was performed. After initial mixing of XFPK and F6P, the putative enolAcThDP intermediate was generated. In the second mixing step the so formed enzyme bound species was mixed with phosphate and the reaction was monitored at 420 nm by UV/vis stopped-flow spectroscopy (Figure 33). Addition of phosphate causes a rapid signal/intermediate depletion within less than 50 ms at a concentration of 3 mM phosphate (red curve). All curves were fitted according to a first order single exponential equation. With increasing phosphate concentrations this

3. Results

process accelerates and reaches a rate constant of $> 400 \text{ s}^{-1}$ for 25 mM phosphate (blue curve). The plotted rate constants do not follow a hyperbolic behaviour, and k_{max} is not reached at 25 mM F6P (~ 20 fold K_M of F6P).

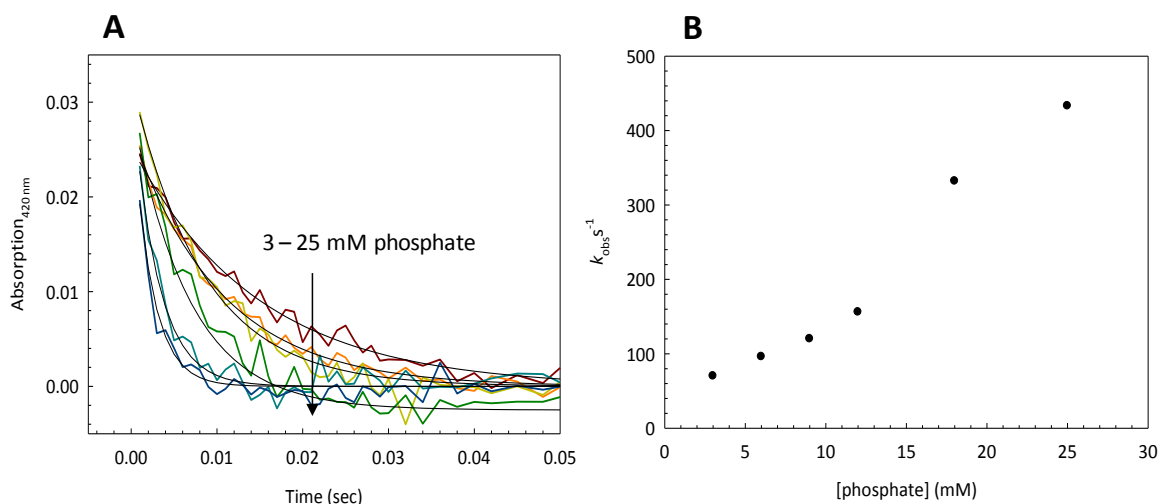


Figure 33: Rapid mixing experiment of wt XFPK bound enolAcThDP with the second substrate phosphate. (A) Sequential stopped-flow experiment with XFPK (2.5 mg/ml) in 20 mM HEPES (pH 7.2) containing 1 mM MgCl_2 and 200 μM ThDP mixed with increasing F6P concentrations at 25 °C. Addition of phosphate was performed in a stopped-flow spectrometer with a path-length of 10 mm and at a temperature of 25 °C. Spectra were fitted according to a single exponential equation first order giving rise to the respective rate constants. (B) Plotting of the first order rate constants against the utilized concentration of F6P.

3.2.8 ^1H NMR spectroscopic H/D exchange experiments to verify the presence of the enol form of AcThDP

To clearly assign the chemical state of the intermediates that are formed during conversion of F6P by XFPK and to better understand their formation ^1H NMR spectroscopical experiments were performed. In brief, when incubating XFPK with F6P, the enzyme converts this donor substrate and E4P will be released while an enzyme bound two carbon fragment (DhEThDP) remains bound to the active site. Dehydration by a yet unknown mechanism yields AcThDP. Our previous experiments implicated that this species dynamically change between ketoAcThDP and enolAcThDP. In case the reaction of XFPK and F6P will be carried out in heavy water the deuterium from the latter would be incorporated continuously into the methyl group of AcThDP yielding a mixture of deuterated species ($-\text{CH}_3$, $-\text{CH}_2\text{D}$, $-\text{CHD}_2$ and $-\text{CD}_3$). Given that AcThDP is depleted by non-enzymatically hydration and subsequent release of acetate this allows

3. Results

for an analysis of this product by ^1H NMR spectroscopy. Deuterated acetate is spectroscopically silent whereas acetate gives a strong signal at 1.93 ppm.

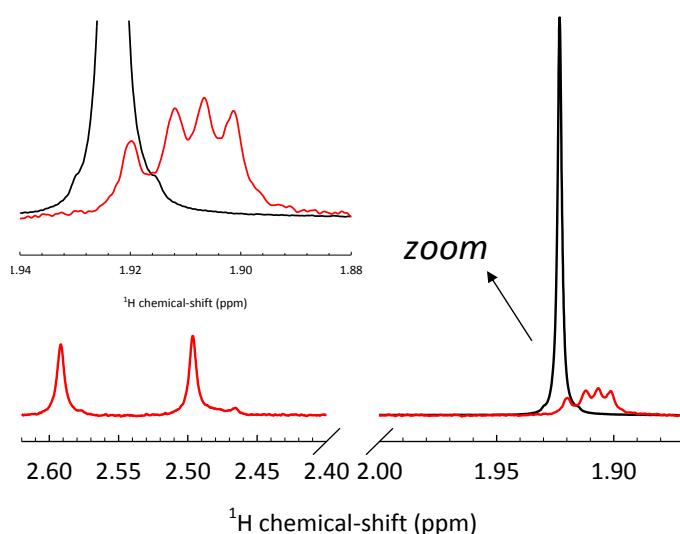


Figure 34: ^1H NMR spectroscopic analysis of produced acetate after wt XFPK driven conversion of F6P in absence of phosphate. Generated acetate can be clearly detected at 1.93 ppm in aqueous solution (black graph). The same experiment performed in deuterium oxide leads to almost full depletion of the signal, due to spectroscopically silent, incorporated deuterium (red graph). The residual multiplet at 1.92-1.93 ppm can be assigned to incomplete deuterated acetate.

As shown in Figure 34 a distinct signal for the methyl group of acetate can be detected after incubation of XFPK with F6P in the absence of phosphate (1.92-1.93 ppm). Performing the same experiment in deuterium oxide, a small residual peak can be detected at the position of the former acetate signal. But moreover a multiplet is visible ~ 0.015 ppm highfield shifted from the methyl-group signal. This multiplet can be assigned as incomplete deuterated acetate ($-\text{CHD}_2$ and $-\text{CH}_2\text{D}$ whereas complete deuterated acetate is spectroscopically silent. The two peaks at ~ 2.5 and 2.6 ppm correspond to the methyl groups located at the thiazolium- and the aminopyrimidine ring of the cofactor. Those signals served as internal standard. These experiments demonstrate that enzyme bound AcThDP indeed changes between the keto and enol form when bound to the active site of XFPK. If this process might have an importance for the reactivity of the intermediate and for catalysis of XFPK will be discussed later.

3.2.9 Interactions of glutamate 437 with the pyrimidinium ring of ThDP

In order to identify the catalytic function of glutamate 437, which is located atop the aminopyrimidine ring of ThDP (see introduction), this residue was exchanged by glutamine by site-directed mutagenesis (Figure 35).

3. Results

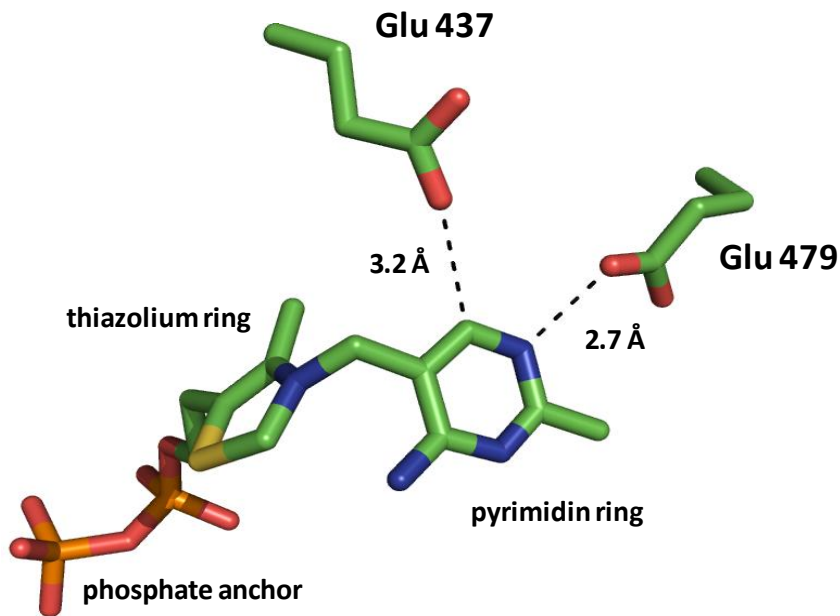


Figure 35: Location of Glu 437 atop the pyrimidinring of the ThDP cofactor. Besides, for orientation the activation Glu 479 is shown.

The variant turned out to have a comparable stability and secondary structure as the wild-type (see thermal unfolding and far-UV CD data in the appendix). Interestingly, the variant showed no activity for formation of acetyl phosphate, as verified by the hydroxamate assay and ITC kinetics even at protein concentrations of up to 2 mg/mL (Figure 36). This underlines a pivotal function for glutamate 437 during catalysis, either by stabilizing the active center of XFPK, coordinating the cofactor or by direct acid/base or electrostatic catalysis. Besides the incapability of the E437 variant to form acetyl phosphate could be confirmed in UV/vis stopped flow measurements since no signal for the putatively enolAcThDP was measurable (Figure 37).

3. Results

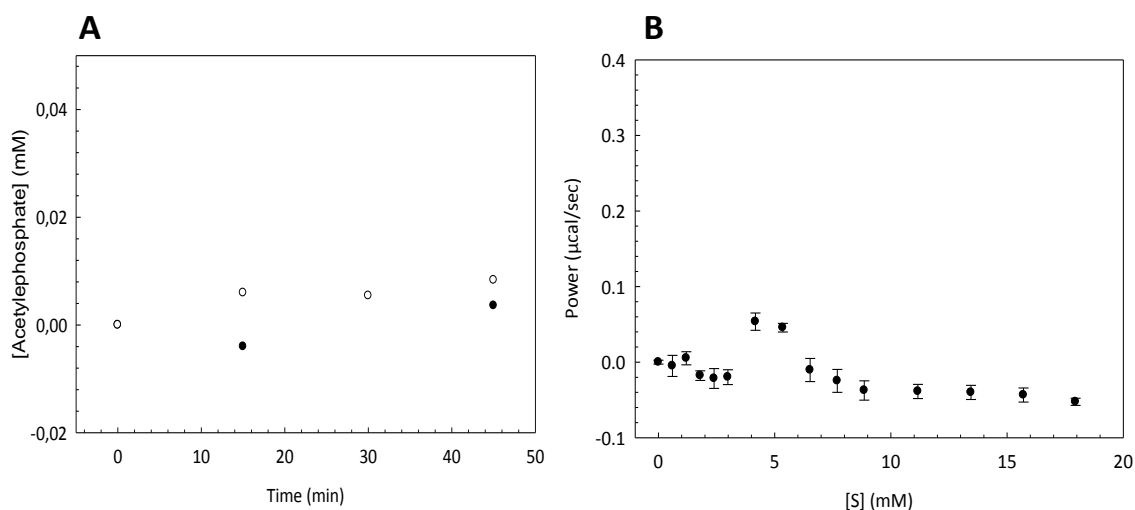


Figure 36: Catalytic activity of XFPK E437Q (A) Hydroxamate assay. 2 mg/mL XFPK E437Q in 25 mM MES pH 6.5, 0.1 mM MgCl₂ and 200 µM ThDP were preincubated with 80 mM Na₂HPO₄ and then mixed with F6P (shown are the progress curves for 0 and 80 mM). (B) 2.1 µM XFPK E437Q in 20 mM Hepes (pH 7.2) containing 1 mM MgCl₂, 50 mM Na₂HPO₄ and 200 µM ThDP were incubated for 120 sec at 25 °C in the ITC cell until thermal equilibrium was established. Afterwards 4 successive injections of 4 times 0.5, 4 times 1 and 4 times 2 µL of 311 mM F6P were performed every 150 seconds.

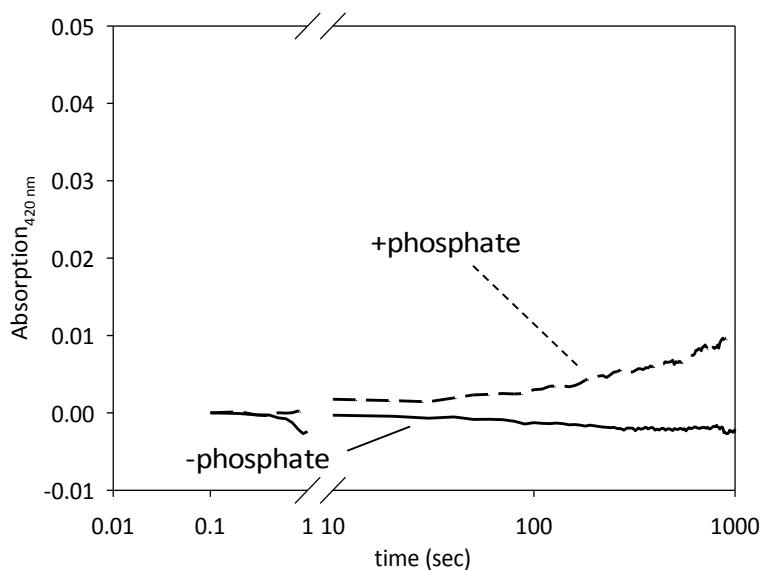


Figure 37: Time resolved PDA spectra of XFPK E437 driven F6P conversion. First phase of F6P conversion by XFPK E437Q in 20 mM HEPES (pH 7.2) containing 1 mM MgCl₂ and 200 µM ThDP at 25 °C in a stopped-flow spectrometer with a pathlength of 10 mm. Besides a slow increase of the absorption, putatively caused by precipitation, no signal of the AcThDP could be detected at 420 nm.

Near-UV pH titration experiments with XFPK E437Q revealed unique spectroscopic signatures (Figure 38). As outlined for the wild-type an increase of the pH leads to a decrease of the APH⁺ signal while the IP form of the cofactor accumulates. The variant shows already an IP specific signal at low pH values which only slightly increases at higher pH. Contrary, the APH⁺ signal shows the same spectroscopical behaviour as wt XFPK instead. It is reasonable to assume that the negative charge of glutamate 437

3. Results

influences the spectroscopic characteristics of the aminopyrimidine ring of ThDP. Especially the IP signal is obviously quenched at lower pH values. After mutagenesis against an uncharged glutamine this restriction does no longer occur and the IP signal can be detected at lower pH values already. Importantly, this is a macroscopic description of absorbance signals. The molecular origins of the alternate spectroscopic behavior after amino acid exchange in the active site of XFPK are most probably disturbed equilibria of IP, AP and APH⁺.

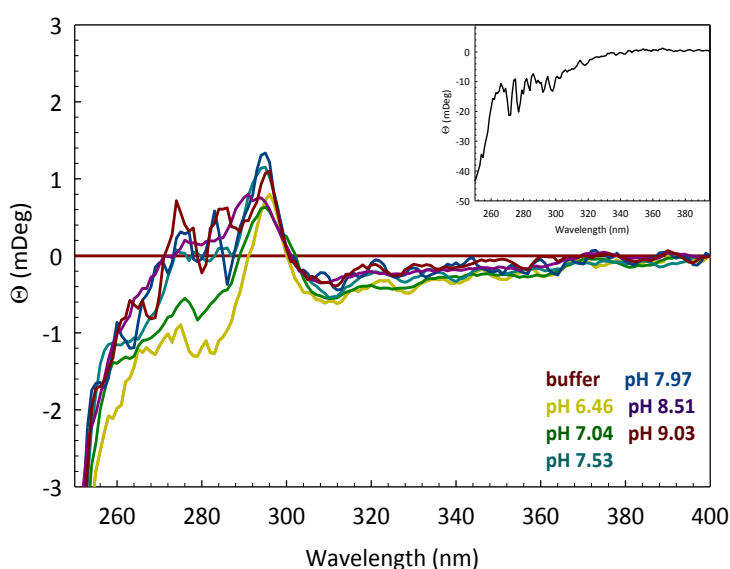


Figure 38: Near-UV spectra analysis of XFPK E437Q at a concentration of 1 mg/mL. Increase of the pH-value leads to a decrease of the APH⁺ signal. The already at low pH values present IP signal does only slightly change. Insert shows the difference spectra (spectrum at pH 6.46-spectrum at pH 9.03) reflecting the overall change of spectroscopic signals.

3.2.10 Structure of XFPK E437Q

In order to correlate our spectroscopical and functional results on the active site variant E473Q with structural information, we crystallized this protein and determined structures in the ground state as well as in complex with DHeThDP/AcThDP.

While the resting state of XFPK E437Q could be determined at a resolution of 1.48 Å, the structure of XFPK E473Q in complex with ThDP-intermediates had a resolution of 1.6 Å (Statistics see appendix). For both structures, residues 5-806 could be traced relying on 2Fo-Fc and FoFc electron density maps. The first 24 amino acids (containing the hexahistidine sequence) and the last 19 amino acids of the C-terminal domain could not be traced because of mixing electron density for these moieties of the structure. As described by Suzuki *et al.* the XFPK monomer consists of three α/β -fold domains, which have been assigned as the N-terminal PP-domain (5-378), the middle Pyr-domain (379-611) and the C-terminal domain (612-806) (see introduction). Interestingly, only the

3. Results

hexameric fractions of XFPK were able to crystallize which was also observable for this variant. As expected, both determined structures of XFPK shown here revealed that ThDP binds in its typical V-conformation to the active site, a characteristic previously described for all ThDP-dependent enzymes. Mutation of glutamate 437 has no effect on the position of the histidine residues, which are important for catalysis. In order to estimate the impact of the substitution of E437Q we superimposed the wt XFPK structure and inspected the close proximity of ThDP and residue 437. While no structural changes are observable for the cofactor as well as for active site residues, residues glutamine 437 and tyrosine 501 revealed an increased flexibility relative to the wt structure (Figure 39).

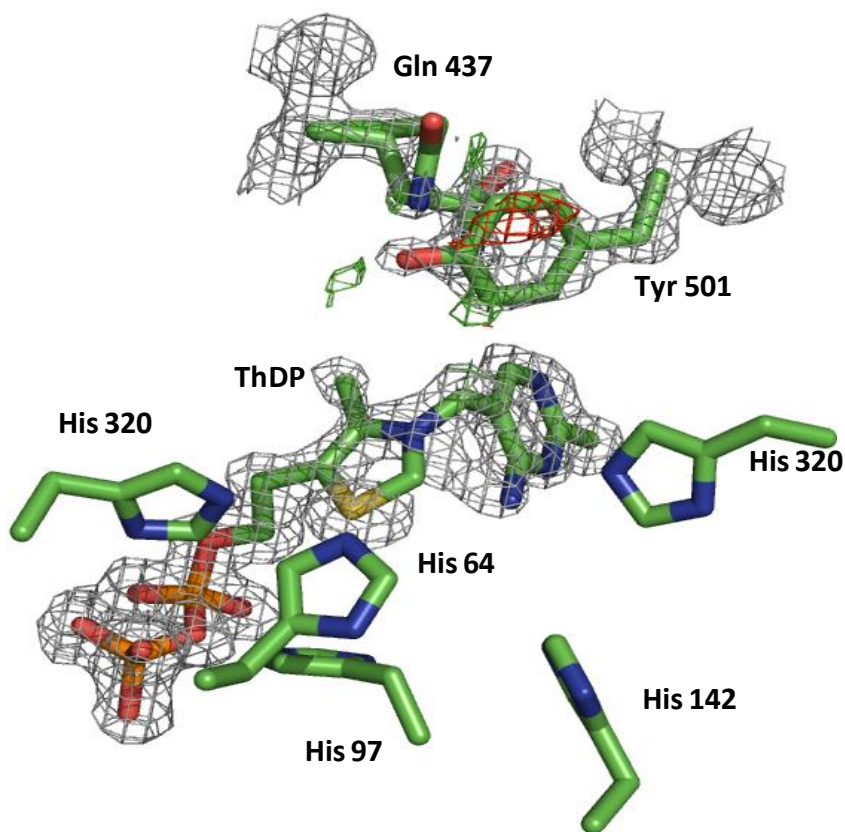


Figure 39: Electron density maps of resting ThDP in the XFPK E437Q variant. $2|F_o|-|F_c|$ omit map of the ThDP cofactor is shown. Missing electron density can be observed between the C2 and the S1 of the thiazolium ring. Beside there seems to be a connection between the C2 and the N4' of the pyrimidinring (for discussion see text). Tyr 501 and Gln 437 show a high flexibility, reflected by their undefined $|F_o|-|F_c|$ maps.

For these two residues diffuse and undefined difference electron density maps $|F_o F_c|$ are observable, that is most likely explained by different, interconverting side chain conformations (Figure 39). Tyrosine 501 was characterized as pivotal interaction partner

3. Results

for the second substrate phosphate. Interestingly, all soaking experiments of the variant with phosphate were so far not successful, strongly indicating that tyrosine 501 is indeed essential for phosphate binding and that increased flexibility of this residues impaires this process. This conclusion is in line with the unability of this variant to generate acetyl phosphate (see section 3.2.9). For glutamine 437 two alternate conformations could be traced. Another interesting observation is missing electron density for the cofactor in 2|Fo|-|Fc| simulated annealing omit map between the C2 and the S1 of the thiazolium ring and a residual electron density between the C2 and the N4' of the aminopyrimidine ring. Suzuki *et al.* reported a comparable phenomenon for the structure of XFPK H64A. They postulated ThDP to exist in a tricyclic state (dihydrothiachromine; structure see appendix)¹¹⁸. Attempts to model this tricyclic form into our observed electron density showed no good accordance (see appendix). Even a ThDP-modell with a broken covalent bond between the C2 and the S1 did not fit into our observed data (see appendix). Besides, the weak electron density for the reactive C2 atom might indicate the presence of a ThDP carbene. Carbenes are highly reactive species and possess an elctron sextet in contrast to an octet in protonated ThDP¹¹³.

In order to accumulate the intermediates, crystals of XFPK E437Q were soaked for several minutes with 54 mM F6P. Strong, additional electron density at the C2 of the thiazolium ring could be observed. Assuming that under the chosen soaking condition several covalent intermediates will be generated and that the stability of each intermediates might be different in the characterized variant we refined our structures with both post-cleavage intermediates (DHeThDP and AcThDP). Analysis of the difference electron density maps after refinements, clearly revealed the accumulation of the AcThDP intermediate (Figure 40).

3. Results

However, we observe weak residual electron density atop the sp^2 hybridised C2 α -atom indicated the presence of a small fraction DhThDP intermediate. This is in accordance to previously published data⁸⁰. These findings underpin, that glutamate 437 has impact on the coordination of the cofactor but directly influences phosphate binding in collaboration with tyrosine 501. NMR studies on the intermediate distribution of this variant could so far not be performed

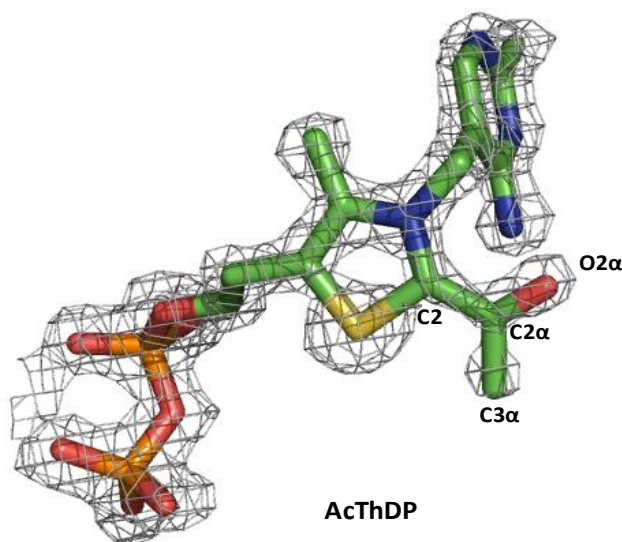


Figure 40: Electron density maps of AcThDP in the XFPK E437Q variant. 2|Fo|-|Fc| omit map of the AcThDP cofactor is shown.

3.3 Transketolase-like proteins 1 and 2

3.3.1 Recombinant expression of TKTL1 and 2 in *E. coli*

In order to functionally characterise TKTL1 and 2 in detail, high amounts of purified enzyme were needed. For that purpose two artificial gene-constructs coding for TKTL1 and 2 were designed (Uni Prot identifier: P51854 (TKTL1); Q9H0I9 (TKTL2)) and subsequently cloned into the pET-SUMO expression vector (provided by Dr. Kathrin Schröder-Tittmann [Department for Bioanalytics, Georg-August-University Göttingen]). In previous experiments using different *E. coli* strains (BL 21 star, Arctic express, SoluBL 21 SG 1309, JM 109, RIL and C600, personal communication Dr. Stefan Lüdtkke), recombinant TKTL1 and 2 expressions resulted in formation of insoluble proteins.

Solubility of the desired proteins could not be increased by lowering the temperature during expression, use of autoinduction media, adding a lower amount of IPTG or addition of up to 2 % ethanol (v/v) to induce chaperone formation. Cloning of TKTL1 and 2 into the pGEX and the pGP172 expression vector to fuse the desired proteins with

3. Results

different tags (GST and Strep) had no effect on protein solubility too (data not shown). This is a common phenomenon when expressing human proteins in *E.coli* since posttranslational modifications, needed for proper protein-folding, can not be performed. To overcome this problem it was intended to establish a eucaryotic cell based expression system.

3.3.2 Recombinant expression of TKTL1 and 2 by usage of the Bac-to-bac™ expression system

To overcome the problem of insoluble TKTL1 and 2 by use of a procaryotic expression system, the Bac-to-bac™ insect cell expression system was used. Therefore genes encoding for TKTL1 and 2 were cloned into a baculovirus genome. Baculovirus-DNA was transfected into three different insect cell cell-lines (Sf9 and Sf21 derived from *Spodoptera frugiperda* as well as Hi5 cells derived from *Trichoplusia ni*). After virus generation in transfected cells, virus particles were used to inoculate expression cultures of the named cell lines and induce TKTL1 and 2 expressions. The Hi5 cell-line turned out to be the most suitable one, due to the strongest expression of the desired proteins and was therefore used for protein expression (Figure 41). However, although expression of TKTL1 and 2 was successful in this expression system, both proteins remain in the insoluble fraction after cell lysis and centrifugation. Even after a first chromatographic purification step by IMAC (TKTL1 and 2 are fused to a hexa-histidine sequence) only trace amounts of the desired proteins were obtained as confirmed by western blotting (Figure 41).

3. Results

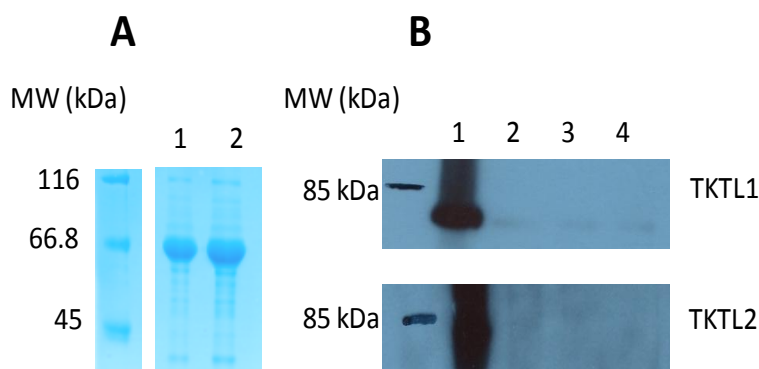


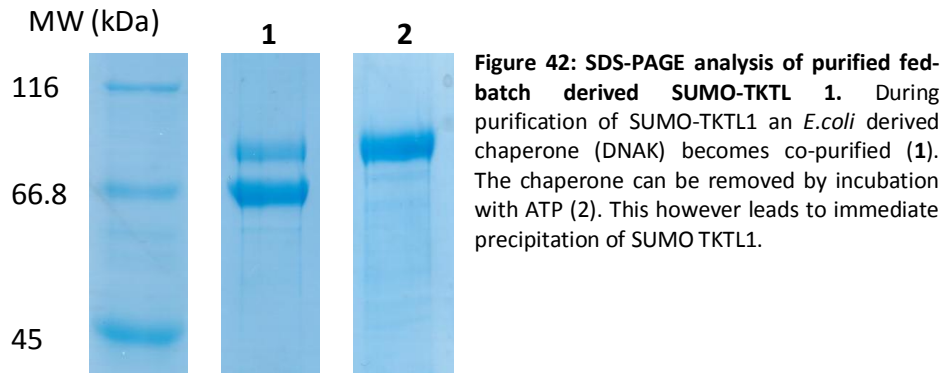
Figure 41: SDS-PAGE analysis of TKTL1 and 2 expression in Hi 5 cells. (A) Cells were lysed after 24 h and total cell lysate was analyzed for TKTL1 and 2 expression **1:** TKTL1, **2:** TKTL2. (B) Western blot analysis of recombinantly expressed TKTL1 and 2 after a first chromatographic purification step. Only trace amounts of soluble protein were obtained in both cases (<0.1 mg). The main portion of the desired proteins remained in the precipitate fraction. **1:** Pelleted fraction after centrifugation, **2:** supernatant, **3:** column flow-through, **4:** eluate fractions

3.3.3 Fed batch expression of TKTL1 and 2

Although TKTL1 and 2 turned out to be located mainly in the insoluble fraction after *E.coli* based expression in baffled flasks, slight amounts of protein could be located in the supernatant fraction (about 0.2 mg from a 20 g cell pellet). To increase the total cell mass, and by this to generate a higher amount of soluble enzyme in-total, a fed batch based expression was performed in analogy to the expression described for native human TKT. For that purpose the pETSUMO TKTL1 and 2 constructs were transformed in *E.coli* BL21 Star cells. Fermentation was performed in a Biostat C Biofermenter (Sartorius, Göttingen) as described in Section 2.8.14. Harvested cells were lysed and TKTL1 and 2 were purified using affinity chromatography. In comparison to baffled flasks expression, lysis of a higher amount of cell material (100 g cells) led to significantly detectable TKTL1 and 2 (Figure 42) in SDS-PAGE analysis after a first IMAC purification step. The amount of purified protein of interest was in the range of several milligrams (up to 2 mg per 40 g cell pellet). As can be seen in Figure 42 a double band appeared in the area of the expected mass of TKTL1 and 2. ESI-MS experiments of trypsin-digested protein samples (performed by Dr. Oliver Valerius [Departement for Molecular Microbiology and Genetic, Georg-August-University Göttingen]) revealed that the upper band corresponds indeed to TKTL1 or 2 in SDS PAGE analysis. The lower one was shown to be DnaK, a chaperone of *E.coli*, whose co-purification was described as a severe problem during recombinant expression in *E. coli*¹¹⁹. DnaK was removed by incubating

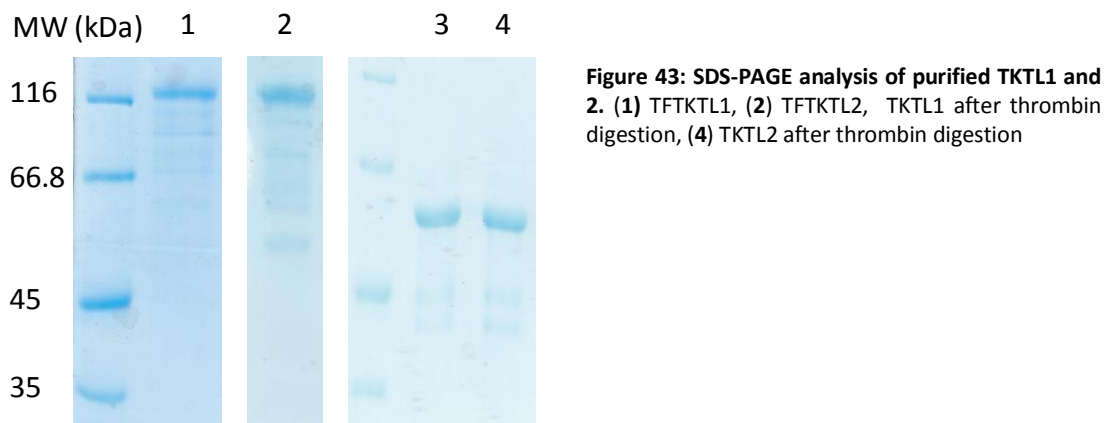
3. Results

the samples with ATP and MgCl₂ (up to 10 mM). However removal of the chaperone severely affects the solubility of TKTL1 leading to precipitation of the mayor fraction of the protein with amounts of below 0.2 mg of soluble protein.



3.3.4 A chaperone TKTL1 and 2 fusion construct for recombinant expression

Since contamination of TKTL1 and 2 with the *E.coli* derived chaperone DnaK turned out to have a positive effect on the solubility of the desired proteins, a different expression strategy was applied. For that purpose TKTL1 and 2 were c-terminally fused to the *E.coli* trigger-factor chaperone, to increase solubility and facilitate purification. For further processing the trigger factor can be removed by protease digestion with i.e. thrombin or the HRV3C-protease. The trigger factor belongs to the best-characterised chaperones and was recently established as suitable tool for recombinant expression of proteins in *E.coli*.



3. Results

Generation of the construct, transformation, expression and purification were performed as outlined in the material and methods section. After a first IMAC purification step high amounts of the desired proteins could be obtained. After an overnight digestion with the HRV3C-protease a SEC step was performed as well as another IMAC to remove undigested proteins and the proteases. Purification of TKTL1 and 2 was successful (Figure 43). The amount of purified protein was in the range of several milligrams (up to 60 mg from a 20 g cell pellet) and the proteins turned out to be stable under the used conditions. While expected molecular weights are 67 kDa for TKTL1 and 69 kDa for TKTL2 it can clearly be seen that the mass of both proteins lies in the range of approximately 60 kDa, independent of whether HRV 3C protease or thrombin were used. This contradicts an unspecific proteolytic cleavage of both proteins by the protease since the cleavage sites clearly differ and the sequences of TKTL1 and 2 contain no such sequence besides the one between protein and trigger-factor. An SDS PAGE analysis of either thrombin or HRV3C digested TFKTL1 and 2 can be found in the appendix. Differences in the apparent molecular weight of TKTL1 in-vivo have been reported earlier by other workgroups⁷⁵ but similar behaviour for TKTL2 has never been reported

3.3.5 Secondary structure and thermal stability of native TKTL1 and TKTL2

To compare structural differences between TKTL1, TKTL2 and native human TKT far-UV CD was applied.

The CD spectrum for the trigger-factor TKTL1 and 2 fusion proteins (TFKTL1 and 2) are comparable to a typical (α/β)-protein with two negative bands at 208 nm and 220 nm, and a positive signal at 195 nm. CD spectra of TKTL1 and 2, whose trigger-factor fusion protein was cleaved off by thrombin digestion, showed similar absorption spectra to the respective trigger-factor fusion constructs. The two negative signals at 208 nm and 220 nm are clearly visible, as well as a positive signal at 195, reflecting a typical (α/β)-protein. CDNN software calculations are summarized in Table 4. These values are in fair agreement with the secondary structural content of TKT derived from crystallographic data (36 % α -helices and 16 % β -sheets estimated by use of the program PROMOTIF, pdb

3. Results

code: 3MOS)¹²⁰ except for the α -helical content of TKTL1 which had significantly dropped down.

Table 4: CDNN analysis of secondary structure contents of TFTKTL1, TFKT2, TKTL1 and TKTL2.

	α -helical content (%)	β -sheet content (%)
TFTKTL1	37	16
TFKT2	29	18
TKTL1	23	19
TKTL2	31	17

The CD spectra of the different constructs are due to the strong absorbance of the used high salt buffer limited to wavelengths above 200 nm. Despite this restriction the overall spectra of TFTKTL1 and 2 look comparable to those of a typical fold of a (α/β)-protein. Noteworthy is a smaller absorption at 222 nm corresponding to a loss of a α -helical based signal (Figure 44).

Next the stability of the proteins was analyzed by thermal unfolding which turned out to be an irreversible process in all cases. The unfolding process of TFTKTL1 and 2 turned out to follow a one phase transition with a transition point at 325 and 323 K. This differs significantly from native TKT with two transition points under high salt conditions at 326 K and 337 K as well as the deletion variant with 317 K. Removing the trigger factor fusion protein does not affect the position of the transition point (Figure 44).

3. Results

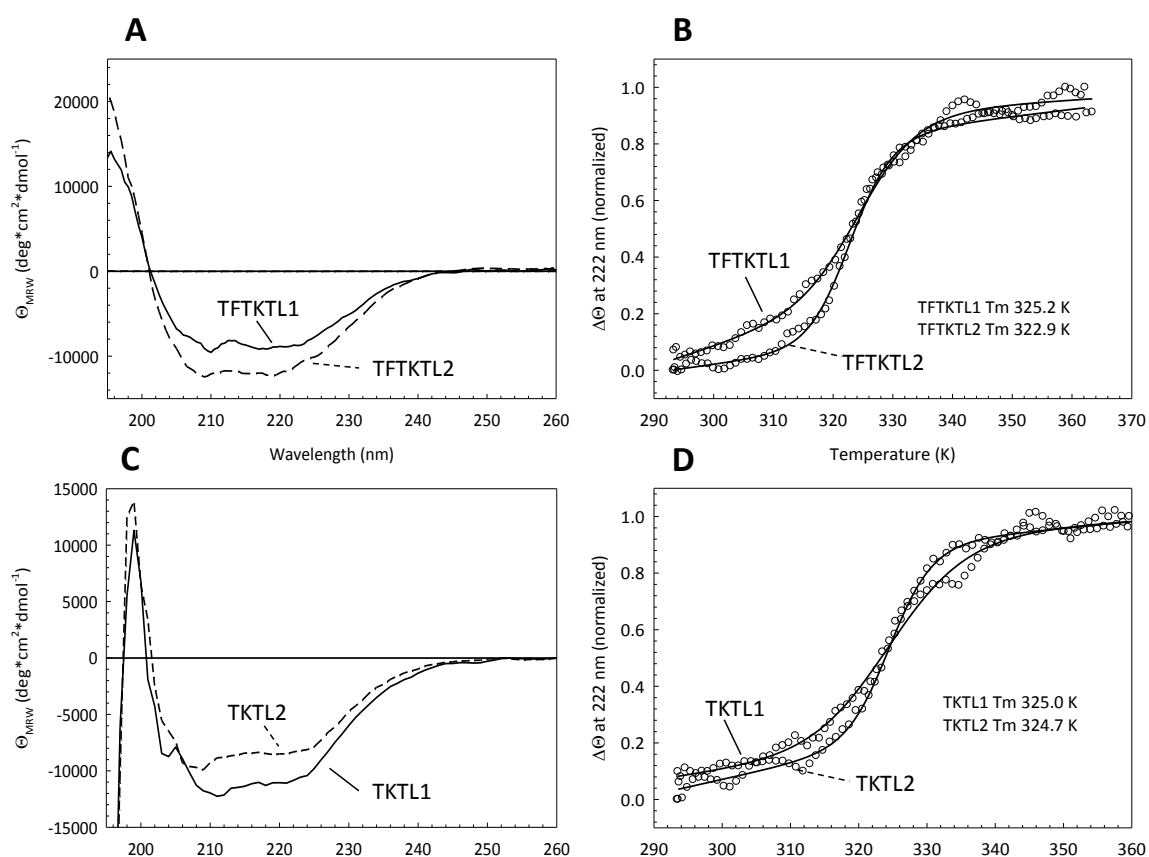


Figure 44: Far-UV spectra and thermal unfolding of TFKTL1 and 2 as well as the trigger-factor released TKTL1 and 2 constructs. (A) Far-UV CD spectra of TFKTL1 and 2 were recorded at a protein concentration of 0.1 mg/mL in 50 mM sodium phosphate buffer, pH 7.6 containing 500 mM NaCl, 2.5 mM MgCl₂ and 200 μM ThDP at 20 °C. **(B)** Thermal unfolding of TFKTL1 and 2 recorded at 222 nm in the same buffer as mentioned for the far-UV CD measurements. **(C)** Far-UV CD spectra of TKTL1 and 2 were recorded at a protein concentration of 0.1 mg/mL in 50 mM sodium phosphate buffer, pH 7.6 containing 500 mM NaCl, 2.5 mM MgCl₂ and 200 μM ThDP at 20 °C. **(D)** Thermal unfolding of TKTL1 and 2 recorded at the change of the far-UV CD signal at 222 nm in the same buffer as mentioned for the far-UV CD measurements.

3.3.6 Enzymatic characterisation of TKTL1 and 2

To verify if TKTL1 and 2 possess a catalytic transketolase function a coupled enzymatic assay was performed. Furthermore X5P and CoA were used since it was reported that TKTL1 cleaves X5P into G3P and a C2-fragment of unknown chemical structure identity which was hypothesized to be further converted to acetyl-CoA. In both assays cleavage product G3P will be processed by auxiliary enzymes linked to the consumption of NADH.

3. Results

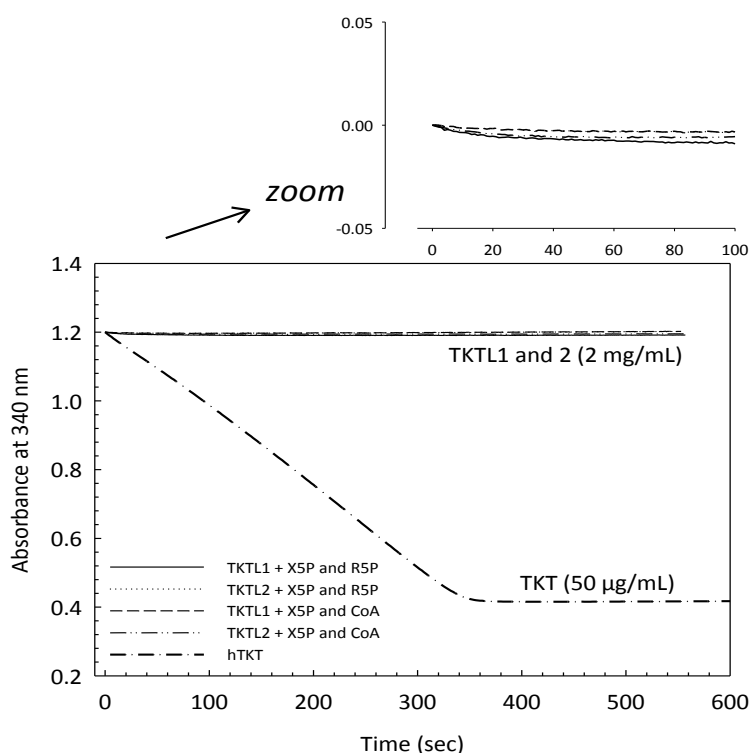


Figure 45: Steady-state kinetic analysis of enzymatic activity of TKTL1 and 2. Conversion of substrates X5P and R5P into S7P and G3P by a TKT-like mediated enzymatic activity were coupled to the consumption of NADH (340 nm) at 30 °C. Moreover the putative cleavage of X5P and transfer of the residual C2-fragment to Coenzyme A was coupled to the consumption of NADH.

As control native TKT was used. No enzymatic activity could be detected for TKTL1 and 2 even after an increase of the used enzyme-concentration of up to 2 mg/mL (Figure 45). While performing the same experiment with the undigested TFTKTL1 and 2 constructs an unspecific oxidation of NADH could be observed, even in the absence of the substrates X5P, R5P and CoA. The observed unspecific NADH-oxidation was presumably caused by co-purified proteins which were present in the used TFTKTL1 and 2 fractions (see appendix).

3.3.7 Product analysis of a putative TKTL1 and 2 activity by mass spectrometry

To further investigate whether the purified TKTL1 and 2 proteins show enzymatic activity, nano-electrospray tandem mass spectrometry experiments were performed by courtesy of Dr. Cornelia Herrfurth (Department for Plant Biochemistry, Georg-August-University Göttingen). After quenching the reaction, the protein was removed by filtration and the supernatant analyzed as described in section 2.8.29. As depicted below neither TKTL1 or TKTL2 showed detectable production of G3P, S7P or acetyl-CoA.

3. Results

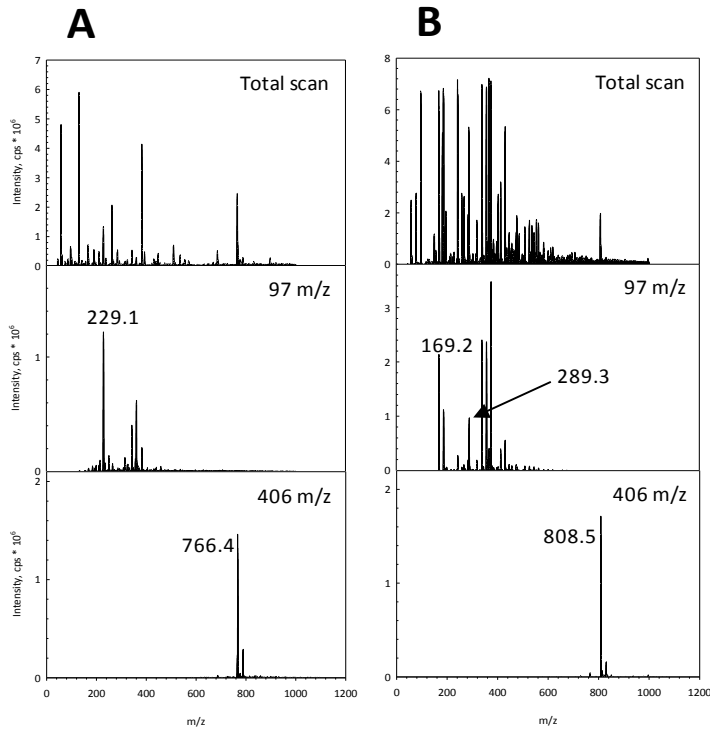


Figure 46: Total scan and ms/ms spectra of the putatively used substrates and generated products of a TKTL1 and 2 mediated enzymatic reaction. (A) Total scan and ms/ms spectra of the used substrates X5P, R5P and Coenzyme A (top). CID derived spectra gave rise to the expected substrate-signals (229.1 for X5P and R5P (middle); 766.4 for CoA (bottom)). **(B)** Total scan and ms/ms spectra of the expected products G3P, S7P and acetyl-CoA (top). CID derived spectra gave rise to the expected product-signals (169.2 for G3P; 289.3 for S7P (middle); 808.5 for acetyl-CoA (bottom)).

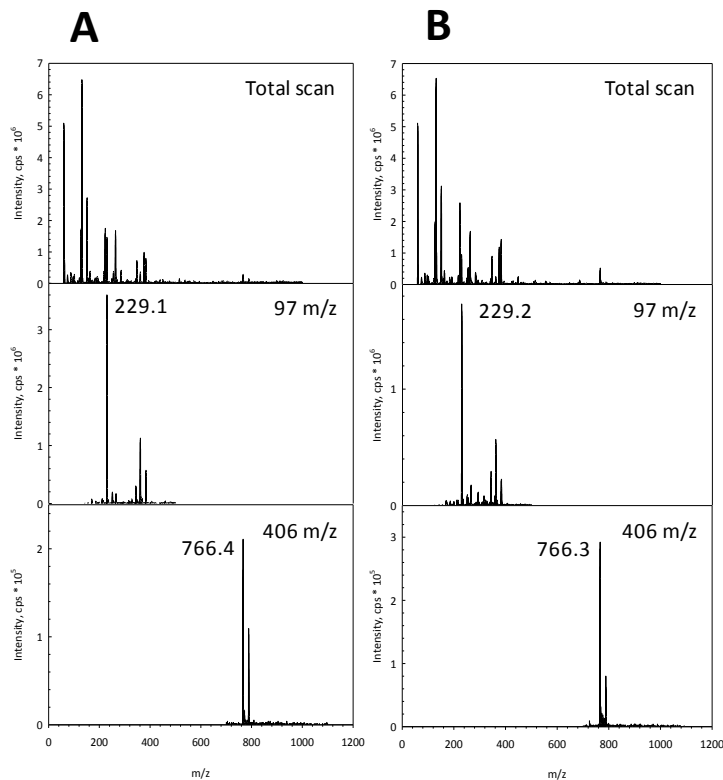


Figure 47: Total scan and ms/ms spectra of the putatively used substrates and generated products of an TFKTL1 and 2 mediated enzymatic reaction. (A) Total scan and ms/ms spectra of the used substrates X5P, R5P and Coenzyme A (top). CID derived spectra gave rise to the expected substrate-signals (229.1 for X5P and R5P (middle); 766.4 for CoA (bottom)). **(B)** Total scan and ms/ms spectra of the expected products G3P, S7P and acetyl-CoA (top). CID derived spectra gave rise to the expected product-signals (169.2 for G3P; 289.3 for S7P (middle); 808.5 for acetyl-CoA (bottom)).

3. Results

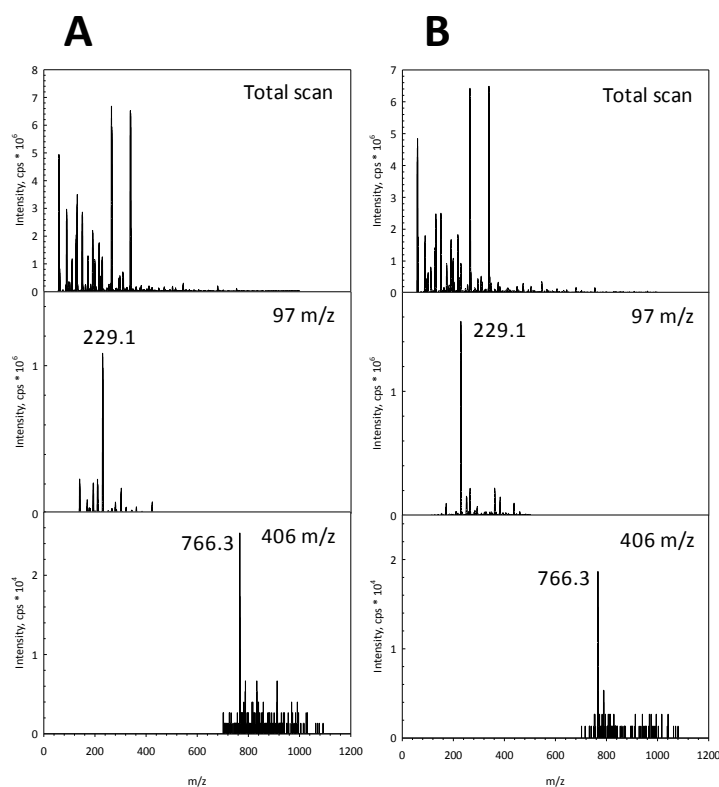


Figure 48: Total scan and ms/ms spectra of the putatively used substrates and generated products of an TFTKTL1 and 2 mediated enzymatic reaction. (A) Total scan and ms/ms spectra of the used substrates X5P, R5P and CoA (top). CID derived spectra gave rise to the expected substrate-signals (229.1 for X5P and R5P (middle); 766.4 for CoA (bottom)). (B) Total scan and ms/ms spectra of the expected products G3P, S7P and acetyl-CoA (top). CID derived spectra gave rise to the expected product-signals (169.2 for G3P; 289.3 for S7P (middle); 808.5 for acetyl-CoA (bottom)).

Based on these results it seems unlikely that TKTL1 and 2 perform a transketolase-like reaction. Moreover, the previously reported cleavage of X5P into G3P and putative formation of acetyl-CoA could not be reproduced.

3.3.8 Analysis of cofactor binding by near UV CD spectroscopy

Binding of the ThDP cofactor in TFTKTL1 and 2 as well as TKTL1 and 2 was investigated in analogy to the previously described deletion variant experiments (section 3.1.4). No TKT specific negative CD signal could be detected in the TFTKTL1 as well as in the TKTL1 and 2 constructs under any tested condition (up to 10 mM ThDP and Ca²⁺) (Figure 49). This outcome either corresponds to an absence of cofactor in the mentioned proteins or a spectroscopically silent protein bound cofactor in all those cases.

3. Results

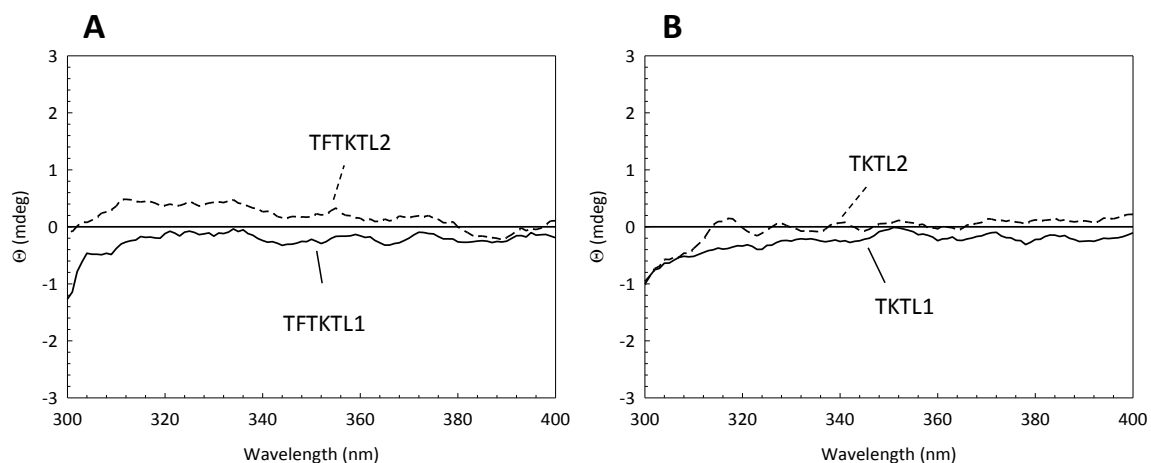


Figure 49: Cofactor binding analysis by near-UV CD. (A) Near-UV spectra analysis of TFKTL1 and 2 at a concentration of 2 mg/mL protein in glycyl glycine buffer, pH 7.6 containing 500 mM NaCl. **(B)** Near-UV spectra analysis of TKTL1 and 2 at a concentration of 2 mg/mL enzyme in glycyl glycine buffer, pH 7.6 containing 500 mM NaCl. Noteworthy is the missing absorption at 320 nm in all recorded spectra.

NMR studies to verify ThDP binding in TKTL1 and 2 could so far not be performed.

4 Discussion

4.1 The $\Delta 38$ deletion variant of human transketolase as model for TKTL1

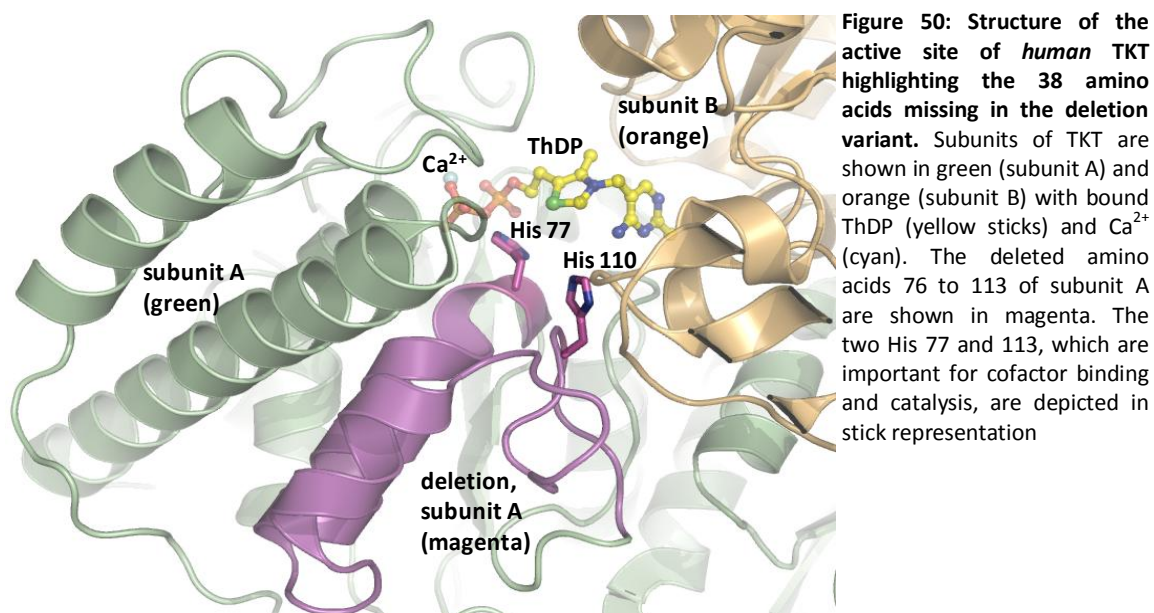
TKTL1 is an isoform of human TKT that has been described to act as a putative key-player in establishing of an altered tumor cell metabolism by a gain of function role. It is supposed to drive a tumor cells' metabolism towards a glycolytic phenotype, despite sufficient oxygen concentrations for respiration⁵³. By quantitative real-time PCR an increased expression of TKTL1 was detected in several cancers^{121 63}. Besides elevated mRNA levels, TKTL1 was detected by immunostaining by use of a monoclonal antibody specific against TKTL1⁵³. Furthermore raised expression levels of TKTL1 have been assigned as a negative factor in terms of metastasis-formation and over-all survival of patients suffering from cancer^{121 122 63}.

TKTL1 was supposed to convert the native TKT substrate X5P into G3P and a two-carbon unit of unknown identity, which was suggested to be acetyl-CoA. This lyase-reaction was hypothesized to be analogue to the reaction of XFPK of lactic acid bacteria that produces acetyl phosphate as product⁵³. In this regard a very low TKT activity of TKTL1 was presented to underpin the proposed enzymatic activity. Specific activities of this TKTL1 reaction were not shown by the authors and substrate consumption was measured over 24 hours. A native human TKT mediated reaction would convert the substrate within a few minutes under the described conditions⁵⁰.

Facing these inconsistent data a deletion variant of native human TKT was generated by an overlap extension PCR method yielding an artificial TKTL1-construct (TKT $\Delta 38$). This pseudo-TKTL1 lacks 38 amino acids in the N-terminus (residue 76-113) which have been described as the main difference between TKT and TKTL1 (Figure 9). After successful expression of this construct in *E.coli* the resulting protein could be purified to homogeneity, yielding several mg of protein. Purified TKT $\Delta 38$ was biochemically characterized and compared to full-length TKT. Native TKT was previously characterized after *E.coli* based recombinant expression as an active enzyme, suggesting that no post-translational modifications are necessary for enzymatic activity. In contrast the data obtained in the present work show that deletion of the 38 amino acids in full-length TKT leads to enzymatically inactive protein, underpinning the importance of this sequence for catalysis (Figure 19) (Figure 50). Comparable results were obtained by *in silico*

4. Discussion

studies, as well as a generated deletion variant lacking the same 38 amino acids as presented in this work^{123 124}. The incapability of cofactor binding in the deletion variant, analysed by near-UV CD and ¹H NMR spectroscopy, can be considered as origin of this lack of enzymatic activity (Figure 20). Although TKTΔ38 is able to fold with a proper secondary structure, its thermal stability was severely reduced in comparison to full-length TKT as distinguished by far-UV CD (Figure 18). Attempts to crystallize the deletion variant failed so far, despite extensive trials with conditions under which the native TKT crystallized reproducibly⁵⁰. This restriction eliminated a further characterization of this variant by means of X-ray crystallography. Moreover the deletion affects formation of the homodimer, suggesting a role of the deleted helix-turn-helix motif in the interaction of the respective monomers as shown by analytical gel filtration (Figure 21). The consensus of TKTL1 and the deletion variant suggest the latter to be a good model, leading us to the assumption that TKTL1 does not possess an enzymatic activity relying on the ThDP cofactor. Therefore our results challenge the model of a proposed enzymatic role in tumor cell metabolism. However our data cannot rule out if a putative enzymatic activity of TKTL1 is performed after binding to so far unknown proteins or protein complexes.



4. Discussion

4.2 Elucidation of the catalytic mechanism of XFPK of *B. breve*

4.2.1 Purification and kinetic analysis of wt XFPK and active site variants

XFPK of *B. breve* was successfully purified according to a previously published protocol⁷⁹. The wild type enzyme as well as the variants H64A, H97A, H142A, H320A and H553A turned out to be stable under the chosen conditions. The only exception was the H142A variant which was prone to denaturation. All variants showed a lower thermal stability in comparison to the wild type. This was most likely caused by improper cofactor binding, whose contribution to the stability of the enzyme seems indispensable. Determining the kinetic parameters of wt XFPK by the discontinuous hydroxamat assay revealed a 2.5 fold elevated K_M (24.6 ± 4.3 mM) and 30 % lowered k_{cat} of $18.6 \text{ s}^{-1} \pm 1.3$ in comparison to previously published data (Figure 24)⁸⁰. The origin of this discrepancy is so far unknown but it is most likely caused by the used error-prone assay or the mentioned product inhibition by E4P. Previously published K_M values for F6P of a phosphoketolase form *Lactobacillus plantarum* were denoted with 24 ± 4 mM which is in a fairer agreement with our data⁸¹. Applying an ITC based method for determining kinetic parameters failed probably due to the mentioned product inhibition by E4P, which has been studied earlier⁸¹. According to Yevenes and Frey the three irreversible steps of XFPK mediated catalysis, dehydration of DhEThDP, tautomerization of the enolAcThDP to ketoAcThDP and phosphorolysis of the ketoAcThDP are the cause for product inhibition by E4P. They describe the way of inhibition as an uncompetitive way of action by E4P with respect to phosphate. It was proposed that this can be explained by Cleland's rules since E4P and phosphate bind to different enzyme forms¹²⁵. Based on this, the only accessible data for our enzyme were the K_M values for F6P (6.3 ± 0.45 mM) which are more comparable to the already published data on XFPK of *B. breve*. These data have to be considered with caution since lowering V_{max} by product inhibition affects K_M also. Moreover it could be shown that S7P does not serve as substrate for XFPK.

4. Discussion

4.2.2 Protonic and tautomeric equilibria of XFPK and active site variants

Since TKT and XFPK share a high degree of homology in the quaternary structure, which is expressed by a nearly equal active center composition, a similar spectroscopic behavior was expected in near-UV CD based measurements. As it was previously described^{100 101 126}. TKTs show a negative CD-absorption centered at 320 nm. Nemeria *et al.* assigned this band to be the AP form of the ThDP cofactor (Figure 51)⁴⁹.

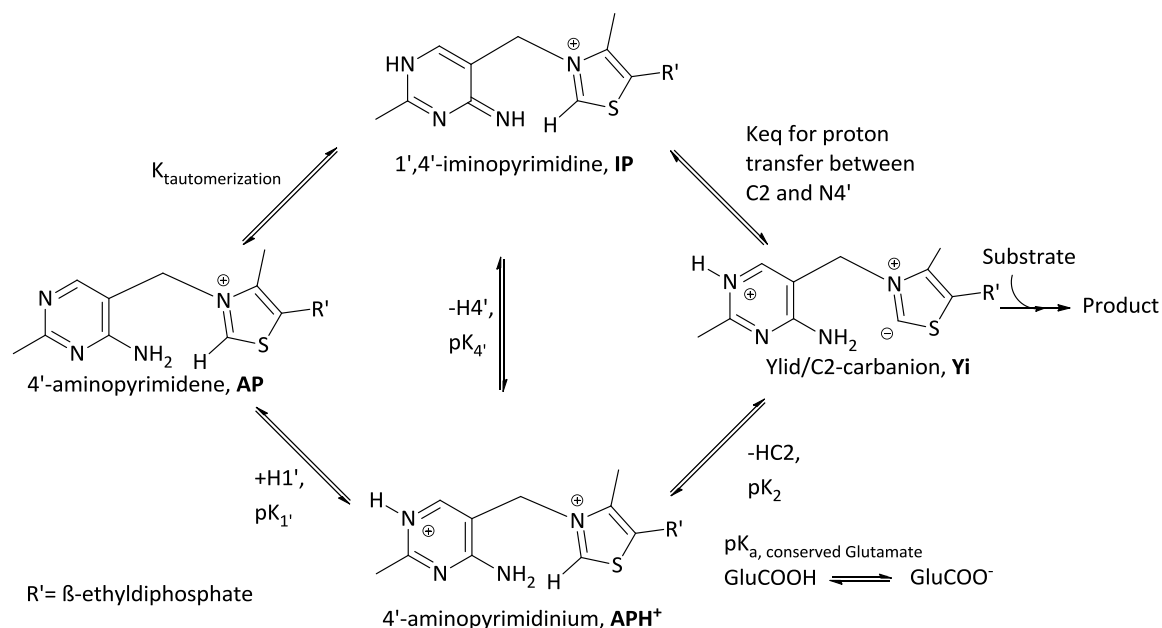


Figure 51: Tautomeric and ionization equilibria of ThDP in the resting state of ThDP-dependent enzymes. Adapted from Nemeria *et al.* (2007)

For XFPK such a signal could not be detected (Figure 28). The reason for this finding is so far unknown since the signals for the putatively APH⁺ and IP form can be detected (this point will be discussed later). Besides, it seems that generation of this AP-signal is not caused by the same set of factors in different ThDP dependent enzymes. Nemeria *et al.* could show that formation of the AP derived signal depends on formation of the Michaelis-complex in the E1 component of the yeast and *E.coli* pyruvate dehydrogenase. However in TKT this signal can already be detected prior substrate addition, indicating that a general mechanism of AP signal generation by Michaelis-complex formation might not exist in this enzyme. Moreover it was shown by Asztalos *et al.* that the generation of the AP signal seems to depend on the presence of the N4' amino group of the aminopyrimidine moiety of the cofactor¹²⁷. While adding F6P to XFPK a change in the generated ThDP signals could not be monitored, since F6P is cleaved into E4P, which

4. Discussion

leads to a strong ellipticity signal in the wavelength range below 320 nm overlapping with the tautomer signals of the ThDP cofactor (see appendix). It should be noted that substrates and amino acid residues as well as smaller molecules (i.e. Cl^{2-}) present in the buffer systems used, can influence the spectroscopic behaviour of the generated near-UV CD signals⁹⁷.

As mentioned above although no AP signal could be detected, a negative signal centered at 280 nm and a positive signal centered at 295 nm could be detected for XFPK (Figure 28). The positive signal has previously been assigned to the IP form of the cofactor⁴⁹. In case of the negative signal we assume it to be the APH^+ for of ThDP since it disappears while increasing the pH of the corresponding buffer (discussed below). Visualization of CD signals below 300 nm is not unambiguous, since proteins show a high signal in this wavelength range that are caused by aromatic amino acid side chains. Moreover the ThDP cofactor gives also rise to a strong CD signal centered at wavelengths below 300 nm (see appendix), due to its strong absorption.

To further assign the generated CD signals pH-titration experiments with wt XFPK and different active site variants have been performed (Figure 29). Titration experiments have already been described for other ThDP dependent enzymes like benzaldehyde lyase, benzoylformate decarboxylase, pyruvate oxidase and the E1 component of the pyruvate dehydrogenase complex⁴⁹. Using titration experiments the putative IP and APH^+ signals could be confirmed for the wild type enzyme. The putative signal of the protonated APH^+ form diminishes with increasing hydroxydion concentrations whereas the IP signal increases. Besides the signal for the AP form could not be visualized, although this was expected for higher pH values since it depicts the deprotonated form of APH^+ as it was already reported for pyruvate decarboxylase¹²⁸. According to Jordan *et al.* ThDP dependent catalysis requires interplay of the different neutral and charged cofactor states but due to the given enzyme environment it is possible that in some cases not all signals can be detected. In case of the active center histidine residues the signal strengths of the recorded spectra were too low to make a qualitative assumption on the chemical state distribution of the cofactor. It seems that the affinity for ThDP is lowered and transferring the variants into cofactor free buffer (a prerequisite for near-UV CD measurements due to the high absorption of free ThDP below 300 nm) leads to

4. Discussion

apo-enzyme formation. A fluorescence based analysis to determine K_A values for ThDP for the wild type XFPK and the different variants could not be performed, since all so far applied protocols to generate XFPK apo-enzyme led to precipitation of the enzyme (data not shown).

4.2.3 UV/vis stopped flow based analysis of enzyme-bound ThDP-intermediate formation

In order to gather more insights into the reaction mechanism of XFPK, UV/vis experiments, employing a stopped-flow instrument have been performed. Stopped-flow has been described as suitable tool for analyzing very fast microscopic steps of ThDP-intermediate formation in TKTs^{113 127 129}. In TKTs signals for different tautomeric states at the aminopyrimidine ring after F6P-adduct formation have been described for the AP-form (320-335 nm) and the IP-form (295-305 nm)¹¹³. Performing UV/vis based approaches to elucidate the catalytic way of action of XFPK revealed an unexpected result after F6P addition. As described within stopped-flow UV/vis experiments, a prominent absorption signal in the wavelength range of ~420 nm can be detected in the absence of the second substrate phosphate (Figure 31). In case of *E.coli* TKT such a spectroscopic behaviour has been assigned to the formation of an enolat-species of the DhThDP cofactor (Figure 52)¹³⁰.

4. Discussion

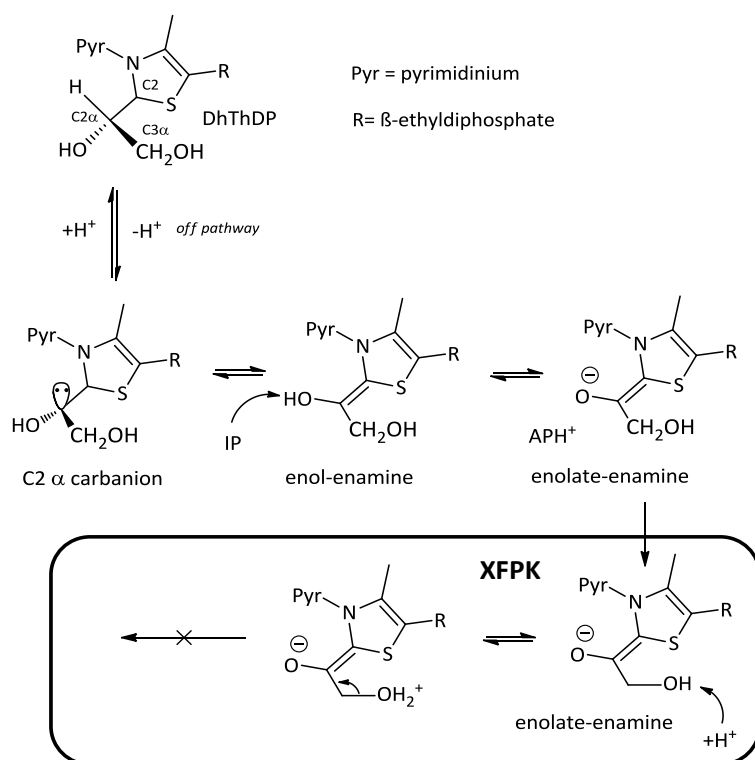


Figure 52: Chemical structure of DhThDP including tautomeric states of the enolat-enamin in *E.coli* TKT. The base being responsible for the putative enolate-enamine formation is so far unknown (either the IP form of the cofactor or an amino acid residue of the active center). In XFPK formation of such a species seems unlikely since it would hamper water elimination at the C3 α . Figure adapted and modified from Meyer *et al.* (2012)

In XFPK such a species seems rather unlikely since formation of an enolate would hamper protonation at the OH-group at the C3 α to induce water elimination (see introduction). The close vicinity of the negative charges at the C3 α would repel electron rearrangement after water elimination.

Although it was still questionable to which chemical species this signal could be assigned (F6P-ThDP adduct, DhThDP, enolAcThDP or ketoAcThP) we suggest this signal represents the enolAcThP intermediate by several indications:

- 1) The intermediate detected in ¹H NMR spectroscopic analysis revealed accumulation of the AcThDP adduct in absence of phosphate (discussed below).
- 2) Analysis of the histidine residues of the active center by UV/vis showed only in the case of the H142A variant formation of this signal (see appendix). These residues have been described as important for either DhThDP-formation or enolAcThDP-formation. This means that all catalytic steps that depend on these histidine residues are upstream from the enolAcThDP in the catalytic cycle of XFPK (Figure 53). Analysis of the variants by stopped-flow would presumably show a strong accumulation of the signal if it

4. Discussion

corresponds to the F6P-ThDP adduct or the DhThDP-intermediate where the respective catalytic step is blocked.

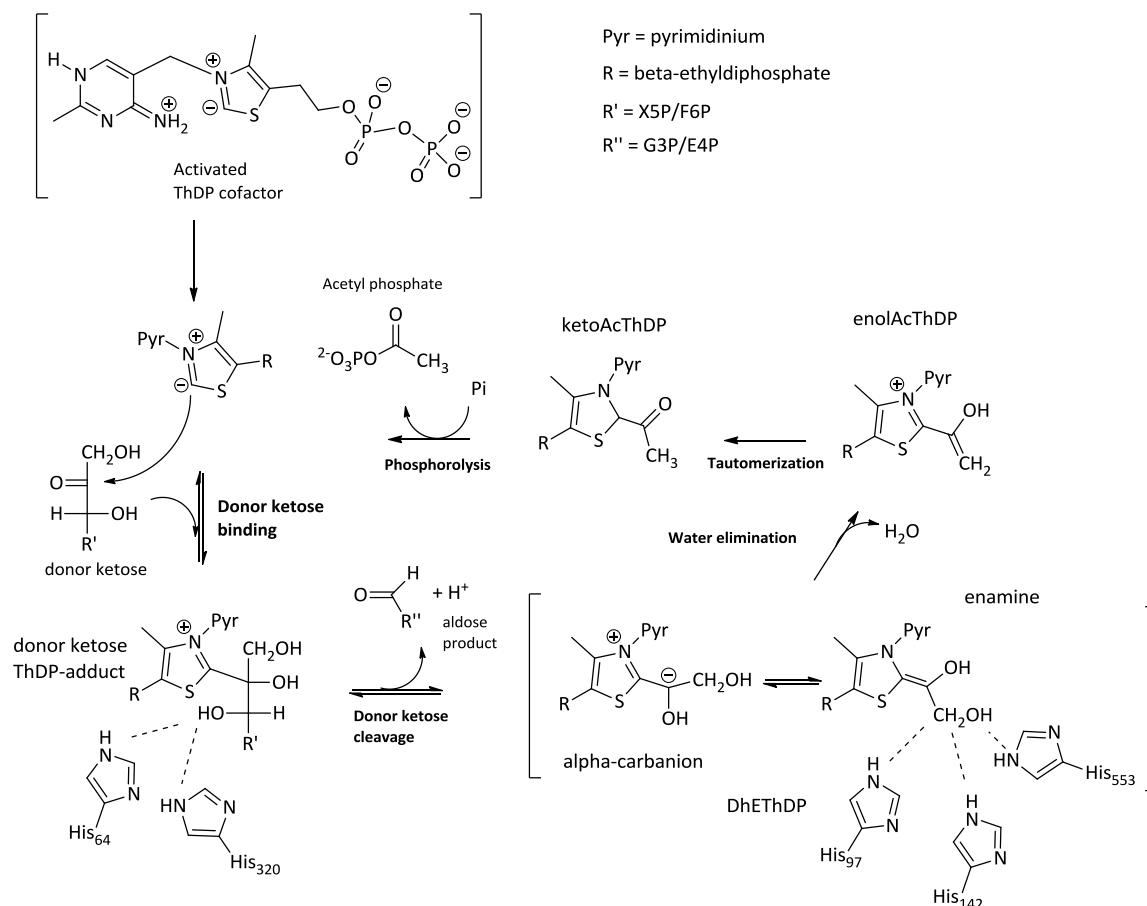


Figure 53: Catalytic steps mediated by the conserved active site His residues in XFPK. His 64 and 320 are hypothesized to be responsible for the first catalytic step, protonation of the ThDP-adduct followed by release of the first product. His 97, His 142 and His 553 are supposed to catalyze interconversion of the second intermediate DhThDP into enolAcThDP.

3) A similar spectroscopic behavior was described for the ThDP-dependent enzyme N²-(2-carboxyethyl) arginine synthase (CEAS). This enzyme ligates the substrates G3P and arginine and is thus responsible for the first step of β -lactam antibiotic synthesis¹³¹. During catalysis an acryloyl-ThDP intermediate is generated showing a comparable absorption at ~ 410 nm in UV/vis analysis. By using synthesized thiazolium analogues the authors could show that the resulting absorption is caused by the conjugated double bond system of the thiazolium and the terminal acryloyl-group.

4) Crystallization attempts performed by Suzuki *et al.* showed difficulties in isolating the DhThDP-intermediate at the reactive center after soaking experiments (discussed

4. Discussion

below). The authors explain that the DhThDP is transiently formed during catalysis and therefore hard to isolate⁸⁰.

If we assign the spectroscopically detectable species to the enolAcThDP it is astonishing that the absorption shows its maximum in a wavelength range of 420 nm. One would expect the enol of such a small ketone to have an absorption maximum at the range of about 280 nm⁸². It seems likely that the π -electrons of the putatively enolAcThDP are delocalized by interacting with the π -electrons of the thiazolium ring. This was explained for free AcThDP earlier, shifting the absorption spectra to ~ 310 nm⁸². In our case there might be some additional interference with the aminopyrimidine ring of the cofactor. As described before, the two aromatic ring systems of ThDP seem to interact by a charge-transfer mechanism leading to the red-shifted absorption signal¹³². In case of enzyme bound ThDP such a mechanism occurs due to the V-orientation of the cofactor (in solution this conformation is thermodynamically not favored, hampering the described interaction) (Figure 54). This possible charge-transfer “communication” could explain the red-shifted absorption spectra of the detected enolAcThDP.

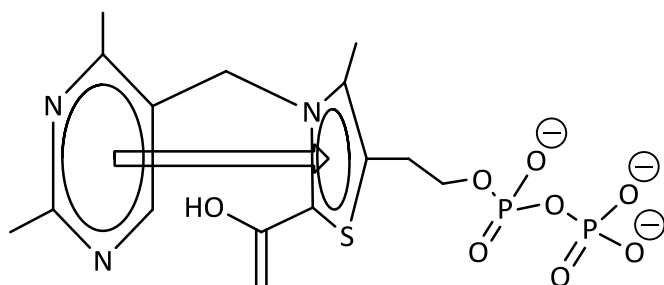


Figure 54: Possible charge-transfer interaction of the aminopyrimidine- and the thiazolium ring of ThDP.

4.2.4 UV/vis stopped-flow based kinetic analysis of phosphate catalyzed enzyme bound ThDP-intermediate conversion

Analyzing the reaction of enzyme-bound enolAcThDP with the second substrate phosphate was performed by UV/vis sequential stopped-flow (Figure 33). After mixing XFPK with F6P, the intermediate was formed and its reaction with the second substrate phosphate was analyzed. Addition of phosphate leads to complete signal depletion within >50 ms even at the lowest used phosphate concentration (3 mM). The rate

4. Discussion

constant for the different used phosphate concentrations were obtained after plotting the different spectra with a single exponential equation showing a k_{cat} of $>400 \text{ s}^{-1}$ for the highest used phosphate concentration of 25 mM. The rate constant for unspecific hydrolysis in absence of phosphate were estimated as described by Gibson *et al.* ¹³³. For hydrolysis the rate constant turned out to be $\sim 0.3 \text{ s}^{-1}$. This means in turn that phosphorolysis is more than three orders of magnitude faster than the described signal depletion in absence of phosphate. This result indicates that phosphate accelerates the tautomerization of the enolAcThDP followed by phosphorolysis. Thus it can be proposed that phosphate not just acts as a substrate but that it has an own catalytic function and participates to the reaction in a substrate assisted catalysis (SAC) manner (Figure 55).

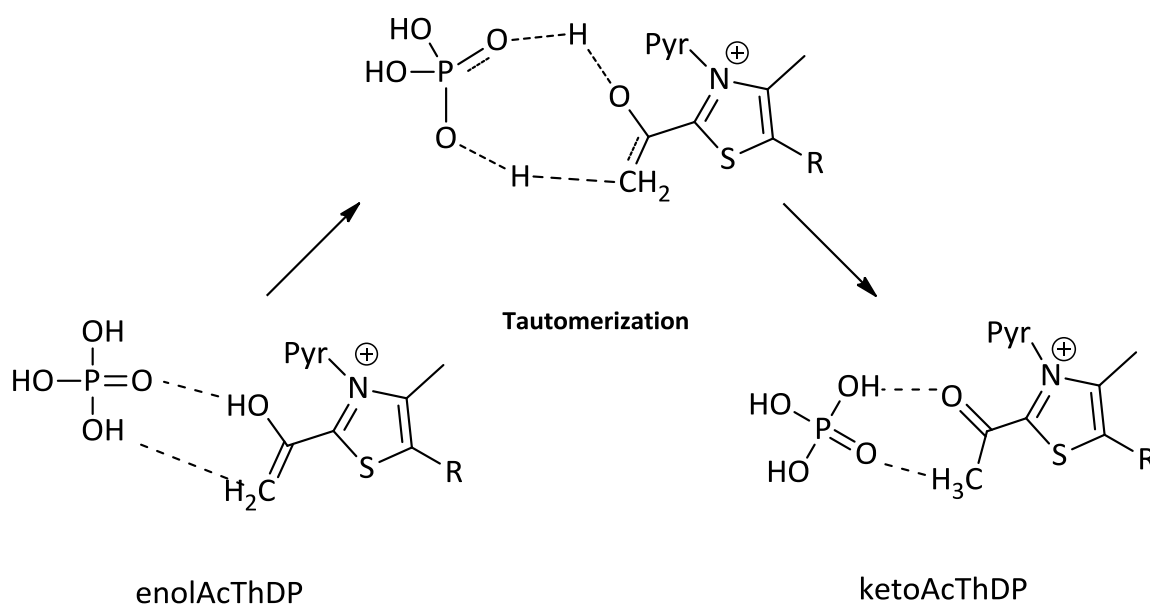


Figure 55: Phosphate catalyzed tautomerization of enolAcThDP to ketoAcThDP.

Substrate assisted catalysis has been described for several enzymes like serine proteases, type II restriction endonucleases and the G protein-coupled receptor RAS ⁸⁶. In this regard the substrate usually performs a catalytic function, which one would usually expect for an amino acid residue within the active center of the respective enzyme. In case of phosphate containing substrates it has been shown that in several cases phosphate acts as acid base catalyst in such enzymes like EcoRI, EcoRV, aspartyl-, and glutamyl t-RNA synthase and aspartate carbamoyl transferase ^{134 135 136 137}.

4. Discussion

Moreover in the G protein-coupled receptor RAS p21 the terminal phosphate of the GTP-substrate stabilizes an occurring intermediate by formation of a hydrogen bond¹³⁸. All these SAC mechanisms have been described on basis of structural studies of the corresponding enzymes, by substrate analog usage, by the stereo-chemistry of the reaction or, in case of ras P21, by free-energy relationships.

4.3 ¹H NMR spectroscopic product analysis

To further validate our assumption that indeed the enol form of AcThDP is accumulated in the active center of XFPK as an intermediate, ¹H NMR spectroscopy experiments have been performed according to a method described earlier¹⁰³. First, ThDP-intermediate analysis has been performed to analyze the over-all distribution of detectable ThDP-intermediates within XFPK driven catalysis. In presence of F6P, the only detectable intermediate was AcThDP (Figure 30). This can be explained with AcThDP either being a dead-end product, or a true occurring intermediate. In light of our UV/vis stopped-flow experiments the latter seems to be more likely, although a distinction between the enol and keto form is under the chosen pH conditions not possible. With F6P and phosphate present the DhThDP-intermediate was detectable (Figure 30). It is reasonable that the AcThDP can be detected only in the absence of phosphate since the tautomerization followed by hydrolysis seems to be the rate limiting step and is accelerated by several orders of magnitude in presence of phosphate. Moreover it is questionable why the expected F6P-ThDP adduct could not be detected, although it should occur under these conditions as it was reported for other F6P-converting ThDP-dependent enzymes³⁸. The most likely explanation might be its transient character⁸⁰. ¹H NMR analysis of the active site histidine variants could not be performed to a greater extend so far, but their evaluation should clearly show which histidine serves as acid/base catalyst at which point of XFPK catalysis by accumulating either the F6P- adduct or DhThDP.

To confirm if the enzyme bound spectroscopically detected ThDP-intermediate can be assigned as the enolAcThDP we performed product analysis ¹H NMR spectroscopy H/D exchange experiments. In aqueous solution XFPK showed production of acetate while incubation with F6P in absence of phosphate (Figure 34). If this intermediate is in a dynamic equilibria between its enol and keto form, provided deuterium should be

4. Discussion

incorporated. Performing this experiment in deuterium oxide revealed almost full depletion of this signal and only a minor amount of mono- and dideuterated acetate (fully deuterated acetate is NMR-silent). This underpins our assumption of the in UV/vis experiments detected ThDP-intermediate being enolAcThDP and of phosphate accelerating the tautomerization into the ketoAcThDP.

Our proposed mechanism of phosphate mediated SAC is to our knowledge the first description of this phenomenon by a direct spectroscopic method and of an inorganic phosphate changing the chemical state of a substrate. In the ThDP-dependent enzyme class this would be an additional catalytic mechanism and might explain, how the enzyme enables the weak nucleophile phosphate to phosphorolyse the enzyme bound AcThDP.

4.3.1 Glutamate 437 seems to play a role in phosphorolysis

The glutamate 437 of XFPK seems to have an important function within XFPK mediated catalysis. ITC and acetyl phosphate detection based activity assays showed that the exchange of glutamate against glutamine led to a variant which is inactive, even with an increase of the used enzyme concentration of up to 2 mg/mL (Figure 36). Moreover in UV/vis stopped-flow analysis no putatively enolAcThDP-intermediate signal could be detected (Figure 37). Near-UV CD pH-titration showed bound cofactor, with the IP signal already present under initial conditions (Figure 38). It seems as if the glutamine either affects the tautomeric equilibrium of the cofactor, or that the glutamate of the wildtype quenches the IP signal at lower pH values. By performing substrate-soaking experiments during crystallization of this variant, additional electron density could be detected at the C2 of the thiazolium ring of the cofactor. This electron density has been assigned to AcThDP (Figure 40). This is contradictory, since in that case the variant is able to catalyze all steps from substrate-binding up to the formation of the last enzyme-bound intermediate (Figure 56).

4. Discussion

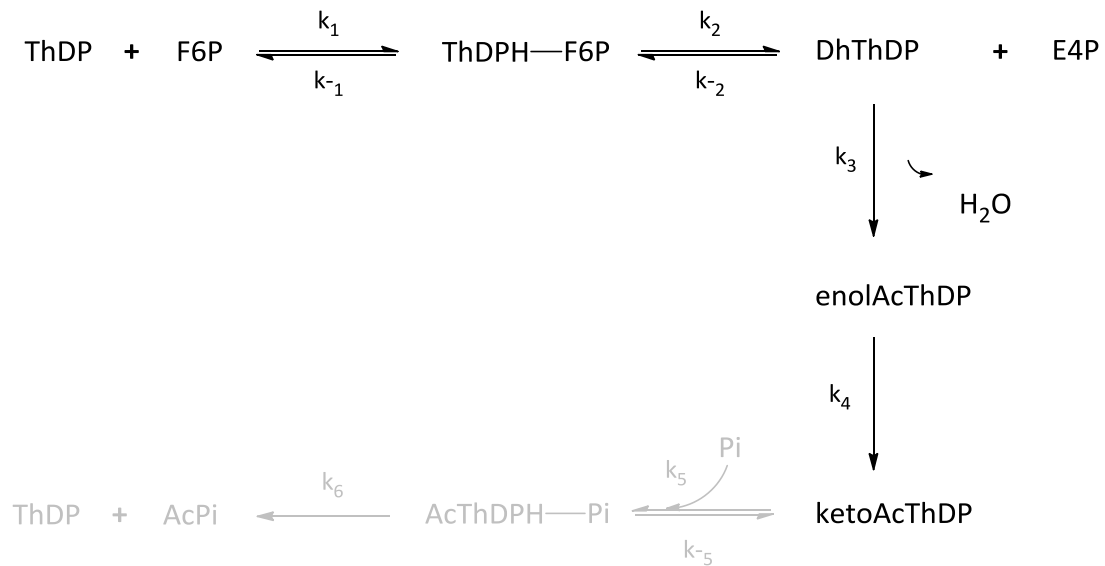


Figure 56: Microscopic steps of XFPK. The E437Q variant seems to be unable to catalyze the last step, nucleophilic attack of phosphate.

Putatively the last step of catalysis (nucleophilic attack of phosphate) is hampered due to the high flexibility of the phosphate binding anchor tyrosine 501. Moreover the exchange of glutamate 437 to glutamine seems to affect the spectroscopic behavior of the intermediate since after the exchanging no enolAcThDP specific signal could be detected. As mentioned above a simple enol should show absorption at 280 nm. In case of the wild-type the red-shifted absorption at 420 nm is most likely caused by an influence of the aminopyrimidine ring of the cofactor. The glutamate seems to play a role in this “information” transfer from the aminopyrimidine to the bound intermediate resulting in the observed absorption pattern.

4.4 Transketolase-like protein 1 and 2

4.4.1 Expression and purification of a chaperone TKTL1 and 2 fusion construct

Attempts to establish a recombinant expression system for TKTL1 and 2 in prokaryotes and eukaryotes failed and led to mainly insoluble protein in both cases (Figure 41) (Figure 42). This is a common problem while expressing human genes in *E.coli* since certain factors like post-translational modifications or interactions with other human derived proteins are not possible¹³⁹. To overcome this restriction a stepwise adaptation of

4. Discussion

the expression protocol can be applied consisting of five different approaches. These are (1) change of the expression vector, (2) change of the host, changing the culture parameters of the host-strain, (4) co-expression of other genes and (5) changing the gene sequence in terms of codon-optimization ¹⁴⁰. All these attempts have been performed as outlined in the results part with the exception of co-expression of other genes. In all cases insufficient amounts of soluble TKTL1 and 2 could be obtained. To enhance this low amount of soluble enzyme a fed-batch derived expression protocol was performed, increasing the total yield of *E.coli* cell material. By this the yield of TKTL1 and 2 that could be obtained was in the mg scale. Besides TKTL1 and 2 the *E.coli* derived chaperone DnaK becomes co-purified, which is a common phenomenon of recombinant expression in *E.coli* ¹¹⁹. Removing DnaK leads to precipitation of TKTL1 and 2. It seems that by the interaction of the TKTL-proteins with the chaperone the desired proteins were held in solution. Basing on this result TKTL1 and 2 were fused to the trigger factor chaperone which increased solubility of the proteins and the solubility-problem could be overcome (Figure 43).

4.4.2 Biochemical analysis cofactor binding and of enzymatic TKTL1 and 2 activity

Biochemical and biophysical analysis of TKTL1 and 2 was performed with established protocols of native human TKT ⁵⁰. TKTL1 and 2 showed no enzymatic activity with X5P as substrate in an enzyme-linked spectroscopically assay as previously reported ⁵³. Moreover, CoA was provided as second substrate for putative TKTL1 or 2 reactions. Neither, in an enzyme-linked spectroscopic assay, nor when performing a product analysis by means of mass spectrometry the expected products G3P or acetyl-CoA could be detected (Figure 45-48). This is in striking contrast to previously published results ⁵³. To rule out if this lack of enzymatic activity is caused by improper protein folding far-UV CD analysis has been performed with the fusion constructs of the TKTL1/2-trigger factor constructs as well as the TKTL1 and 2 obtained after protease cleavage of the trigger factor. All constructs seem to generate a secondary structure which is characteristic for correctly folded proteins, although thermal stability was slightly decreased in comparison to the wild-type (Figure 44). Analysis whether TKTL1 and 2 are able to bind

4. Discussion

ThDP as cofactor near-UV CD experiments have been performed as outlined for TKT and TKTΔ38. None of the constructs showed a characteristic negative AP signal centered at 320 nm. This suggests that TKTL1 and 2 either cannot bind ThDP or that the cofactor is in a spectroscopically silent state (Figure 49). So far ¹H NMR spectroscopy experiments and crystallization could not be performed to confirm the absence of ThDP within TKTL1.

Based on these results it seems unlikely for TKTL1 to feed-forward a malignant cells' glycolytic metabolism by an intrinsic catalytic function. On the other hand it is astonishing that TKTL2 shows no ThDP-derived enzymatic activity since it has a higher homology to native TKT. The deletion of 38 amino acids which mainly differs TKTL1 from TKT is not present in TKTL2 and despite two additional amino acid changes (see appendix) all invariant TKT-specific residues are conserved³⁵.

Slow consumption of X5P by TKTL1 as published earlier was measured over a period of more than 24 h⁵³. While incubating the trigger factor fused TKTL1 and 2 constructs under the same conditions as reported without adding substrate, a very slow oxidation of NADH can be detected (see appendix). This is most likely caused by co-purified protein impurities. These impurities can be removed after protease-mediated release of TKTL1 and 2 (followed by SEC) and the unspecific oxidation of NADH vanishes (Figure 45). The published enzymatic data of TKTL1 were performed with samples showing a comparable impure band pattern in SDS-PAGE analysis⁵³. The authors assume these impurities to be unspecific C-terminal cleavage products but they do not underpin this assumption by mass spectrometric analysis or western-blotting against the fused hexahistidine sequence. Within the published coupled NADH-consumption assays no control has been shown where TKTL1 was incubated without X5P. Therefore it seems likely that the reflected slow NADH consumption after substrate addition over 24 h is an unspecific side effect based on impure TKTL1 samples as detected for our trigger-factor TKTL1 constructs. This outcome once more emphasizes the inconsistencies in the field of TKTL1 research.

The only evidences of an intrinsic TKTL1-activity are the previously discussed NADH consumption assay, and another study in which TKTL1 was described as capable of restoring the function of TKT in the PPP. In the mentioned study chronic myeloid leukemia cells were investigated in terms of the shift from the chronic phase to so called

4. Discussion

blast-crisis¹⁴¹. This transition is characterized by developing a resistance against Imatinib, an inhibitor of the BCR-ABL kinase, whose activity is indispensable for this type of cancer. It was shown that the non-oxidative part of the PPP seems to play an important role in this resistance mechanism and that knock-down of TKT can restore sensitivity towards Imatinib. TKT knocked-down cells which were additionally transfected with a TKTL1 construct regained their resistance towards Imatinib. In light of a likely missing intrinsic catalytic function of TKTL1 this result is hard to explain.

4.4.3 The role of TKTL1 in tumorigenesis needs to be further evaluated

If TKTL1 plays a role in tumorigenesis it will, due to the above mentioned reasons, rather be caused by an enzymatic activity and more likely based on an interaction with other proteins. In this regard HIF1 α , one of the two subunits of the transcription factor HIF, has come into focus⁷⁰. Overexpression of TKTL1 was shown to stabilize the oxygen-sensitive HIF1 α subunit under normoxic conditions, leading to induction of several downstream target genes of the HIF1 transcription factor cascade. Dysregulation of HIF1 α has previously been reported as potential cause for an increased “aerobic glycolysis” in breast cancer cell lines¹⁴². However, this stabilizing effect of TKTL1 on Hif1 α is disputable in light of the described unspecificity of the TKTL1 antibody JFC12T10⁷⁵. Most of the so far published studies on TKTL1 expression on the protein level used this antibody for TKTL1 detection. Especially immunohistochemical staining by using this antibody against surgically removed specimens have been performed showing a correlation of TKTL1 expression and cancer progression^{143 144 145}. As discussed by Mayer *et al.* there are alternative TKTL1 antibodies available but so far no studies have been published using these antibodies. By comparing immunohistochemical validation studies with one of these alternative antibody (HPA000505) (proteintlas.org) Mayer *et al.* could show that the derived data are in contradiction to the so far published TKTL1 results^{122 121}. Previously published results on colon, urothelial and renal cell carcinoma could not be confirmed with the alternative antibody^{121 146}. Based on this the role in tumorigenesis of TKTL1 can neither be confirmed nor neglected. To ascribe TKTL1 a function as global switch from a respiratory to a glycolytic

4. Discussion

phenotype in cancer relying on the available data is, to our understanding, highly speculative.

5 Summary

Transketolase (TKT) is a ubiquitous distributed enzyme in all three domains of life. Its catalytic function is fulfilled within the pentose phosphate pathway (PPP) and the Calvin-Benson-Bassham cycle of photosynthetic plants. TKTs catalyze the transfer of 1,2-dihydroxyethyl-fragments from donor ketoses to acceptor aldose in a reversible manner. TKT requires bivalent cations and thiamine diphosphate (ThDP) as cofactors. ThDP belongs to the best characterized cofactors and enables enzymes to perform a whole variety of reactions like formation and breaking of carbon-carbon bonds. Beside its central role in carbon metabolism, TKT has been described as potential factor in human disease development. Diabetes, Alzheimers' Disease, the neurological disorder Wernicke-Korsakoff syndrome as well as cancer have been described as affected in terms of a TKT mediated disease development. Especially the role of TKT in cancer seems to be a promising approach to overcome resistance mechanisms of tumor cells. In the recent years the concept of an abnormal metabolism in malignant cells has been elucidated in more detail since this abnormality could provide an alternative target side for cancer drugs. In this context malignant cells have to adjust their metabolic program in terms of glucose processing. Glucose can either be used to provide energy in form of adenosine triphosphate (ATP) via glycolysis or for generation of reductive equivalents and nucleotide precursors in form of nicotinamide adenine dinucleotide phosphate (NADPH) and ribose 5-phosphate (R5P) within the PPP. Especially malignant cells have a high consumption of R5P and NADPH since these molecules are indispensable for anabolic reactions and DNA-synthesis, the two prerequisites for cell division. By inhibiting respiration and thereby providing more glucose for the PPP tumor cells seem to adjust this balance towards a glycolytic phenotype, ignoring ample oxygen concentrations for respiration.

As mentioned above TKT plays the central role in the PPP and its connection to the aforementioned metabolic reprogramming of malignant cells seems reasonable. Besides two isoforms of TKT have been discovered sharing a high homology to TKT. One of them, the transketolase-like protein 1 (TKTL1) was described to play an important role in tumorigenesis. It was shown for several cancer entities that an overexpression of TKTL1 on the mRNA as well as the protein level was assigned to an increased aggressiveness of

5. Summary

the corresponding cancer. This was expressed by a higher histopathological staging of the corresponding cancers and a lowered over time survival of patients suffering from cancer.

TKTL1 has been described to act on xylulose 5-phosphate (X5P) one of the used substrates of native TKT. TKTL1 is supposed to cleave X5P into glyceraldehyde 3-phosphate (G3P) and a C2 fragment of unknown identity. This C2 fragment was supposed to be acetyl Coenzyme A, which would be further processed (i.e. lipid synthesis).

Since biochemical data of TKTL1 is rather scarce and inconclusive, we attempted to elucidate the proposed function of TKTL1 in more detail. For that purpose a minimal construct of TKTL1 was generated to gain insights into the biochemical features of TKTL1. This construct was generated by deleting 38 amino acids out of TKT, since this deletion displays the main difference of TKT and TKTL1. Biochemical characterization by established protocols for TKT analysis revealed that this deletion leads to a catalytically inactive protein. This inactivity can be explained by an absent binding of the ThDP cofactor. The deleted amino acid sequence contains nine residues which are conserved among all known TKTs. Two of them (histidine 77 and 110) are important for cofactor binding and catalysis, which explains the loss of catalytic function. Moreover the deleted motif seems to affect assembly of the catalytic dimer, a prerequisite for TKT mediated catalysis since the dimer represents the smallest catalytically active subunit of this enzyme.

As a second approach phosphoketolase (XFPK) of *Bifidobacterium breve* was characterized in terms of its reaction mechanism, since TKTL1 was supposed to show a comparable catalytic activity. XFPK performs a partially comparable reaction as TKT. XFPK also uses ThDP and bivalent cations as cofactors and acts on the same set of substrates (X5P and [fructose 6-phosphate]). However XFPK performs a carbo-lyase reaction whereas TKTs show carbo-ligase activity. The substrate X5P or F6P is cleaved by XFPK which gives rise to G3P and acetyl phosphate. During this reaction a nucleophilic attack of inorganic phosphate at an enzyme-bound ThDP-substrate intermediate takes place. To compare a putative intrinsic TKTL1 activity, XFPK was recombinantly expressed, purified and characterized.

5. Summary

To our surprise XFPK seems to fulfill a unique catalytic way of action among the ThDP enzyme family. It was already proposed that XFPK performs a set of irreversible reactions like the dehydration of the enzyme bound dihydroxyethylthiamin diphosphate intermediate (DhEThDP), leading to acetyl thiamine diphosphate (AcThDP). The latter is subject to phosphorolysis which gives rise to the above mentioned acetyl phosphate.

In UV/vis stopped-flow experiments we were able to detect an intermediate-species, which gave rise to a characteristic absorption at ~ 420 nm. By comparative analysis of active site variants in terms of UV/vis and ^1H NMR spectroscopic intermediate analysis we propose the detected species to be the enol form of the AcThDP. In this regard the addition of phosphate after formation of enolAcThDP led to complete signal depletion within a few milliseconds showing that the detected species is a true occurring intermediate. Prior to phosphorolysis the enolAcThDP needs to tautomerize into its keto form, so phosphate can attack in a nucleophilic manner. By H/D exchange experiments we could show that the enzyme bound AcThDP indeed changes dynamically between its enol- and keto-form.

Based on this it seems that phosphate accelerates this tautomerization by more than three orders of magnitude, acting in a substrate assisted catalytic manner. This unique catalytic mechanism has to our knowledge not been described in terms of a direct spectroscopic observation with inorganic phosphate as catalyst, changing the chemical nature on an enzyme bound intermediate.

To further characterize a putative TKTL1 mediated catalytic function TKTL1 as well as TKTL2 were recombinantly expressed and analysed for enzymatic activity and ThDP cofactor binding as the previously described deletion variant. Neither in a coupled enzymatic assay, nor while performing mass spectrometric product analysis a noteworthy catalytic activity was detected. This absence of a ThDP mediated catalytic activity seems to be caused by the disability of TKTL1 and 2 to bind the ThDP cofactor, as judged by circular dichroism measurements. Therefore a role in tumorigenesis of TKTL1 by an intrinsic catalytic activity seems rather unlikely.

6 Bibliography

1. **Haberland, J.; Bertz, J.; Wolf, U.; Ziese, T.; Kurth, B. M.**, German cancer statistics 2004. *BMC cancer* 2010, *10*, 52.
2. **Luengo-Fernandez, R.; Leal, J.; Gray, A.; Sullivan, R.**, Economic burden of cancer across the European Union: a population-based cost analysis. *The lancet oncology* 2013.
3. **Bertram, J. S.**, The molecular biology of cancer. *Molecular aspects of medicine* 2000, *21* (6), 167-223.
4. **Weinberg, R. A.**, Oncogenes and tumor suppressor genes. *CA: a cancer journal for clinicians* 1994, *44* (3), 160-70.
5. **Hanahan, D.; Weinberg, R. A.**, The hallmarks of cancer. *Cell* 2000, *100* (1), 57-70.
6. **Hanahan, D.; Weinberg, R. A.**, Hallmarks of cancer: the next generation. *Cell* 2011, *144* (5), 646-74.
7. **Cairns, R. A.; Harris, I. S.; Mak, T. W.**, Regulation of cancer cell metabolism. *Nature reviews. Cancer* 2011, *11* (2), 85-95.
8. **Herling, A.; Konig, M.; Bulik, S.; Holzhutter, H. G.**, Enzymatic features of the glucose metabolism in tumor cells. *The FEBS journal* 2011, *278* (14), 2436-59.
9. **Altenberg, B.; Greulich, K. O.**, Genes of glycolysis are ubiquitously overexpressed in 24 cancer classes. *Genomics* 2004, *84* (6), 1014-20.
10. **Furuta, E.; Okuda, H.; Kobayashi, A.; Watabe, K.**, Metabolic genes in cancer: their roles in tumor progression and clinical implications. *Biochimica et biophysica acta* 2010, *1805* (2), 141-52.
11. **Warburg, O.; Wind, F.; Negelein, E.**, The Metabolism of Tumors in the Body. *The Journal of general physiology* 1927, *8* (6), 519-30.
12. **Warburg, O.**, On the origin of cancer cells. *Science* 1956, *123* (3191), 309-14.
13. **Warburg, O.**, On respiratory impairment in cancer cells. *Science* 1956, *124* (3215), 269-70.
14. **Stryer, L. B., J. M.; Tymoczko, J. L.**, *Biochemistry (5th ed.)*. W. H. Freeman: New York, 2002.
15. **Jang, M.; Kim, S. S.; Lee, J.**, Cancer cell metabolism: implications for therapeutic targets. *Experimental & molecular medicine* 2013, *45*, e45.

6. Bibliography

16. **Heiden, M. G. V.; Cantley, L. C.; Thompson, C. B.**, Understanding the Warburg Effect: The Metabolic Requirements of Cell Proliferation. *Science* 2009, *324* (5930), 1029-1033.
17. **Vanhaesebroeck, B.; Stephens, L.; Hawkins, P.**, PI3K signalling: the path to discovery and understanding. *Nature reviews. Molecular cell biology* 2012, *13* (3), 195-203.
18. **Deberardinis, R. J.; Sayed, N.; Ditsworth, D.; Thompson, C. B.**, Brick by brick: metabolism and tumor cell growth. *Current opinion in genetics & development* 2008, *18* (1), 54-61.
19. **Shackelford, D. B.; Shaw, R. J.**, The LKB1-AMPK pathway: metabolism and growth control in tumour suppression. *Nature reviews. Cancer* 2009, *9* (8), 563-75.
20. **Bensaad, K.; Tsuruta, A.; Selak, M. A.; Vidal, M. N.; Nakano, K.; Bartrons, R.; Gottlieb, E.; Vousden, K. H.**, TIGAR, a p53-inducible regulator of glycolysis and apoptosis. *Cell* 2006, *126* (1), 107-20.
21. **Stambolic, V.; MacPherson, D.; Sas, D.; Lin, Y.; Snow, B.; Jang, Y.; Benchimol, S.; Mak, T. W.**, Regulation of PTEN transcription by p53. *Molecular cell* 2001, *8* (2), 317-25.
22. **DeBerardinis, R. J.; Cheng, T.**, Q's next: the diverse functions of glutamine in metabolism, cell biology and cancer. *Oncogene* 2010, *29* (3), 313-24.
23. **Sprenger, G. A.; Schorken, U.; Sprenger, G.; Sahm, H.**, Transketolase A of *Escherichia coli* K12. Purification and properties of the enzyme from recombinant strains. *European journal of biochemistry / FEBS* 1995, *230* (2), 525-32.
24. **Schneider, G.; Lindqvist, Y.**, Crystallography and mutagenesis of transketolase: mechanistic implications for enzymatic thiamin catalysis. *Biochimica et biophysica acta* 1998, *1385* (2), 387-98.
25. **Schenk, G.; Duggleby, R. G.; Nixon, P. F.**, Heterologous expression of human transketolase. *Int J Biochem Cell B* 1998, *30* (3), 369-378.
26. **Hammes, H. P.; Du, X.; Edelstein, D.; Taguchi, T.; Matsumura, T.; Ju, Q.; Lin, J.; Bierhaus, A.; Nawroth, P.; Hannak, D.; Neumaier, M.; Bergfeld, R.; Giardino, I.; Brownlee, M.**, Benfotiamine blocks three major pathways of hyperglycemic damage and prevents experimental diabetic retinopathy. *Nature medicine* 2003, *9* (3), 294-9.
27. **Heroux, M.; Raghavendra Rao, V. L.; Lavoie, J.; Richardson, J. S.; Butterworth, R. F.**, Alterations of thiamine phosphorylation and of thiamine-dependent enzymes in Alzheimer's disease. *Metabolic brain disease* 1996, *11* (1), 81-8.

6. Bibliography

28. **Boros, L. G.; Puigjaner, J.; Cascante, M.; Lee, W. N.; Brandes, J. L.; Bassilian, S.; Yusuf, F. I.; Williams, R. D.; Muscarella, P.; Melvin, W. S.; Schirmer, W. J.**, Oxythiamine and dehydroepiandrosterone inhibit the nonoxidative synthesis of ribose and tumor cell proliferation. *Cancer research* 1997, *57* (19), 4242-8.
29. **Pacal, L.; Tomandl, J.; Svojanovsky, J.; Krusova, D.; Stepankova, S.; Rehorova, J.; Olsovsky, J.; Belobradkova, J.; Tanhauserova, V.; Tomandlova, M.; Muzik, J.; Kankova, K.**, Role of thiamine status and genetic variability in transketolase and other pentose phosphate cycle enzymes in the progression of diabetic nephropathy. *Nephrology, dialysis, transplantation : official publication of the European Dialysis and Transplant Association - European Renal Association* 2011, *26* (4), 1229-36.
30. **Zahr, N. M.; Kaufman, K. L.; Harper, C. G.**, Clinical and pathological features of alcohol-related brain damage. *Nat Rev Neurol* 2011, *7* (5), 284-294.
31. **Thomas, A. A.; De Meese, J.; Le Huerou, Y.; Boyd, S. A.; Romoff, T. T.; Gonzales, S. S.; Gunawardana, I.; Kaplan, T.; Sullivan, F.; Condroski, K.; Lyssikatos, J. P.; Aicher, T. D.; Ballard, J.; Bernat, B.; DeWolf, W.; Han, M.; Lemieux, C.; Smith, D.; Weiler, S.; Wright, S. K.; Vigers, G.; Brandhuber, B.**, Non-charged thiamine analogs as inhibitors of enzyme transketolase. *Bioorganic & medicinal chemistry letters* 2008, *18* (2), 509-12.
32. **Thomas, A. A.; Le Huerou, Y.; De Meese, J.; Gunawardana, I.; Kaplan, T.; Romoff, T. T.; Gonzales, S. S.; Condroski, K.; Boyd, S. A.; Ballard, J.; Bernat, B.; DeWolf, W.; Han, M.; Lee, P.; Lemieux, C.; Pedersen, R.; Pheneger, J.; Poch, G.; Smith, D.; Sullivan, F.; Weiler, S.; Wright, S. K.; Lin, J.; Brandhuber, B.; Vigers, G.**, Synthesis, in vitro and in vivo activity of thiamine antagonist transketolase inhibitors. *Bioorganic & medicinal chemistry letters* 2008, *18* (6), 2206-10.
33. **Le Huerou, Y.; Gunawardana, I.; Thomas, A. A.; Boyd, S. A.; de Meese, J.; Dewolf, W.; Gonzales, S. S.; Han, M.; Hayter, L.; Kaplan, T.; Lemieux, C.; Lee, P.; Pheneger, J.; Poch, G.; Romoff, T. T.; Sullivan, F.; Weiler, S.; Wright, S. K.; Lin, J.**, Prodrug thiamine analogs as inhibitors of the enzyme transketolase. *Bioorganic & medicinal chemistry letters* 2008, *18* (2), 505-8.
34. **Lindqvist, Y.; Schneider, G.; Ermler, U.; Sundstrom, M.**, **Three-dimensional structure of transketolase**, a thiamine diphosphate dependent enzyme, at 2.5 Å resolution. *The EMBO journal* 1992, *11* (7), 2373-9.
35. **Schenk, G.; Layfield, R.; Candy, J. M.; Duggleby, R. G.; Nixon, P. F.**, Molecular evolutionary analysis of the thiamine-diphosphate-dependent enzyme, transketolase. *Journal of molecular evolution* 1997, *44* (5), 552-72.
36. **Kluger, R.**, Thiamin Diphosphate - a Mechanistic Update on Enzymatic and Nonenzymic Catalysis of Decarboxylation. *Chem Rev* 1987, *87* (5), 863-876.
37. **Jordan, F.**, Current mechanistic understanding of thiamin diphosphate-dependent enzymatic reactions. *Natural product reports* 2003, *20* (2), 184-201.

6. Bibliography

38. **Kluger, R.; Tittmann, K.**, Thiamin diphosphate catalysis: enzymic and nonenzymic covalent intermediates. *Chem Rev* 2008, *108* (6), 1797-833.
39. **Pohl, M.; Sprenger, G. A.; Muller, M.**, A new perspective on thiamine catalysis. *Current opinion in biotechnology* 2004, *15* (4), 335-42.
40. **Williams, R. R.**, Structure of Vitamin B1. *J. Am. Chem. Soc.* **1936**, *58* (6), 1063-1064.
41. **Breslow, R.**, Rapid deuterium exchange in thiazolium salts. *J. Am. Chem. Soc.* 1957, *79* (7), 1762-1763.
42. **Breslow, R.**, On the Mechanism of Thiamine Action IV. Evidence from Studies on Model Systems. *J. Am. Chem. Soc.* 1958, *80* (14), 3719-3726.
43. **Kemp, D. S.; O'Brien, J. T.**, Base catalysis of thiazolium salt hydrogen exchange and its implications for enzymatic thiamine cofactor catalysis. *Journal of the American Chemical Society* 1970, *92* (8), 2554-5.
44. **Washabaugh, M. W.; Jencks, W. P.**, Thiazolium C(2)-proton exchange: structure-reactivity correlations and the pKa of thiamin C(2)-H revisited. *Biochemistry* 1988, *27* (14), 5044-53.
45. **Muller, Y. A.; Lindqvist, Y.; Furey, W.; Schulz, G. E.; Jordan, F.; Schneider, G.**, A thiamin diphosphate binding fold revealed by comparison of the crystal structures of transketolase, pyruvate oxidase and pyruvate decarboxylase. *Structure* 1993, *1* (2), 95-103.
46. **Kern, D.; Kern, G.; Neef, H.; Tittmann, K.; Killenberg-Jabs, M.; Wikner, C.; Schneider, G.; Hubner, G.**, How thiamine diphosphate is activated in enzymes. *Science* 1997, *275* (5296), 67-70.
47. **Hubner, G.; Tittmann, K.; Killenberg-Jabs, M.; Schaffner, J.; Spinka, M.; Neef, H.; Kern, D.; Kern, G.; Schneider, G.; Wikner, C.; Ghisla, S.**, Activation of thiamin diphosphate in enzymes. *Biochimica et biophysica acta* 1998, *1385* (2), 221-8.
48. **Jordan, F.; Nemeria, N. S.**, Experimental observation of thiamin diphosphate-bound intermediates on enzymes and mechanistic information derived from these observations. *Bioorganic chemistry* 2005, *33* (3), 190-215.
49. **Nemeria, N.; Korotchkina, L.; McLeish, M. J.; Kenyon, G. L.; Patel, M. S.; Jordan, F.**, Elucidation of the chemistry of enzyme-bound thiamin diphosphate prior to substrate binding: defining internal equilibria among tautomeric and ionization states. *Biochemistry* 2007, *46* (37), 10739-44.

6. Bibliography

50. **Mitschke, L.; Parthier, C.; Schroder-Tittmann, K.; Coy, J.; Ludtke, S.; Tittmann, K.**, The crystal structure of human transketolase and new insights into its mode of action. *The Journal of biological chemistry* 2010, *285* (41), 31559-70.
51. **Ludtke, S.; Neumann, P.; Erixon, K. M.; Leeper, F.; Kluger, R.; Ficner, R.; Tittmann, K.**, Sub-angstrom-resolution crystallography reveals physical distortions that enhance reactivity of a covalent enzymatic intermediate. *Nature chemistry* 2013, *5* (9), 762-7.
52. **Coy, J. F.; Dubel, S.; Kioschis, P.; Thomas, K.; Micklem, G.; Delius, H.; Poustka, A.**, Molecular cloning of tissue-specific transcripts of a transketolase-related gene: implications for the evolution of new vertebrate genes. *Genomics* 1996, *32* (3), 309-16.
53. **Coy, J. F.; Dressler, D.; Wilde, J.; Schubert, P.**, Mutations in the transketolase-like gene TKTL1: clinical implications for neurodegenerative diseases, diabetes and cancer. *Clinical laboratory* 2005, *51* (5-6), 257-73.
54. **Needleman, S. B.; Wunsch, C. D.**, A general method applicable to the search for similarities in the amino acid sequence of two proteins. *Journal of molecular biology* 1970, *48* (3), 443-53.
55. **Foldi, M.; Stickeler, E.; Bau, L.; Kretz, O.; Watermann, D.; Gitsch, G.; Kayser, G.; Zur Hausen, A.; Coy, J. F.**, Transketolase protein TKTL1 overexpression: A potential biomarker and therapeutic target in breast cancer. *Oncology reports* 2007, *17* (4), 841-5.
56. **Volker, H. U.; Hagemann, C.; Coy, J.; Wittig, R.; Sommer, S.; Stojic, J.; Haubitz, I.; Vince, G. H.; Kammerer, U.; Monoranu, C. M.**, Expression of transketolase-like 1 and activation of Akt in grade IV glioblastomas compared with grades II and III astrocytic gliomas. *American journal of clinical pathology* 2008, *130* (1), 50-7.
57. **Chen, H.; Yue, J. X.; Yang, S. H.; Ding, H.; Zhao, R. W.; Zhang, S.**, Overexpression of transketolase-like gene 1 is associated with cell proliferation in uterine cervix cancer. *Journal of experimental & clinical cancer research : CR* 2009, *28*, 43.
58. **Wikner, C.; Meshalkina, L.; Nilsson, U.; Backstrom, S.; Lindqvist, Y.; Schneider, G.**, His103 in yeast transketolase is required for substrate recognition and catalysis. *European journal of biochemistry / FEBS* 1995, *233* (3), 750-5.
59. **Madigan, M. T.; Martinko, J. M.**, *Brock biology of microorganisms*. 12th edition ed.; Pearson/Benjamin Cummings: San Francisco, CA, USA, 2009.
60. **Hawkins, C. F.; Borges, A.; Perham, R. N.**, A common structural motif in thiamin pyrophosphate-binding enzymes. *FEBS letters* 1989, *255* (1), 77-82.
61. **Xu, X. J.; zur Hausen, A.; Coy, J. F.; Lochelt, M.**, Transketolase-like protein 1 (TKTL1) is required for rapid cell growth and full viability of human tumor cells. *International Journal of Cancer* 2009, *124* (6), 1330-1337.

6. Bibliography

62. **Yuan, W. J.; Wu, S. B.; Guo, J. W.; Chen, Z. K.; Ge, J.; Yang, P.; Hu, B.; Chen, Z. H.**, Silencing of TKTL1 by siRNA inhibits proliferation of human gastric cancer cells in vitro and in vivo. *Cancer biology & therapy* 2010, 9 (9), 710-716.
63. **Zerilli, M.; Amato, M. C.; Martorana, A.; Cabibi, D.; Coy, J. F.; Cappello, F.; Pompei, G.; Russo, A.; Giordano, C.; Rodolico, V.**, Increased expression of transketolase-like-1 in papillary thyroid carcinomas smaller than 1.5 cm in diameter is associated with lymph-node metastases. *Cancer* 2008, 113 (5), 936-944.
64. **Krockenberger, M.; Honig, A.; Rieger, L.; Coy, J. F.; Sutterlin, M.; Kapp, M.; Horn, E.; Dietl, J.; Kammerer, U.**, Transketolase-like 1 expression correlates with subtypes of ovarian cancer and the presence of distant metastases. *International journal of gynecological cancer : official journal of the International Gynecological Cancer Society* 2007, 17 (1), 101-6.
65. **Schmidt, M.; Voelker, H. U.; Kapp, M.; Krockenberger, M.; Dietl, J.; Kammerer, U.**, Glycolytic phenotype in breast cancer: activation of Akt, up-regulation of GLUT1, TKTL1 and down-regulation of M2PK. *Journal of cancer research and clinical oncology* 2010, 136 (2), 219-25.
66. **Kayser, G.; Kassem, A.; Sienel, W.; Schulte-Uentrop, L.; Mattern, D.; Aumann, K.; Stickeler, E.; Werner, M.; Passlick, B.; zur Hausen, A.**, Lactate-dehydrogenase 5 is overexpressed in non-small cell lung cancer and correlates with the expression of the transketolase-like protein 1. *Diagnostic pathology* 2010, 5, 22.
67. **Kohrenhagen, N.; Voelker, H. U.; Schmidt, M.; Kapp, M.; Krockenberger, M.; Frambach, T.; Dietl, J.; Kammerer, U.**, Expression of transketolase-like 1 (TKTL1) and p-Akt correlates with the progression of cervical neoplasia. *The journal of obstetrics and gynaecology research* 2008, 34 (3), 293-300.
68. **Bentz, S.; Pesch, T.; Wolfram, L.; de Valliere, C.; Leucht, K.; Fried, M.; Coy, J. F.; Hausmann, M.; Rogler, G.**, Lack of transketolase-like (TKTL) 1 aggravates murine experimental colitis. *American journal of physiology. Gastrointestinal and liver physiology* 2011, 300 (4), G598-607.
69. **Wanka, C.; Steinbach, J. P.; Rieger, J.**, Tp53-induced glycolysis and apoptosis regulator (TIGAR) protects glioma cells from starvation-induced cell death by up-regulating respiration and improving cellular redox homeostasis. *The Journal of biological chemistry* 2012, 287 (40), 33436-46.
70. **Sun, W.; Liu, Y.; Glazer, C. A.; Shao, C.; Bhan, S.; Demokan, S.; Zhao, M.; Rudek, M. A.; Ha, P. K.; Califano, J. A.**, TKTL1 is activated by promoter hypomethylation and contributes to head and neck squamous cell carcinoma carcinogenesis through increased aerobic glycolysis and HIF1alpha stabilization. *Clinical cancer research : an official journal of the American Association for Cancer Research* 2010, 16 (3), 857-66.

6. Bibliography

71. **Smith, I. M.; Glazer, C. A.; Mithani, S. K.; Ochs, M. F.; Sun, W.; Bhan, S.; Vostrov, A.; Abdullaev, Z.; Lobanenkov, V.; Gray, A.; Liu, C.; Chang, S. S.; Ostrow, K. L.; Westra, W. H.; Begum, S.; Dhara, M.; Califano, J.**, Coordinated activation of candidate proto-oncogenes and cancer testes antigens via promoter demethylation in head and neck cancer and lung cancer. *PLoS one* 2009, 4 (3), e4961.
72. **Lu, H.; Dalgard, C. L.; Mohyeldin, A.; McFate, T.; Tait, A. S.; Verma, A.**, Reversible inactivation of HIF-1 prolyl hydroxylases allows cell metabolism to control basal HIF-1. *The Journal of biological chemistry* 2005, 280 (51), 41928-39.
73. **Kaelin, W. G., Jr.; Ratcliffe, P. J.**, Oxygen sensing by metazoans: the central role of the HIF hydroxylase pathway. *Molecular cell* 2008, 30 (4), 393-402.
74. **Vaupel, P.**, The role of hypoxia-induced factors in tumor progression. *Oncologist* 2004, 9, 10-17.
75. **Mayer, A.; Von Wallbrunn, A.; Vaupel, P.**, Glucose metabolism of malignant cells is not regulated by transketolase-like (TKTL)-1. *International journal of oncology* 2010, 37 (2), 265-71.
76. **Hartmannsberger, D.; Mack, B.; Eggert, C.; Denzel, S.; Stepp, H.; Betz, C. S.; Gires, O.**, Transketolase-like protein 1 confers resistance to serum withdrawal in vitro. *Cancer letters* 2011, 300 (1), 20-9.
77. **Heath, E. C.; Hurwitz, J.; Horecker, B. L.; Ginsburg, A.**, Pentose fermentation by *Lactobacillus plantarum*. I. The cleavage of xylulose 5-phosphate by phosphoketolase. *The Journal of biological chemistry* 1958, 231 (2), 1009-29.
78. **Takahashi, K.; Tagami, U.; Shimba, N.; Kashiwagi, T.; Ishikawa, K.; Suzuki, E.**, Crystal structure of *Bifidobacterium longum* phosphoketolase; key enzyme for glucose metabolism in Bifidobacterium. *FEBS letters* 2010, 584 (18), 3855-61.
79. **Suzuki, R.; Kim, B. J.; Shibata, T.; Iwamoto, Y.; Katayama, T.; Ashida, H.; Wakagi, T.; Shoun, H.; Fushinobu, S.; Yamamoto, K.**, Overexpression, crystallization and preliminary X-ray analysis of xylulose-5-phosphate/fructose-6-phosphate phosphoketolase from *Bifidobacterium breve*. *Acta crystallographica. Section F, Structural biology and crystallization communications* 2010, 66 (Pt 8), 941-3.
80. **Suzuki, R.; Katayama, T.; Kim, B. J.; Wakagi, T.; Shoun, H.; Ashida, H.; Yamamoto, K.; Fushinobu, S.**, Crystal structures of phosphoketolase: thiamine diphosphate-dependent dehydration mechanism. *The Journal of biological chemistry* 2010, 285 (44), 34279-87.
81. **Yevenes, A.; Frey, P. A.**, Cloning, expression, purification, cofactor requirements, and steady state kinetics of phosphoketolase-2 from *Lactobacillus plantarum*. *Bioorganic chemistry* 2008, 36 (1-3), 121-127.

6. Bibliography

82. **Gruys, K. J.; Halkides, C. J.; Frey, P. A.**, Synthesis and properties of 2-acetylthiamin pyrophosphate: an enzymatic reaction intermediate. *Biochemistry* 1987, 26 (24), 7575-85.
83. **Gruys, K. J.; Datta, A.; Frey, P. A.**, 2-Acetylthiamin pyrophosphate (acetyl-TPP) pH-rate profile for hydrolysis of acetyl-TPP and isolation of acetyl-TPP as a transient species in pyruvate dehydrogenase catalyzed reactions. *Biochemistry* 1989, 28 (23), 9071-80.
84. **Tittmann, K.; Golbik, R.; Ghisla, S.; Hubner, G.**, Mechanism of elementary catalytic steps of pyruvate oxidase from *Lactobacillus plantarum*. *Biochemistry* 2000, 39 (35), 10747-54.
85. **Wille, G.; Meyer, D.; Steinmetz, A.; Hinze, E.; Golbik, R.; Tittmann, K.**, The catalytic cycle of a thiamin diphosphate enzyme examined by cryocrystallography. *Nature chemical biology* 2006, 2 (6), 324-8.
86. **Dall'Acqua, W.; Carter, P.**, Substrate-assisted catalysis: molecular basis and biological significance. *Protein science : a publication of the Protein Society* 2000, 9 (1), 1-9.
87. **Ausubel F.M., B. R. E., Kingston D.D., Seidmann J.R., Smith J.A., Struhl K.**, *Current Protocolls in Molecular Biology*. Green Publishing Associates and John Wiley and Sons Inc.: New York, New York, USA, 1993.
88. **Corpet, F.**, Multiple sequence alignment with hierarchical clustering. *Nucleic acids research* 1988, 16 (22), 10881-90.
89. **Gouet, P.; Courcelle, E.; Stuart, D. I.; Metz, F.**, ESPript: analysis of multiple sequence alignments in PostScript. *Bioinformatics* 1999, 15 (4), 305-8.
90. **Bertani, G.**, Studies on lysogenesis. I. The mode of phage liberation by lysogenic *Escherichia coli*. *Journal of bacteriology* 1951, 62 (3), 293-300.
91. **Taylor, R. G.; Walker, D. C.; McInnes, R. R.**, *E. coli* host strains significantly affect the quality of small scale plasmid DNA preparations used for sequencing. *Nucleic acids research* 1993, 21 (7), 1677-8.
92. **Inoue, H.; Nojima, H.; Okayama, H.**, High efficiency transformation of *Escherichia coli* with plasmids. *Gene* 1990, 96 (1), 23-8.
93. **Horton, R. M.; Hunt, H. D.; Ho, S. N.; Pullen, J. K.; Pease, L. R.**, Engineering hybrid genes without the use of restriction enzymes: gene splicing by overlap extension. *Gene* 1989, 77 (1), 61-8.
94. **Laemmli, U. K.**, Cleavage of structural proteins during the assembly of the head of bacteriophage T4. *Nature* 1970, 227 (5259), 680-5.

6. Bibliography

95. **Bradford, M. M.**, A rapid and sensitive method for the quantitation of microgram quantities of protein utilizing the principle of protein-dye binding. *Analytical biochemistry* 1976, 72, 248-54.
96. **Kochetov, G. A.**, Transketolase from yeast, rat liver, and pig liver. *Methods in enzymology* 1982, 90 Pt E, 209-23.
97. **Kelly, S. M.; Jess, T. J.; Price, N. C.**, How to study proteins by circular dichroism. *Biochimica et biophysica acta* 2005, 1751 (2), 119-39.
98. **Bohm, G.; Muhr, R.; Jaenicke, R.**, Quantitative analysis of protein far UV circular dichroism spectra by neural networks. *Protein engineering* 1992, 5 (3), 191-5.
99. **Pace, C. N.; Hebert, E. J.; Shaw, K. L.; Schell, D.; Both, V.; Krajcikova, D.; Sevcik, J.; Wilson, K. S.; Dauter, Z.; Hartley, R. W.; Grimsley, G. R.**, Conformational stability and thermodynamics of folding of ribonucleases Sa, Sa2 and Sa3. *Journal of molecular biology* 1998, 279 (1), 271-86.
100. **Kochetov, G. A.; Usmanov, R. A.; Merzlov, V. P.**, Thiaminepyrophosphate induced changes in the optical activity of baker's yeast transketolase. *FEBS letters* 1970, 9 (5), 265-266.
101. **Heinrich, C. P.; Noack, K.; Wiss, O.**, A circular dichroism study of transketolase from baker's yeast. *Biochemical and biophysical research communications* 1971, 44 (2), 275-9.
102. **Tittmann, K.** Untersuchungen zu Katalysemechanismen von Flavin- und Thiamindiphosphat-abhängigen Enzymen. Aktivierung von Thiamindiphosphat in Enzymen. Katalysemechanismus der Pyruvateoxidase aus *Lactobacillus plantarum*. Martin-Luther-University, Halle an der Saale, 2000.
103. **Tittmann, K.; Golbik, R.; Uhlemann, K.; Khailova, L.; Schneider, G.; Patel, M.; Jordan, F.; Chipman, D. M.; Duggleby, R. G.; Hubner, G.**, NMR analysis of covalent intermediates in thiamin diphosphate enzymes. *Biochemistry* 2003, 42 (26), 7885-91.
104. **Lipmann, F.; Tuttle, L. C.**, The detection of activated carboxyl groups with hydroxylamine as interceptor. *The Journal of biological chemistry* 1945, 161, 415.
105. **Goldberg, M. L.; Racker, E.**, Formation and isolation of a glycolaldehyde-phosphoketolase intermediate. *The Journal of biological chemistry* 1962, 237, 3841-2.
106. **Todd, M. J.; Gomez, J.**, Enzyme kinetics determined using calorimetry: a general assay for enzyme activity? *Analytical biochemistry* 2001, 296 (2), 179-87.

6. Bibliography

107. **Haynes, C. A.; Allegood, J. C.; Sims, K.; Wang, E. W.; Sullards, M. C.; Merrill, A. H., Jr.**, Quantitation of fatty acyl-coenzyme As in mammalian cells by liquid chromatography-electrospray ionization tandem mass spectrometry. *Journal of lipid research* 2008, *49* (5), 1113-25.
108. **Kabsch, W.**, Xds. *Acta crystallographica. Section D, Biological crystallography* 2010, *66* (Pt 2), 125-32.
109. **Adams, P. D.; Afonine, P. V.; Bunkoczi, G.; Chen, V. B.; Davis, I. W.; Echols, N.; Headd, J. J.; Hung, L. W.; Kapral, G. J.; Grosse-Kunstleve, R. W.; McCoy, A. J.; Moriarty, N. W.; Oeffner, R.; Read, R. J.; Richardson, D. C.; Richardson, J. S.; Terwilliger, T. C.; Zwart, P. H.**, PHENIX: a comprehensive Python-based system for macromolecular structure solution. *Acta crystallographica. Section D, Biological crystallography* 2010, *66* (Pt 2), 213-21.
110. **Schuttelkopf, A. W.; van Aalten, D. M.**, PRODRG: a tool for high-throughput crystallography of protein-ligand complexes. *Acta crystallographica. Section D, Biological crystallography* 2004, *60* (Pt 8), 1355-63.
111. **Emsley, P.; Lohkamp, B.; Scott, W. G.; Cowtan, K.**, Features and development of Coot. *Acta crystallographica. Section D, Biological crystallography* 2010, *66* (Pt 4), 486-501.
112. **Mitschke, L.** Kinetische und strukturelle Charakterisierung humaner Transketolase. Martin-Luther-University, Halle an der Saale, 2008.
113. **Lüdtke, S.** Structural and functional studies on vitamin B1-Dependent human and bacterial transketolases. Georg-August University Göttingen, 2012.
114. **Freyer, M. W.; Lewis, E. A.**, Isothermal titration calorimetry: experimental design, data analysis, and probing macromolecule/ligand binding and kinetic interactions. *Methods in cell biology* 2008, *84*, 79-113.
115. **Leavitt, S.; Freire, E.**, Direct measurement of protein binding energetics by isothermal titration calorimetry. *Current opinion in structural biology* 2001, *11* (5), 560-6.
116. **Turnbull, W. B.; Daranas, A. H.**, On the value of c: can low affinity systems be studied by isothermal titration calorimetry? *Journal of the American Chemical Society* 2003, *125* (48), 14859-66.
117. **Liang, Y.**, Applications of isothermal titration calorimetry in protein science. *Acta biochimica et biophysica Sinica* 2008, *40* (7), 565-76.
118. **Washabaugh, M. W.; Yang, C. C.; Hollenbach, A. D.; Chen, P.**, Hydrolysis of Thiamin - Evidence for Rate-Limiting Breakdown of the Tricyclic Dihydrothiachromine Intermediate in Neutral Aqueous-Solution. *Bioorganic chemistry* 1993, *21* (2), 170-191.

6. Bibliography

119. **Rial, D. V.; Ceccarelli, E. A.**, Removal of DnaK contamination during fusion protein purifications. *Protein expression and purification* 2002, 25 (3), 503-7.
120. **Hutchinson, E. G.; Thornton, J. M.**, PROMOTIF--a program to identify and analyze structural motifs in proteins. *Protein science : a publication of the Protein Society* 1996, 5 (2), 212-20.
121. **Langbein, S.; Zerilli, M.; Zur Hausen, A.; Staiger, W.; Rensch-Boschert, K.; Lukan, N.; Popa, J.; Ternullo, M. P.; Steidler, A.; Weiss, C.; Grobholz, R.; Willeke, F.; Alken, P.; Stassi, G.; Schubert, P.; Coy, J. F.**, Expression of transketolase TKTL1 predicts colon and urothelial cancer patient survival: Warburg effect reinterpreted. *British journal of cancer* 2006, 94 (4), 578-85.
122. **Volker, H. U.; Scheich, M.; Schmausser, B.; Kammerer, U.; Eck, M.**, Overexpression of transketolase TKTL1 is associated with shorter survival in laryngeal squamous cell carcinomas. *European archives of oto-rhino-laryngology : official journal of the European Federation of Oto-Rhino-Laryngological Societies* 2007, 264 (12), 1431-6.
123. **Maslova, A. O.; Meshalkina, L. E.; Kochetov, G. A.**, Computer modeling of transketolase-like protein, TKTL1, a marker of certain tumor tissues. *Biochemistry. Biokhimiia* 2012, 77 (3), 296-9.
124. **Meshalkina, L. E.; Druitsa, V. L.; Koroleva, O. N.; Solovjeva, O. N.; Kochetov, G. A.**, Is transketolase-like protein, TKTL1, transketolase? *Biochimica et biophysica acta* 2013, 1832 (3), 387-90.
125. Cleland, W. W., *The Enzymes*.
126. **Fiedler, E.; Thorell, S.; Sandalova, T.; Golbik, R.; Konig, S.; Schneider, G.**, Snapshot of a key intermediate in enzymatic thiamin catalysis: crystal structure of the alpha-carbanion of (alpha,beta-dihydroxyethyl)-thiamin diphosphate in the active site of transketolase from *Saccharomyces cerevisiae*. *Proceedings of the National Academy of Sciences of the United States of America* 2002, 99 (2), 591-5.
127. **Asztalos, P.** Untersuchungen zu molekularen, strukturellen und biokatalytischen Aspekten des Vitamin B1-abhängigen Enzyms Transketolase A aus *Escherichia coli*. Martin-Luther-University, Halle an der Saale, 2008.
128. **Meyer, D.** Kinetische und strukturelle Untersuchung der Katalysemechanismen ausgewählter Kofaktor-abhängiger Enzyme - Implikationen für die Decarboxylierung von α -Ketosäuren durch Thiamindiphosphat-abhängige Enzyme. Martin-Luther-University, Halle an der Saale, 2011.
129. **Fiedler, E.** Kinetische und strukturelle Untersuchungen zur Donorsubstrat- und Ligandenbindung an Transketolase aus *Saccharomyces cerevisiae*. Martin-Luther-University, Halle an der Saale, 2002.

6. Bibliography

130. **Meyer, D.; Neumann, P.; Koers, E.; Sjuts, H.; Ludtke, S.; Sheldrick, G. M.; Ficner, R.; Tittmann, K.**, Unexpected tautomeric equilibria of the carbanion-enamine intermediate in pyruvate oxidase highlight unrecognized chemical versatility of thiamin. *Proceedings of the National Academy of Sciences of the United States of America* 2012, *109* (27), 10867-72.
131. **Merski, M.; Townsend, C. A.**, Observation of an acryloyl-thiamin diphosphate adduct in the first step of clavulanic acid biosynthesis. *Journal of the American Chemical Society* 2007, *129* (51), 15750-1.
132. **Nemeria, N.; Baykal, A.; Joseph, E.; Zhang, S.; Yan, Y.; Furey, W.; Jordan, F.**, Tetrahedral intermediates in thiamin diphosphate-dependent decarboxylations exist as a 1',4'-imino tautomeric form of the coenzyme, unlike the michaelis complex or the free coenzyme. *Biochemistry* 2004, *43* (21), 6565-75.
133. **Gibson, Q. H.; Swoboda, B. E.; Massey, V.**, Kinetics and Mechanism of Action of Glucose Oxidase. *The Journal of biological chemistry* 1964, *239*, 3927-34.
134. **Horton, N. C.; Newberry, K. J.; Perona, J. J.**, Metal ion-mediated substrate-assisted catalysis in type II restriction endonucleases. *Proceedings of the National Academy of Sciences of the United States of America* 1998, *95* (23), 13489-94.
135. **Cavarelli, J.; Eriani, G.; Rees, B.; Ruff, M.; Boeglin, M.; Mitschler, A.; Martin, F.; Gangloff, J.; Thierry, J. C.; Moras, D.**, The active site of yeast aspartyl-tRNA synthetase: structural and functional aspects of the aminoacylation reaction. *The EMBO journal* 1994, *13* (2), 327-37.
136. **Perona, J. J.; Rould, M. A.; Steitz, T. A.**, Structural basis for transfer RNA aminoacylation by Escherichia coli glutaminyl-tRNA synthetase. *Biochemistry* 1993, *32* (34), 8758-71.
137. **Gouaux, J. E.; Lipscomb, W. N.**, Three-dimensional structure of carbamoyl phosphate and succinate bound to aspartate carbamoyltransferase. *Proceedings of the National Academy of Sciences of the United States of America* 1988, *85* (12), 4205-8.
138. **Kosloff, M.; Selinger, Z.**, Substrate assisted catalysis application to G proteins. *Trends Biochem Sci* 2001, *26* (3), 161-166.
139. **Makrides, S. C.**, Strategies for achieving high-level expression of genes in Escherichia coli. *Microbiological reviews* 1996, *60* (3), 512-38.
140. **Gopal, G. J.; Kumar, A.**, Strategies for the Production of Recombinant Protein in Escherichia coli. *Protein J* 2013, *32* (6), 419-425.

6. Bibliography

141. **Zhao, F.; Mancuso, A.; Bui, T. V.; Tong, X.; Gruber, J. J.; Swider, C. R.; Sanchez, P. V.; Lum, J. J.; Sayed, N.; Melo, J. V.; Perl, A. E.; Carroll, M.; Tuttle, S. W.; Thompson, C. B.**, Imatinib resistance associated with BCR-ABL upregulation is dependent on HIF-1 alpha-induced metabolic reprogramming. *Oncogene* 2010, 29 (20), 2962-2972.
142. **Robey, I. F.; Lien, A. D.; Welsh, S. J.; Baggett, B. K.; Gillies, R. J.**, Hypoxia-inducible factor-1 alpha and the glycolytic phenotype in tumors. *Neoplasia* 2005, 7 (4), 324-330.
143. **Diaz-Moralli, S.; Tarrado-Castellarnau, M.; Alenda, C.; Castells, A.; Cascante, M.**, Transketolase-like 1 expression is modulated during colorectal cancer progression and metastasis formation. *PloS one* 2011, 6 (9), e25323.
144. **Wu, H. T.; Allie, N.; Myer, L.; Govender, D.**, Anaplastic nephroblastomas express transketolase-like enzyme 1. *Journal of clinical pathology* 2009, 62 (5), 460-463.
145. **Schultz, H.; Kahler, D.; Branscheid, D.; Vollmer, E.; Zabel, P.; Goldmann, T.**, TKTL1 is overexpressed in a large portion of non-small cell lung cancer specimens. *Diagnostic pathology* 2008, 3, 35.
146. **Langbein, S.; Frederiks, W. M.; zur Hausen, A.; Popa, J.; Lehmann, J.; Weiss, C.; Alken, P.; Coy, J. F.**, Metastasis is promoted by a bioenergetic switch: new targets for progressive renal cell cancer. *International journal of cancer. Journal international du cancer* 2008, 122 (11), 2422-8.
147. **Pang, S. S.; Duggleby, R. G.; Schowen, R. L.; Guddat, L. W.**, The crystal structures of *Klebsiella pneumoniae* acetolactate synthase with enzyme-bound cofactor and with an unusual intermediate. *The Journal of biological chemistry* 2004, 279 (3), 2242-53.

7. Appendix

7 Appendix

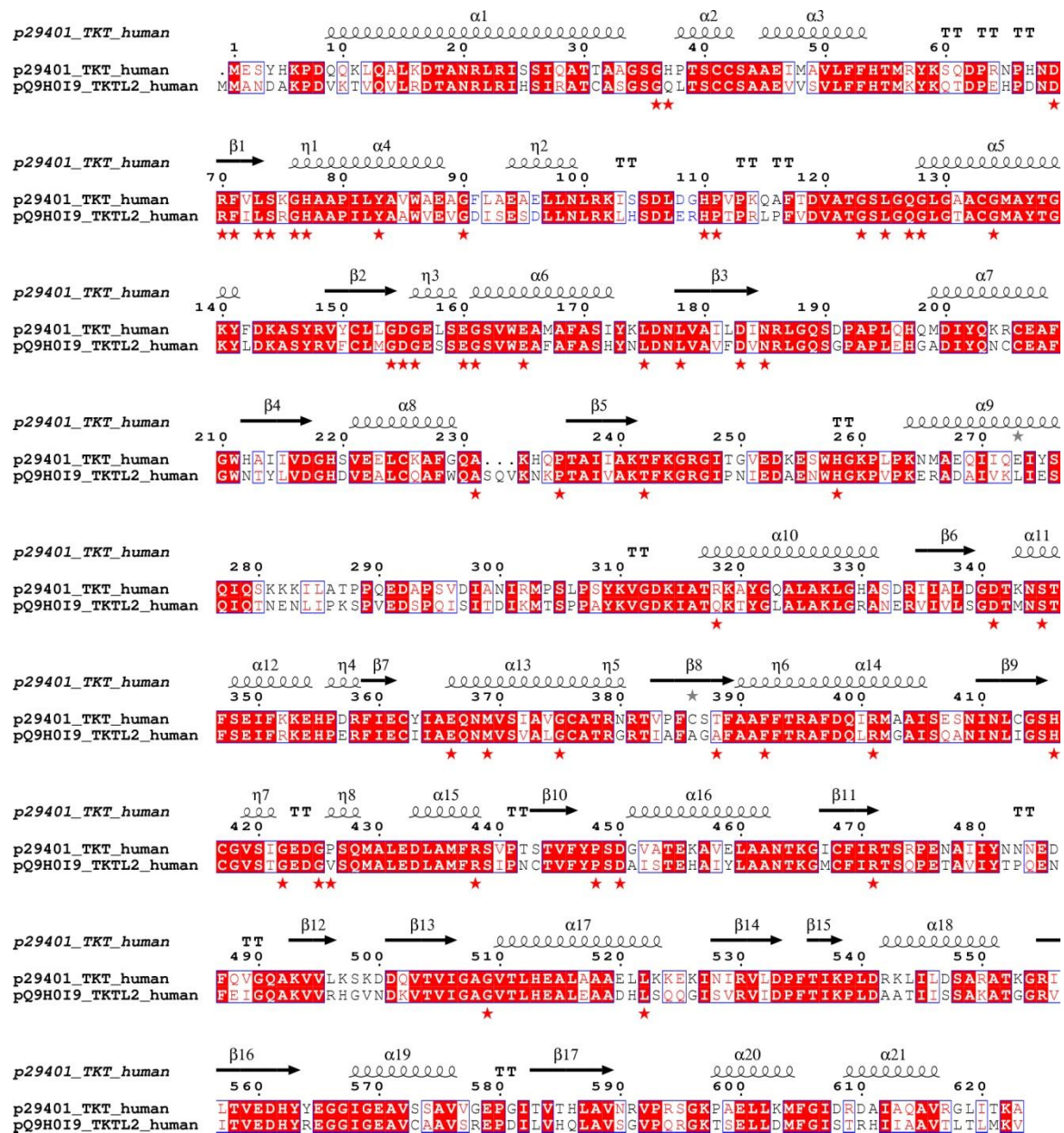


Figure 57: Sequence alignment of *h*TKT (p29401) against TKTL2 (pQ9H0I9). Numbering corresponds to the sequence of *human* TKT. Secondary structure elements are extracted from pdb-structure **3MOS** (*h*TKT). Identical residues are highlighted by a red background, similar ones by red characters. Asterisks mark residues which are invariant amongst all TKT sequences. Alignment and data presentation was performed with ClustalW2 and ESPrnt 2.3 respectively.

7. Appendix

Table 5: X-ray statistics for *B.breve* XFPK in ground state with native cofactor ThDP, or refined with Dihydrothiachromin.

Data set	XFPK E437Q Resting	XFPK E437Q Dihydrothiachromin	XFPK E437Q Dihydrothiachromin
Data collection statistics			
Space group	"	I422	"
Unit cell (Å)		<i>a</i> = 174.7 <i>b</i> = 174.7 <i>c</i> = 163.6	
Beam line		P111 P13	
Wavelength (Å)		0.8248	
Resolution Range (Å)		50-1.48 (1.604-1.48)	
Number reflections		1227798 (256166)	
Unique reflections		206660 (44003)	
Completeness (%)		99.8 (99.9)	
R _{merge} (%)		6.8 (58.3)	
<i>I</i> / σ <i>I</i>		17.19 (3.31)	
Redundancy		5.9 (5.8)	
Refinement statistics			
Resolution range (Å)	46.4-1.48	50-1.48	41.14-1.48
No. of reflections	196316 (10333)	196316 (10333)	196316 (10333)
R-factor/R _{free} (%)	16.02/17.37	16.02/17.37	15.56/17.12
Number of atoms			
Protein	6381	6420	6420
Ligands	97	71	71
Water	812	1026	1027
B-factor protein	26.23	19.75	19.49
B-factor ligands	27.52	19.85	21.68
B-factor Water	37.25	35.29	34.99
Deviations from ideal (r.m.s.d.)			
Bond distances (Å)	0.007	0.007	0.007
Bond angles (°)	1.221	1.223	1.23
Dihedrals (°)	13.689	14.06	14.13
Ramachandran plot			
Favoured regions (%)	96.75	96.6	96.75
Allowed regions (%)	3.25	3.4	3.25
Outlier regions (%)	0	0	0

7. Appendix

Table 6: X-ray statistics for *B.breve* XFPK in complex with 1,2-dihydroxyethyl thiamindiphosphate (DhETHDP) or 2-acetyl thiamindiphosphate (AcThDP).

Data set	XFPK E437Q AcThDP	XFPK DhThDP
Data collection statistics		
Space group	I422	"
Unit cell (Å)	$a = 174.3$ $b = 174.3$ $c = 163.3$	
Beam line	P111 P13	
Wavelength (Å)	0.8248	
Resolution Range (Å)	50-1.6 (1.7- 1.6)	
Number reflections	592371 (97584)	
Unique reflections	160690 (26467)	
Completeness (%)	98.2 (98)	
R _{merge} (%)	8 (86.1)	
I/σI	(15.78 (2.22))	
Redundancy	7.37	
Refinement statistics		
Resolution range (Å)	1.6-38.8	1.6-38.8
No. of reflections	160625	160625
R-factor/R _{free} (%)	16.56(19.31)	16.3/19.1
Number of atoms		
Protein	7533	6391
Ligands	75	74
Water	1043	1059
B-factor protein	16.2	16.41
B-factor ligands	22.9	23.81
B-factor Water	30.49	30.89
Deviations from ideal (r.m.s.d.)		
Bond distances (Å)	0.018	0.018
Bond angles (°)	1.787	1.773
Dihedrals (°)	14.08	14.08
Ramachandran plot		
Favoured regions (%)	96.5	96.5
Allowed regions (%)	3.5	3.5
Outlier regions (%)	0	0

7. Appendix

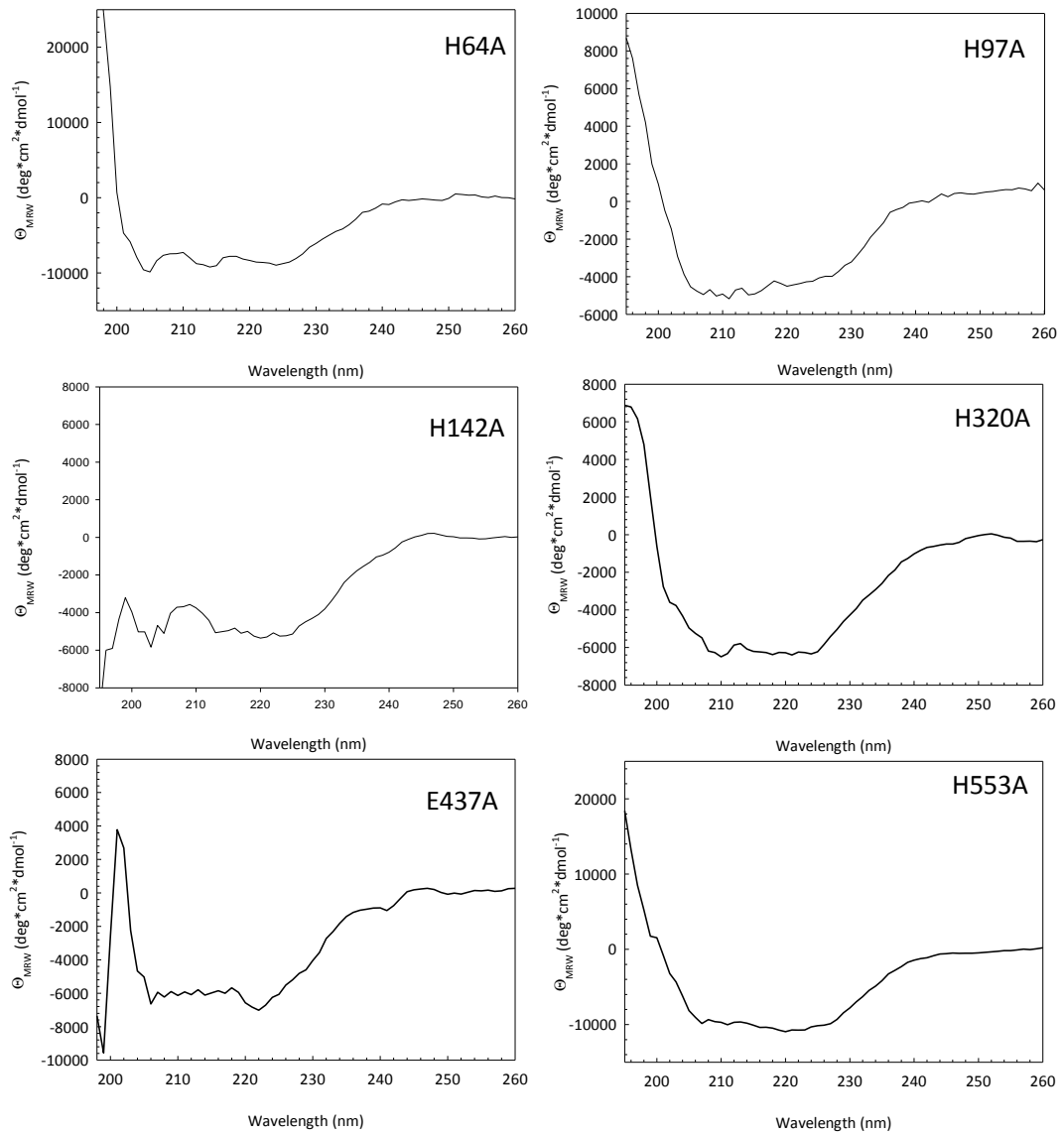


Figure 58: XFPK variants (0.1 mg/mL) were analysed by far-UV CD to estimate their secondary structural content.



Figure 59: SDS PAGE analysis of purified XFPK variants.

1) H64A, 2) H97A, 3) H142A, 4) H320A, 5) E437Q, 6) H553A

7. Appendix

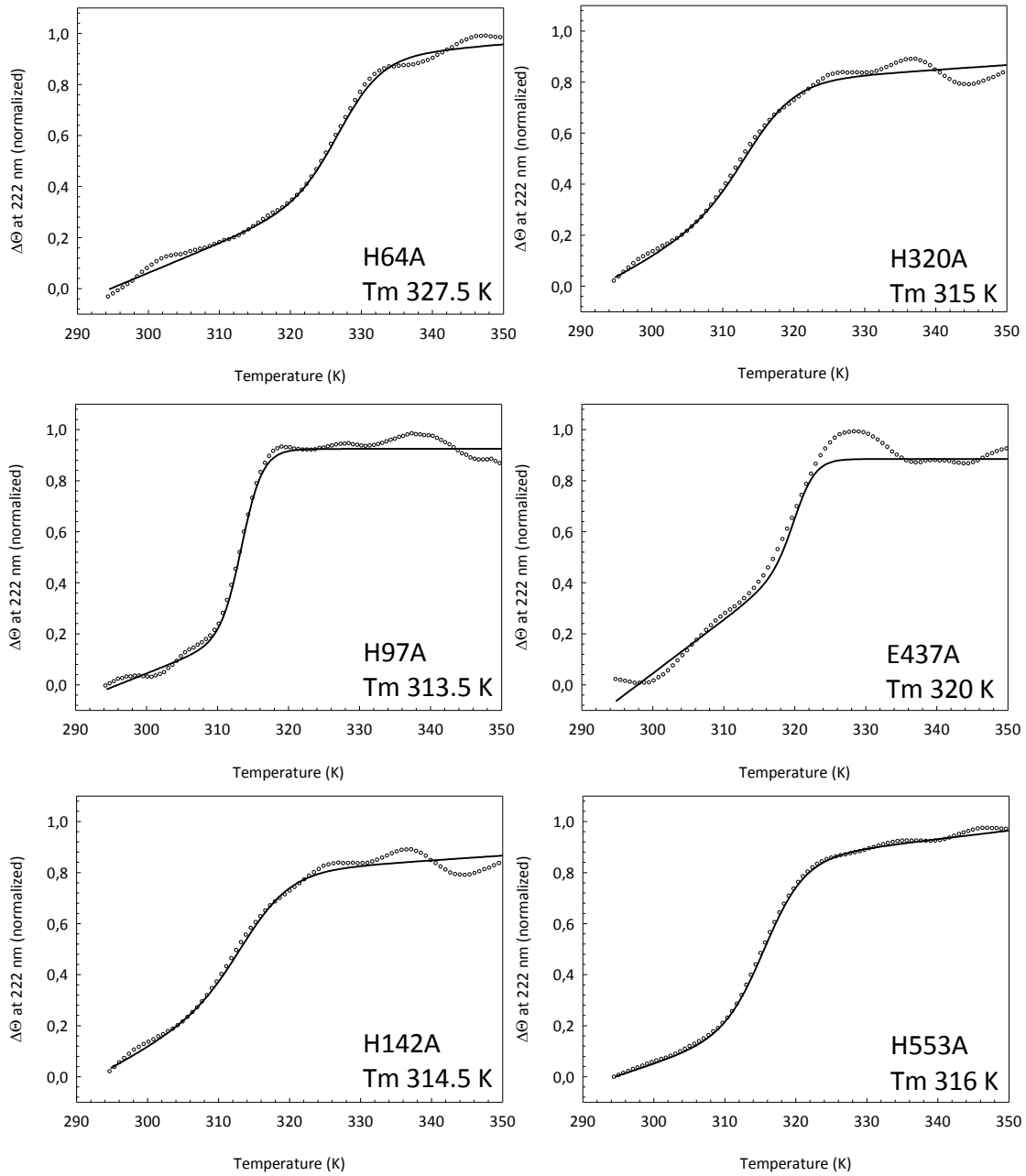


Figure 60: Temperature-induced unfolding of selected XFPK variants. Thermal unfolding was performed as described for the wild type. Apparent T_m was estimated by fitting the progress curves to equation 2.

7. Appendix

ITC kinetics calculations

Chemical reactions are driven by decrease in free energy which is summed up by the entropic and enthalpic term:

$$\Delta G = \Delta H - T\Delta S \quad [3]$$

Therefore by determining the amount of heat that is produced within an enzyme mediated substrate conversion, the reaction rate is accessible. In this case power is determined as the measured heat (Q) over time (dt).

$$Power = \frac{dQ}{dt} \quad [4]$$

The conversion of n moles of substrates to product is associated with the amount of produced heat by

$$Q = n * \Delta H_{app} = [P]_{total} * V * \Delta H_{app} \quad [5]$$

V = volume of the solution in the reaction cell

P = concentration of the generated product

ΔH_{app} = experimentally determined molar enthalpie of the reaction

By this the reaction rate of an enzymatically driven reaction can be deduced from the amount of generated power by

$$Power = \frac{dQ}{dt} = \frac{d[P]}{dt} * V * \Delta H_{app} \quad [6]$$

Rearranging gives

$$Rate = \frac{d[P]}{dt} = \frac{1}{V * \Delta H_{app}} * \frac{dQ}{dt} \quad [7]$$

7. Appendix

The reaction rate (units of power) needs to be converted into enzyme turnover to get a full kinetic characterization of the reaction. For this the apparent molar enthalpy (ΔH_{app}) of the reaction must be known. This can be done by determining the total amount of produced heat depending on the used substrate concentration

$$\Delta H_{app} = \frac{1}{[S]_{total} * V} \int_{t=0}^{t=\infty} \frac{dQ_t}{dt} dt \quad [8]$$

7. Appendix

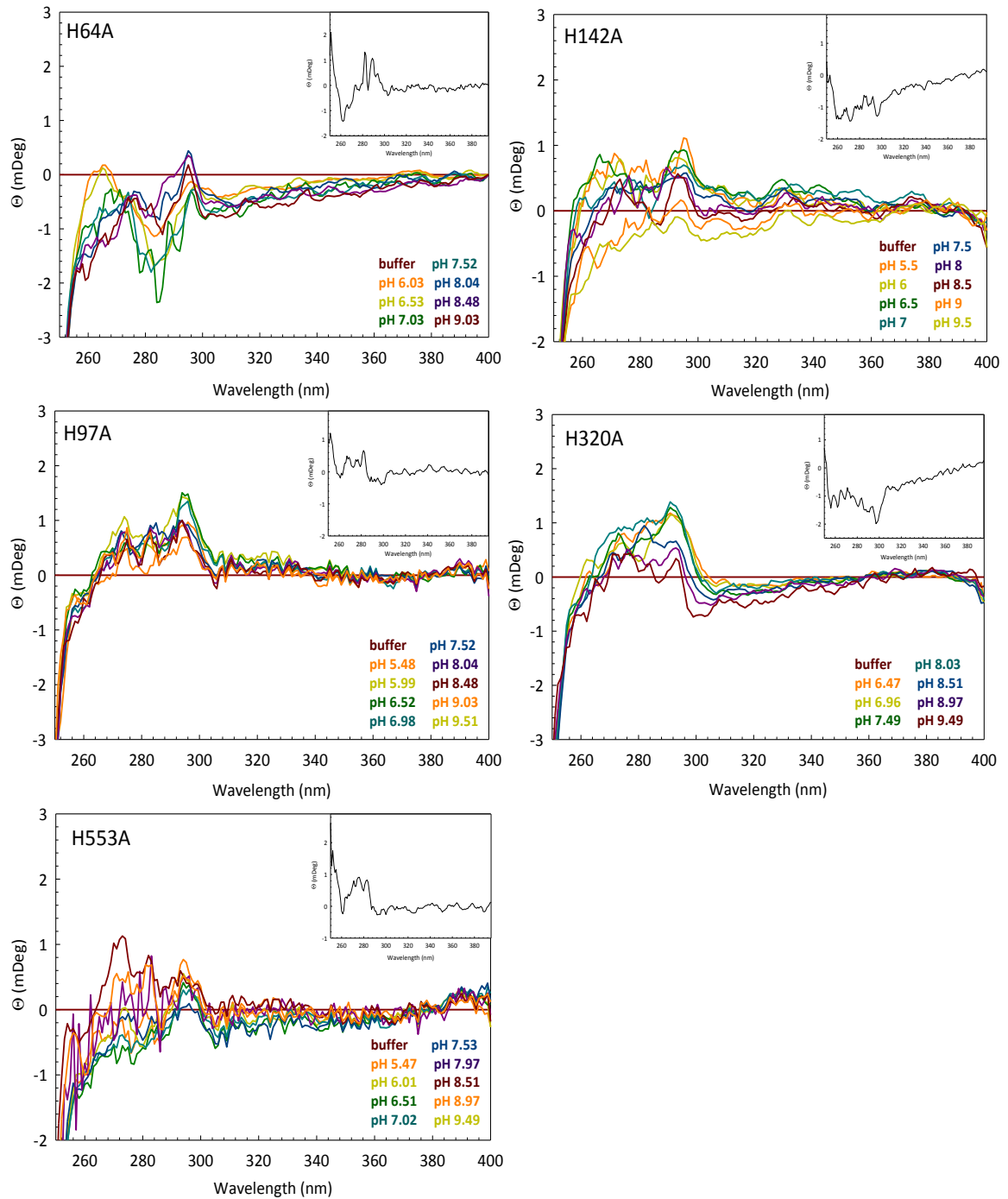


Figure 61: The active center histidine variants of XPK were analyzed by near-UV CD spectroscopy for ThDP binding and generation of the AP, APH⁺ and IP signal

7. Appendix

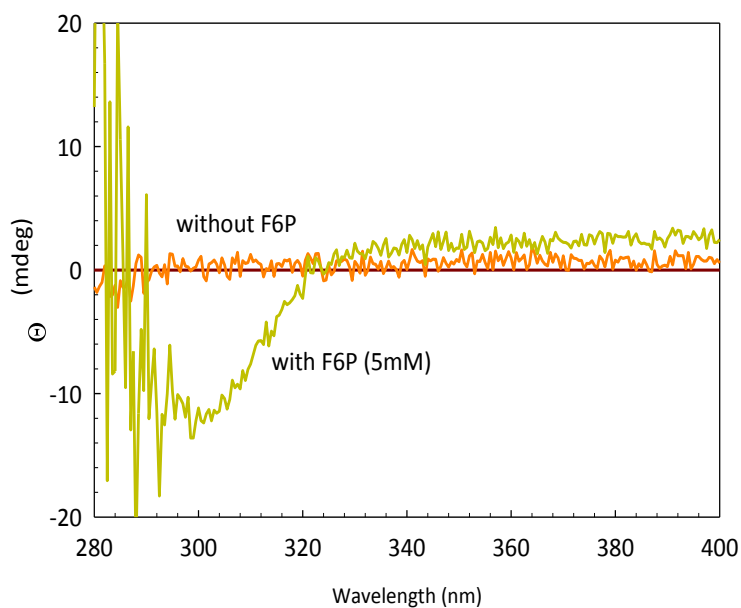


Figure 62: Near-UV spectra analysis of XFPK at a concentration of 1 mg/mL enzyme in Hepes (pH 7.2). Addition of 5 mM F6P leads to a strong absorption signal below 320 nm since the released E4P gives a strong ellipticity signal.

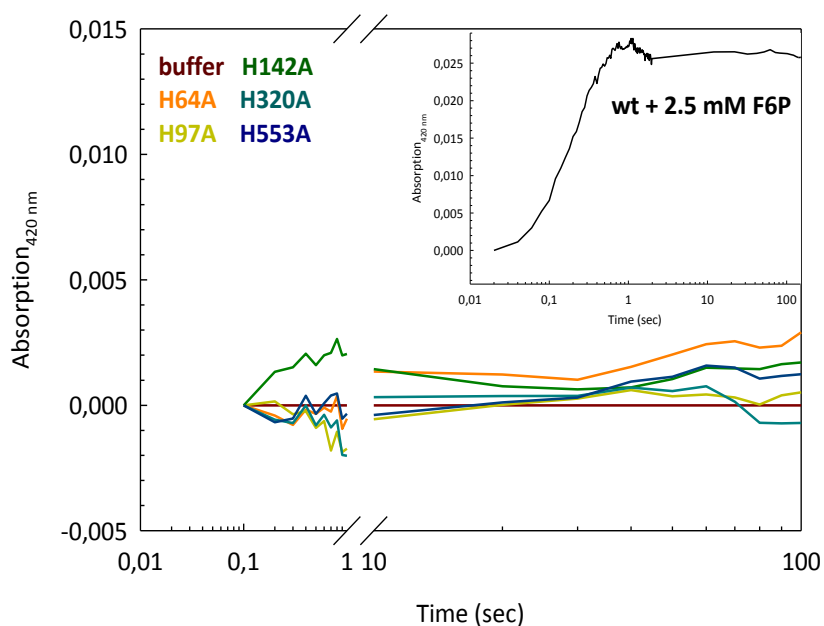


Figure 63: Time resolved PDA spectra of XFPK driven F6P conversion. First phase of F6P conversion by XFPK variants in 20 mM Hepes (pH 7.2) containing 1 mM $MgCl_2$ and 100 μM ThDP at 25 °C in a stopped-flow spectrometer with a pathlength of 10 mm. Only the H142A variant shows slight intermediate formation. Insert shows reaction of wild type XFPK with 2.5 mM F6P.

7. Appendix

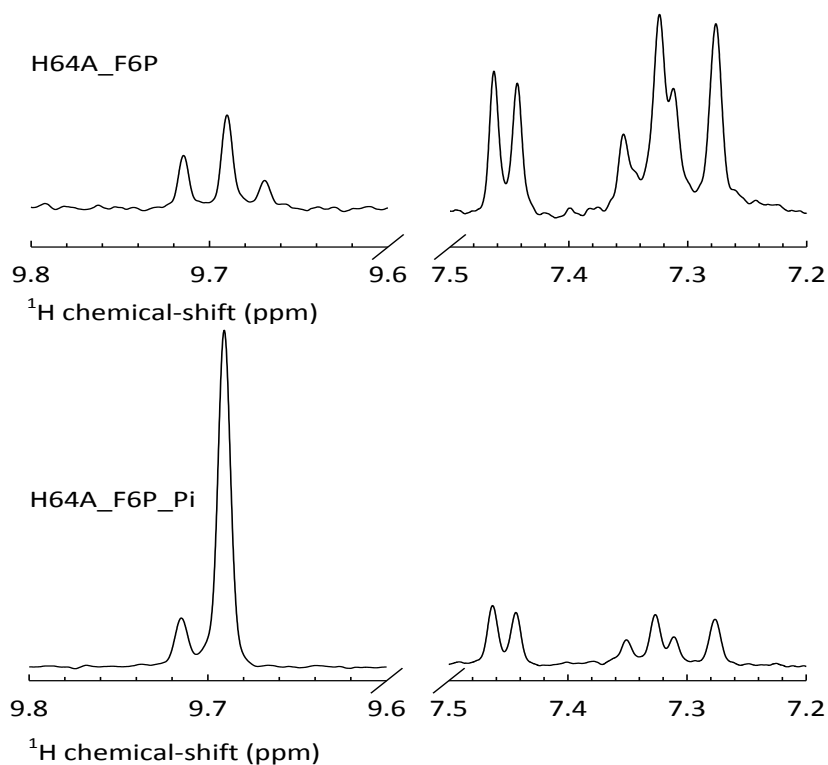


Figure 65: Analysis of intermediate generation after XFPK H64A variant driven conversion of F6P by ^1H -NMR spectroscopy. Addition of F6P or F6P and phosphate leads to generation of multiple signals in the intermediate region. This is caused most likely by cofactor dephosphorolation, which excludes a distinct signal assignment.

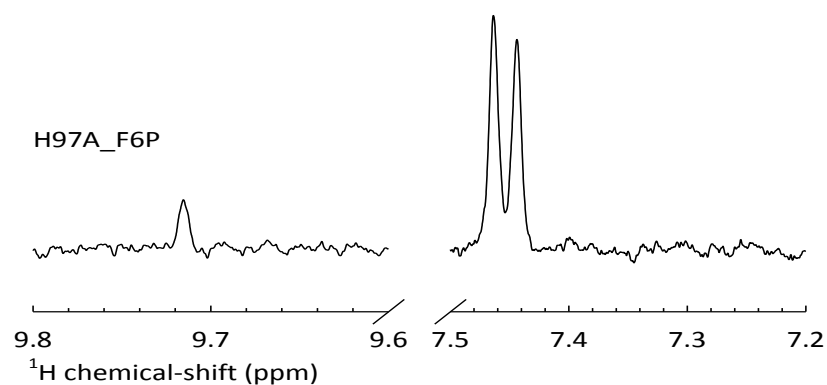


Figure 64: Analysis of intermediate generation after XFPK H97A variant driven conversion of F6P by ^1H -NMR spectroscopy. It seems as if this variant is unable to bind ThDP after dialysis against cofactor free buffer. No intermediate signals could be detected.

7. Appendix

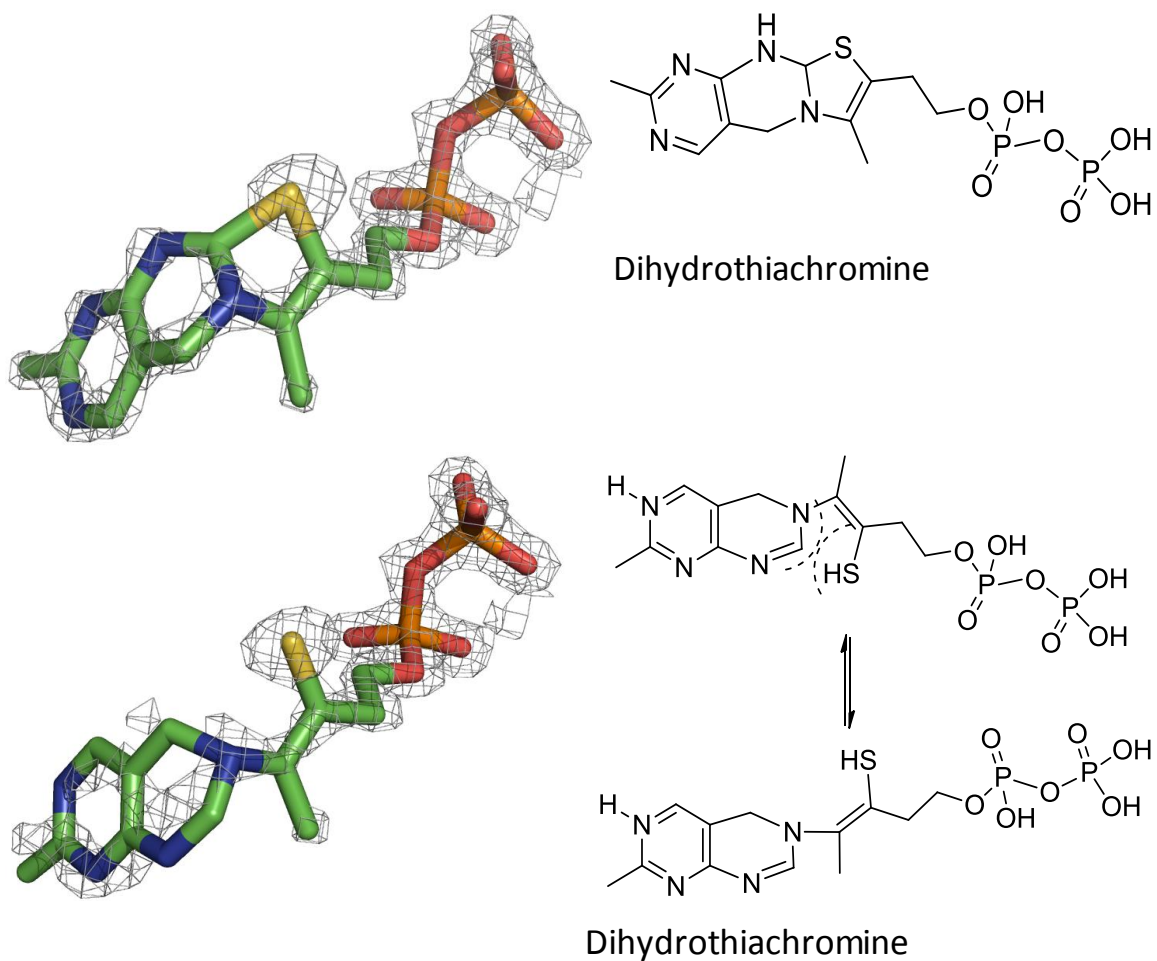


Figure 66: Simulated annealing 2[Fo]-[Fc] omit map of dihydrothiachromin. As outlined in the results part, in the resting state of the E437Q variant missing electron density at the C2 of the thiazolium could be observed. Besides additional electron density seems to be located between the mentioned C2 and the N4' of the aminopyrimidine ring of the cofactor. Suzuki *et al.* reported a comparable phenomenon while determining the structure of the H64A variant. They stated the additional electron density to be a tricyclic form of the ThDP cofactor as reported earlier by Washabaugh *et al.* for free ThDP and Pang *et al.* for ThDP bound to the active center of *Klebsiella pneumoniae* acetolactat synthase¹⁴⁷. Attempts to fit such postulated structures into our electron density gave no good accordance.

7. Appendix

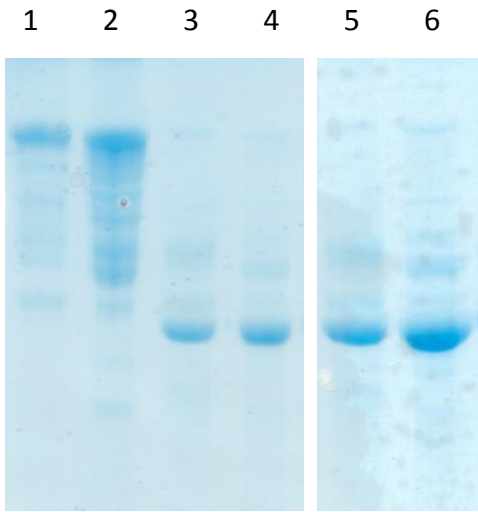


Figure 67: SDS-PAGE analysis of thrombin and HRV 3C digested TFTKTL1 and 2. 1) TFTKTL2 2) TFTKTL1 3) thrombin digested TKTL2 4) thrombin digested TKTL1 5) HRV 3C TKTL2 6) HRV 3C TKTL1

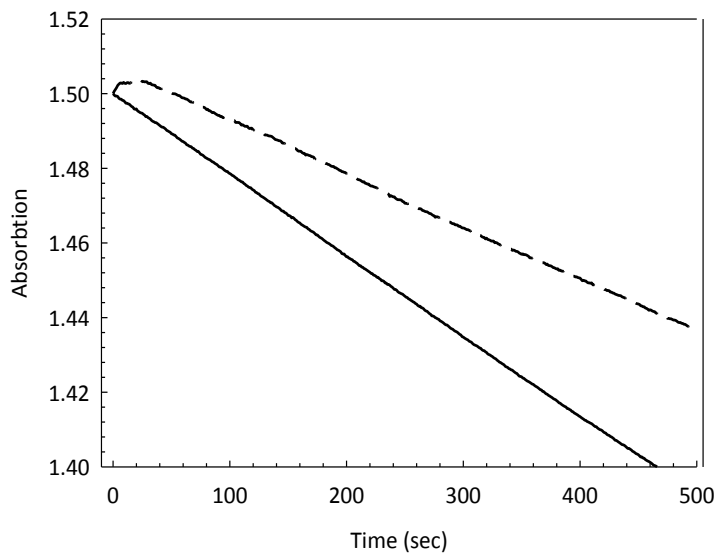


Figure 68: Steady-state kinetic analysis of enzymatic activity of TFTKTL1 and 2. The TKTL1 (solid line) and 2 (dashed line) fusion constructs showed slow consumption of NADH (340 nm) at 30 °C even in the absence of the putative substrates (X5P, R5P and CoA).

7. Appendix

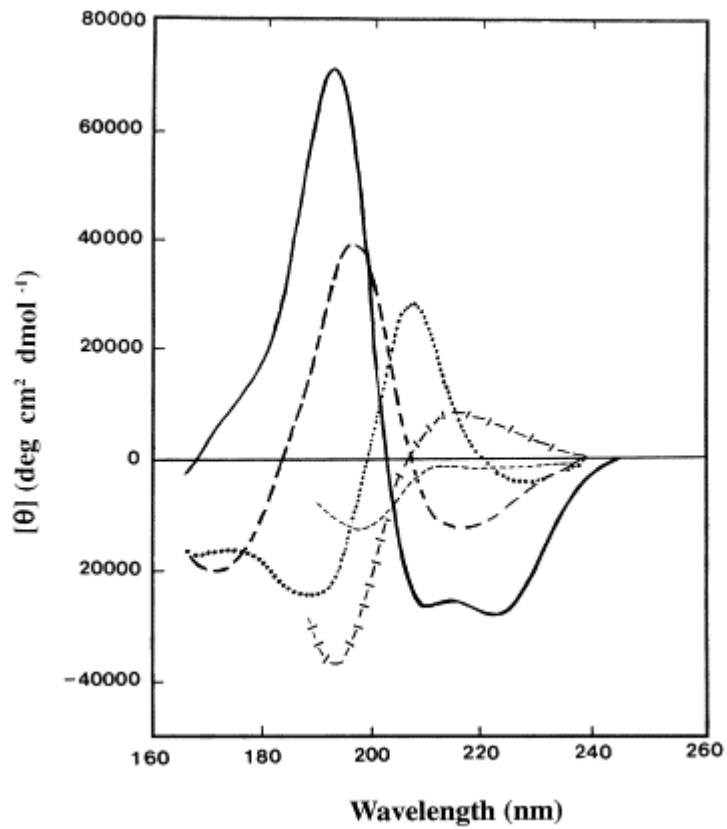


Figure 69: Secondary structure signals as recorded by circular dichroism. Solid line α -helix, long dashed line β -sheet, dotted line type I β -turn, cross dashed line, extended 3_1 helix or poly (pro) II helix, short dashed .line, irregular structure. Adapted from Kelly *et al.* (2005)

Acknowledgements

Acknowledgements

I would like to thank *Prof. Dr. Kai Tittmann* for supervising this thesis and for contribution of numerous fruitful discussions and ideas. I also would like to thank him for NMR data collection.

Furthermore I would like to thank *Prof. Dr Jörg Stülke* for external co-supervision of this thesis and for taking part in the thesis committees.

Moreover I am grateful to *Prof. Dr. Matthias Dobbstein* for external co-supervision of this thesis and for contributing in the thesis committees.

Besides, I am thankful to *Prof. Dr. Ralf Ficner* for being member of my extended thesis committee and for the generous ability to use the instruments and facilities in his department.

Furthermore I would like to thank *Dr. Michael Hoppert* and *Dr. Lars Kuhn* for being members of my extended thesis committee

I also want to thank *Dr. Piotr Neumann* for crystallographic data collection and processing, as well as discussing aspects on protein crystallography.

I especially would like to thank *Dr. Cornelia Herrfurth* for performing mass spectrometric product analysis.

Moreover I want to thank *Dr. Oliver Valerius* for performing mass spectrometric analysis to confirm the identity of the used TKTL1 and 2 proteins.

Especially I would like to thank *Dr. Danilo Meyer* and *Dr. Stefan Lüdtkke*, whose ideas, discussions and critical proofreading of the initial abstract have contributed in numerous ways to this thesis.

Besides I also want to thank *Dr. Kathrin Schröder-Tittmann* who was always open for discussions in terms of molecular biological problems and biofermentation.

Moreover I want to thank *Dr. Florian Brodhun* for final proofreading of this thesis and discussions. Furthermore I would like to thank *Cindy Wechsler* for analysing my NMR samples.

Special thanks goes to my labmates *Dr. Astrid Sitte, Alexander Piontek, Michael Tietzel, Viktor Sautner, Oliver Kupski* and *Fabian Rabe von Pappenheim*.

Finally I want to thank the Göttingen Graduate School for Neuroscience, Biophysics and Molecular Bioscience office, in particular *Kirstin Pöhlker, Christina Bach, Christin Fischer*,

Acknowledgements

Simone Pairan, Dr. Steffen Burkhard and Prof. Dr. Reinhard Jahn for the organization of the graduate school. Moreover I am thankful for the GGNB as recipient of junior group (recipient Prof. Dr. Kai Tittmann) and bridging stipends that allowed me to finish this thesis.

Thanks to my family, whose aid was indispensable for the success of this work.

Last but not least I want to express my gratitude to Caroline Ripp for unconditional support.

Curriculum Vitae

Stefan Schneider

Georg-August-University Göttingen

Department of Bioanalytics

Justus-von-Liebig Weg 11

Göttingen, Germany

Phone: +49 551 3914422

e-mail: sschnei2@gwdg.de

Date of Birth: August 19th 1984

Place of Birth: Göttingen

Nationality: German

Education

1995 – 03/2004	Geschwister Scholl comprehensive school, Göttingen, graduated with general qualification for university entrance
10/2004 – 09/2006	Undergraduate Studies, Diplom Biology, Georg-August-University, Göttingen
10/2006 – 07/2008	Graduate Studies, Diplom Biology, Georg-August-University, Göttingen
10/2008 – 06/2009	Mayors: <i>Biochemistry, Microbiology, Organic chemistry</i> Göttingen center of molecular biology, Department: Biochemistry of the plant, Diploma Candidate Subject: "Characterization of psi-producing Oxygenase C of <i>Aspergillus nidulans</i> " Degree: Diplom-Biologist (1.2)
11/2009 - 10/2013	PhD student, Georg-August-University Göttingen, Department of Bioanalytics „Functional characterization of transketolase-like proteins and related model systems with respect to thiamin diphosphate mediated chemistry", "magna cum laude" Thesis committee: Prof. Dr. Kai Tittmann, Prof. Dr. Jörg Stülke, Prof. Dr. Matthias Dobbelstein
11/2013 - 02/2014	Postdoctoral fellow with Prof. Dr. Kai Tittmann

Curriculum vitae

Scientific contribution

Publications

Brodhun F, Schneider S, Göbel C, Hornung E, Feussner I.: "PpoC from Aspergillus nidulans is a fusion protein with only one active haem." Biochem J. 2010 Jan 15; 425:553-65.

Schneider S, Lüdtke S, Schröder-Tittmann K, Wechsler C, Meyer D, Tittmann K.: "A Δ 38 deletion variant of human transketolase as a model of transketolase-like protein 1 exhibits no enzymatic activity." PLoS One. 2012;7(10):e48321.

Awards and distinctions

11/2009-10/2013	Member of the Göttingen Graduate School for Neurosciences, Biophysics, and Molecular Biosciences (GGNB), Program: Biomolecules: Structure-Function-Dynamics
11/2009-10/2010	Recipient of a GGNB junior group stipend
11/2012-01/2013	Recipient of a GGNB bridging fund stipend
02/2013-10/2013	Recipient of a GGNB junior group stipend